

VIBRATION AND ACOUSTIC MEASUREMENTS OF GUITARS WITH
APPLICATIONS TO LUTHIERY, SYNTHESIS, AND AUDIO EFFECTS

A DISSERTATION
SUBMITTED TO THE DEPARTMENT OF MUSIC
AND THE COMMITTEE ON GRADUATE STUDIES
OF STANFORD UNIVERSITY
IN PARTIAL FULFILLMENT OF THE REQUIREMENTS
FOR THE DEGREE OF
DOCTOR OF PHILOSOPHY

Mark Gregory Rau
November 2023

© 2023 by Mark Gregory Rau. All Rights Reserved.
Re-distributed by Stanford University under license with the author.

This dissertation is online at: <https://purl.stanford.edu/kx813bh3027>

I certify that I have read this dissertation and that, in my opinion, it is fully adequate in scope and quality as a dissertation for the degree of Doctor of Philosophy.

Julius Smith, III, Primary Adviser

I certify that I have read this dissertation and that, in my opinion, it is fully adequate in scope and quality as a dissertation for the degree of Doctor of Philosophy.

Jonathan Abel

I certify that I have read this dissertation and that, in my opinion, it is fully adequate in scope and quality as a dissertation for the degree of Doctor of Philosophy.

Doug James

Approved for the Stanford University Committee on Graduate Studies.

Stacey F. Bent, Vice Provost for Graduate Education

This signature page was generated electronically upon submission of this dissertation in electronic format.

Abstract

Integral to the music-making process is the instrument being played by the musician. Musicians are particular about their instruments, often searching long and hard for the sound they desire. Instrument makers regularly aim to build an instrument with a specific sound to support a given style of music or a player's preferences. However, the acoustic effects of these design changes are not well understood, and systematically testing the auditory effect of geometry or material changes with physical instruments is highly costly and time-consuming. This thesis explores methods designed to allow researchers and luthiers to more easily study design and material changes to instruments, providing a framework for auralizing the sound of an instrument that does not physically exist. Particular emphasis is placed on the acoustic guitar and its construction. Vibration and acoustic measurement methods for analyzing stringed instruments and their components are discussed. In particular, low-cost tools, such as impact hammers, accelerometers, and microphones, are presented, along with an augmentation of a laser Doppler vibrometer to perform scanning measurements. A purpose-built wood measurement device is presented with analysis to measure the internal material parameters of the wood. Simulated vibrational responses from finite element models are compared to the measurements with an optimization routine to predict the material parameters more accurately. A signal processing method is presented to process an electric guitar pickup to sound like an arbitrary virtual acoustic guitar. This method relies on the measured or simulated bridge admittance of the electric and acoustic instrument and provides an opportunity to study the sound of an instrument before it is constructed. Lastly, four studies into the guitar and its acoustics are presented. The first two focus on the construction process of acoustic guitars, the third looks at the influence of neck resonances, and the fourth explores the vibratory behavior of a resonator guitar. This thesis provides a framework for future studies into the construction and sound of stringed instruments, focusing on guitars.

Acknowledgments

A Ph.D. is a rewarding but challenging journey. My journey wouldn't have been possible without the support of an incredible group of advisors and mentors, collaborators, peers, friends, and family. This thesis would not be what it is without your help, so I thank you.

I am grateful to my dissertation and defense committee members: Julius Smith, Jonathan Abel, Doug James, Chris Chafe, and Ronaldo Borja. Thank you to my advisor, Julius Smith, for teaching me about physical models and encouraging my research directions involving the study of guitars. Thank you to my co-advisor, Jonathan Abel, for all of the signal processing discussions and for encouraging me to explore the area of guitar pickup processing. Thank you to my co-advisor, Doug James, for helping me learn about numerical methods and expanding my interests outside of the guitar, though we still spent a lot of time discussing the guitar. Thank you, Chris Chafe, for the steadfast leadership at CCRMA and the support of the CCRMA acoustics lab. Thank you, Ronaldo Borja, for first teaching me the foundations of the finite element method and then serving on my defense as the external chair.

I have had and continue to have the pleasure of working with many brilliant collaborators who helped me become a better researcher. Thank you, Elliot Canfield-Dafilou, Orchisama Das, Prateek Murgai, Jatin Chowdhury, Champ Darabundit, Samuel Clarke, Mason Wang, Mark Sheinin, Esteban Maestre, and Sebastian Gonzalez. I am indebted to Gary Scavone, who took me in as an undergraduate researcher and introduced me to research in music technology.

Shortly after writing my qualifying exams, on a whim, I contacted Richard Hoover, founder of the Santa Cruz Guitar Company, who enthusiastically met with me. This meeting sparked an enduring research collaboration with the luthiers at the Santa Cruz Guitar Company and shaped the direction of much of my research. Thank you, Richard Hoover, for all of our discussions about the guitar and how we can work to understand it better and share this knowledge. Thank you, Rick Barto, for always coming up with a new research idea and working with me to investigate. Thank you, Adam Rose, Brenda Martinez, Carolyn Sills, Darren Webb, William Casper, Forest McCoy, Joshua Huver, Will Kahn, and everyone else for welcoming me and sharing your expert knowledge of the guitar.

Throughout my time in California, I think I spent more time at CCRMA than at my apartment.

While the Knoll may be a beautiful building, it is the people that make CCRMA special. The support of the staff and faculty at CCRMA and the music department has been invaluable. Thank you Matt Wright, Nette Worthey, Jonathan Berger, Takako Fujioka, Ge Wang, Fernando Lopez-Lezcano, Constantin Basica, Dave Kerr, Jarosław Kapuściński, Blair Kaneshiro, Dave Berners, Marina Bosi, John Chowning, Chris Jette, Eoin Callery, Carlos Sanchez, Nils Tonnätt, Sasha Leitman, Victoria Shen, Herb Meyers, Debbie Barney, Marisa Cheng, and Bryan Hardester.

Playing music has always been an enormous part of my life, and thankfully, I had many opportunities to keep playing at Stanford. Thank you, Jim Nadel, for running the Stanford jazz program, and Joshua Redman and Mike Galisatus for teaching and running ensembles. While at Stanford, I started learning the upright bass; thank you, Joshua Thurston-Milgrom, for being my teacher. I am incredibly thankful to have made many incredible friends playing music. In particular, I would like to thank Nolan Miranda, Michael Hayes, Daiki Nakajima, and Joe Goldfrank for their musicianship and friendship.

I have made many incredible friends at and before my time at Stanford. I value every minute I spend with you; your kindness and support are immeasurable. Thank you Jack Atherton, Michael Thomson, Xuan Sun, Chetan Pal Ashta, Lloyd May, Nima Farzaneh, Luna Valentin, Celeste Bentancur, Mike Mulshine, Camille Noufi, Megan Jarek, Juan Sierra, François Germain, Kurt Werner, Dirk Roosenburg, Hassan Estakhrian, Romain Michon, Kimia Koochakzadeh-Yazdi, Kunwoo Kim, Barbara Nerness, Kim Kawczinski, Madeline Huberth, Yuval Adler, Marise van Zyl, Julia Yu, Noah Fram, Doga Buse Cavdir, Nick Gang, Walker Davis, John Granzow, Taylor Goss, Nolan Lem, Eito Murakami, Scott Oshiro, Iran Roman, Jan Stoltenberg, Cara Turnbull, Bernard Wang, Lei Lopez, Christien Raymakers, Sam Sipos, Job de Groot, Connie Choi, Alex Lett, Jane Panangaden, Melissa Pipe, Sam Silverstein, Jerry Xie, Anna Landry, Ryan MacPherson, Jean-Maxime Caron, Henna Tahvanainen and many more.

Though I don't come from a musical family, my family always encouraged my passion for music and my academic journey. Thank you to my parents, Donna and Brian Rau, for all the love and support. Thank you to my brother, Peter Rau, for keeping me sane and bearing the brunt of explaining our research to the rest of the family.

Finally, I am incredibly thankful for the enduring support and encouragement of my partner and best friend, Mariane Generale. You make me a better version of myself, and I could not have done this without you. A bonus thank you goes out to our cat, Daisy; thanks for all the cuddles and meows.

Contents

| | |
|--|----|
| Abstract | iv |
| Acknowledgments | v |
| 1 Introduction: The Guitar and its Acoustics | 1 |
| 1.1 Motivation | 1 |
| 1.2 The American Guitar | 2 |
| 1.3 The Guitar and its Acoustics | 3 |
| 1.4 Modal Representation of the Guitar | 5 |
| 1.4.1 Mode Frequency | 5 |
| 1.4.2 Mode Damping | 6 |
| 1.4.3 Mode Shape | 8 |
| 1.5 Chapter Breakdown | 8 |
| 2 Acoustic and Vibratory Measurements of Plucked String Instruments | 10 |
| 2.1 Instrument Measurement Practices and Methods | 10 |
| 2.1.1 Location and Mounting | 10 |
| 2.1.2 Admittance | 11 |
| 2.1.3 Radiation | 13 |
| 2.2 Lab Tools Built for This Thesis | 13 |
| 2.2.1 Automated Impact Hammer | 13 |
| 2.2.2 Scanning Vibrometer [96] | 14 |
| 2.3 Low-Cost Measurement Devices | 25 |
| 2.3.1 Impact Hammers | 25 |
| 2.3.2 Vibration Sensors | 27 |
| 2.3.3 Wood Speed of Sound Meter | 29 |
| 2.3.4 Wood Measurement Device [93] | 31 |

| | |
|--|-----------|
| 3 Modal and Material Parameter Extraction | 44 |
| 3.1 A Comparison of Modal Parameter Extraction Methods when Applied to Measurements of Stringed Instruments [95] | 44 |
| 3.1.1 Introduction | 45 |
| 3.1.2 Data | 46 |
| 3.1.3 Mode Fitting Algorithms | 47 |
| 3.1.4 Evaluation | 48 |
| 3.1.5 Discussion and Conclusions | 55 |
| 3.1.6 Acknowledgments | 56 |
| 3.2 Wood Material Parameter Extraction and Optimization | 57 |
| 3.2.1 Introduction | 57 |
| 3.2.2 Wood Materials | 57 |
| 3.2.3 Measurements | 58 |
| 3.2.4 Modeling | 61 |
| 3.2.5 Optimization | 63 |
| 3.2.6 Results and Discussion | 63 |
| 4 Electric-to-Acoustic Pickup Processing | 65 |
| 4.1 Introduction | 66 |
| 4.2 Processing Method | 68 |
| 4.2.1 Transient Detection | 71 |
| 4.2.2 Pitch Detection | 72 |
| 4.2.3 Damping Correction | 73 |
| 4.2.4 Sound Radiation | 75 |
| 4.3 Test Case: Measured Guitar | 76 |
| 4.3.1 Measurements | 76 |
| 4.3.2 Mode Fitting | 77 |
| 4.3.3 Reflectance Filter | 80 |
| 4.3.4 Radiation Filter | 81 |
| 4.3.5 Sound Processing | 82 |
| 4.3.6 Evaluation | 82 |
| 4.3.7 Altered Guitar | 86 |
| 4.4 Discussion and Conclusions | 87 |
| 5 Studies in Guitar Measurement and Modeling | 90 |
| 5.1 Study 1: Measurements of Acoustic Guitar Top Plates During The Voicing Process [92] | 90 |
| 5.1.1 Introduction | 90 |
| 5.1.2 Brace Carving | 91 |

| | |
|---|------------|
| 5.1.3 Measurements | 95 |
| 5.1.4 Results | 96 |
| 5.1.5 Discussion | 99 |
| 5.2 Study 2: Measurements of an Acoustic Guitar During the Full Construction Process [88] | 101 |
| 5.2.1 Introduction | 101 |
| 5.2.2 Guitars | 101 |
| 5.2.3 Measurements | 102 |
| 5.2.4 Results and Conclusions | 111 |
| 5.3 Study 3: An Exploration of Guitar Neck Admittance Measurements Taken at Different String Stopping Locations [94] | 121 |
| 5.3.1 Introduction | 121 |
| 5.3.2 Measurements | 122 |
| 5.3.3 Observations | 125 |
| 5.3.4 Discussion and Future Work | 128 |
| 5.4 Study 4: Measurement and modeling of a resonator guitar [97] | 129 |
| 5.4.1 Introduction | 129 |
| 5.4.2 Measurements | 131 |
| 5.4.3 Modal Analysis | 132 |
| 5.4.4 Digital Waveguide Model | 134 |
| 5.4.5 Results and Discussion | 136 |
| 5.4.6 Conclusions | 137 |
| 6 Conclusions | 139 |
| 6.1 Chapter 1 | 139 |
| 6.2 Chapter 2 | 139 |
| 6.3 Chapter 3 | 140 |
| 6.4 Chapter 4 | 140 |
| 6.5 Chapter 5 | 141 |
| 6.6 Future Work | 141 |
| A Electric-to-Acoustic Pickup Processing | 143 |
| A.1 Notch Filter Design | 143 |
| A.2 Mode Fitting | 144 |
| B Publications at CCRMA | 146 |
| B.1 Journal Articles | 146 |
| B.2 Conference Papers | 146 |
| B.3 Conference Presentations | 147 |

List of Tables

| | | |
|-----|--|-----|
| 3.1 | Wood material parameters before and after optimization. | 64 |
| 5.1 | Measured and predicted decay times for the first 5 harmonics of the open low E string to decay by 15 dB. | 127 |
| 5.2 | Center frequency and slope of the linear fitting to calculate the amplitude-dependent nonlinear resonance center frequencies. | 136 |

List of Figures

| | |
|--|----|
| 2.1 Vertical and horizontal mounting of guitars. | 11 |
| 2.2 Hammer and LDV admittance measurement. | 13 |
| 2.3 Mirror galvanometer and control circuits. | 15 |
| 2.4 3D printed galvanometer base, mounted mirror galvanometer, and mounted circuitry. | 16 |
| 2.5 Scanning vibrometer setup. | 17 |
| 2.6 Whiteboard time-domain wave propagation. | 19 |
| 2.7 Spruce board time-domain wave propagation. | 20 |
| 2.8 Spruce board frequency domain modal scans. The admittance is shown on the top. | 21 |
| 2.9 Guitar top plate mode scans. The admittance is shown on the top. | 23 |
| 2.10 Guitar back plate mode scans. The admittance is shown on the top. | 24 |
| 2.11 3D printed force hammer. | 26 |
| 2.12 3D printed force hammer measurement. | 27 |
| 2.13 Low-cost vibration sensor. | 28 |
| 2.14 3D printed force hammer measurement. | 29 |
| 2.15 3D printed device to measure the speed of sound in wood. | 30 |
| 2.16 Tonewood measurement device. | 33 |
| 2.17 Mounting hardware and load cell. | 34 |
| 2.18 Bounding box of board outline. | 35 |
| 2.19 Thickness calipers. | 35 |
| 2.20 Impact hammer and clip-on vibration sensor. | 36 |
| 2.21 Mounting hardware with a board on top. | 37 |
| 2.22 Measurement to pick the longitudinal (first arrow) and transverse (right arrow) flexural frequencies. | 38 |
| 2.23 Example wood board measurement showing equalization and decay. | 40 |
| 2.24 Longitudinal stiffness plots for various tonewood boards. | 41 |
| 2.25 Transverse stiffness plots for various tonewood boards. | 42 |
| 2.26 Longitudinal radiation coefficient plots for various tonewood boards. | 42 |
| 2.27 Transverse radiation coefficient plots for various tonewood boards. | 43 |

| | | |
|------|--|----|
| 3.1 | Generated fitting time. | 49 |
| 3.2 | Generated number of modes fit. | 50 |
| 3.3 | Generated fitting frequency response error. | 50 |
| 3.4 | Generated fitting mode frequency error. | 51 |
| 3.5 | Generated fitting mode damping ratio error. | 51 |
| 3.6 | Generated fitting mode amplitude error. | 52 |
| 3.7 | Guitar admittance. | 53 |
| 3.8 | Bass admittance. | 53 |
| 3.9 | Cello admittance. | 54 |
| 3.10 | Mug admittance. | 54 |
| 3.11 | Redwood board admittance. | 55 |
| 3.12 | Wood measurement. | 59 |
| 3.13 | Flexural (top) and torsional (bottom) mounting velocity vibration. The circle, square, and triangle mark the first and second flexural mode frequencies and the first torsional mode frequency respectively. | 60 |
| 3.14 | First flexural mode (top), second flexural mode (middle), and first torsional mode (bottom). | 62 |
| 3.15 | Mean squared error between the measured and simulated mode frequencies vs iteration number of the optimization. | 64 |
| 4.1 | Single-polarization string model for (a) an acoustic instrument, and (b) an electric instrument with a reflectance correction. | 69 |
| 4.2 | Signal processing block diagram. | 71 |
| 4.3 | Bridge admittance measurement setup for the acoustic guitar. | 77 |
| 4.4 | Mode fitting of the acoustic guitar admittance using $M_a = 50$ modes. | 79 |
| 4.5 | Mode fitting of the electric guitar admittance using $M_e = 11$ modes. | 79 |
| 4.6 | Reflectance of the acoustic and electric guitars as well as the combined reflectance with and without limits. | 80 |
| 4.7 | Comparison of the original reflectance with a 2048 tap FIR and frequency-warped FIR filter. | 81 |
| 4.8 | Radiation filter for the acoustic guitar with $M_a = 50$ modes. | 82 |
| 4.9 | Open low E string pluck comparison. | 83 |
| 4.10 | 3rd fret high E string pluck comparison. | 84 |
| 4.11 | T60 of the first 10 harmonics of the (a) open low E, and (b) 3rd fret high E strings. | 85 |
| 4.12 | Pluck comparison with the measured and mode frequency scaled processing. | 87 |
| 5.1 | Bracing pattern diagram. | 92 |
| 5.2 | Brace carving of OM2. | 94 |

| | | |
|------|---|-----|
| 5.3 | Measurement setup. | 96 |
| 5.4 | Pseudo-bridge admittance of OM1 at the four bracing stages. | 97 |
| 5.5 | Pseudo-bridge admittance of OM2 at the four bracing stages. | 97 |
| 5.6 | Example of mode fitting for OM2. | 98 |
| 5.7 | Mode frequencies and damping ratios of select modes of OM1 and OM2 \pm one standard deviation. | 99 |
| 5.8 | Measurement setup for guitar stages. | 103 |
| 5.9 | 000-28 top carving stages. Un-carved (top left), carving stage 1 (top right), carving stage 2 (bottom left), and the final carving (bottom right). | 104 |
| 5.10 | Guitar box before final sanding. 000-28 with top and sides (top left), 000-28 box (top right), OM1 box (bottom left), and OM2 box (bottom right) | 106 |
| 5.11 | Guitar box after final sanding: OM1 (top left), and OM2 (top right), and 000-28 (bottom) | 108 |
| 5.12 | 000-28 finish stages. First coat (top left), Four coats (top right), and fully polished (bottom left). | 109 |
| 5.13 | 000-28 stages with neck: with neck (top left), with bridge (top right), and complete (bottom left). | 110 |
| 5.14 | OM1 (left) and OM2 (right) complete. | 111 |
| 5.15 | OM1 Body stages measurements. | 112 |
| 5.16 | OM2 Body stages measurements. | 113 |
| 5.17 | 000-28 top carve measurements. | 114 |
| 5.18 | 000-28 body stage measurements. | 115 |
| 5.19 | 000-28 finishing stage measurements. | 116 |
| 5.20 | 000-28 neck on stage measurements. | 117 |
| 5.21 | Mode frequency evolution of OM1 (blue), OM2 (orange), and 000-28 (yellow). | 118 |
| 5.22 | Mode damping ratio evolution of OM1 (blue), OM2 (orange), and 000-28 (yellow). | 119 |
| 5.23 | Mode amplitude evolution of OM1 (blue), OM2 (orange), and 000-28 (yellow). | 120 |
| 5.24 | Experimental setup for admittance measurements. | 123 |
| 5.25 | Magnitude response of the vertical admittance measurements made at the bridge, open position, 4th fret, and 8th fret. | 125 |
| 5.26 | Magnitude response of the horizontal admittance measurements made at the bridge, open position, 4th fret, and 8th fret. | 126 |
| 5.27 | Magnitude responses (lower) of the bridge and open position admittance in the vertical and horizontal directions. The bridge admittance measurements are scaled by -40 dB for clarity. String decay times (upper plot) for the first 5 harmonics to decay by 15 dB. | 127 |
| 5.28 | Low-E string reflectance magnitudes for the vertical direction, corresponding to the bridge and different stopping locations. | 129 |

| | |
|---|-----|
| 5.29 Measurement setup showing the LDV, force hammer, and shaker. Note the shaker's force sensor is not shown. | 132 |
| 5.30 Figure 5.30a shows the measured and fit admittance from the hammer taps with M = 24 modes. Figure 5.30b Shows the measured and fit admittance from the shaker sweeps having RMS velocity of 0.000041, 0.0032, and 0.0102 m s ⁻¹ with M = 14, 16, and 18 modes respectively. The shaker sweeps are offset by -40, 0, and 40 dB for clarity. | 133 |
| 5.31 Admittance from the upward frequency trajectory shaker sweep measurements at 13 different levels. The 12 highest levels are offset in increments of 5 dB for clarity. | 134 |
| 5.32 Block diagram of the waveguide synthesis architecture. | 135 |
| 5.33 Bridge velocity and normalized frequencies of the nonlinear resonances during a pluck of the low G string at 98 Hz. Spectrograms are shown, one with only linear modes, and one which includes the nonlinear resonances. | 137 |

Chapter 1

Introduction: The Guitar and its Acoustics

1.1 Motivation

At the age of ten, I started playing the guitar and have since been captivated by the instrument and everything related to it. I have spent countless hours practicing and studying the guitar, playing with other musicians, and performing. Like many guitarists, I have never been satisfied with just one instrument and am always looking for another with a different sound. I spend a lot of time listening to the sonic details of each instrument, wondering what makes them different and why I prefer one instrument to another for a particular style of music. These differences move me to create music and motivate my study of the acoustics of the guitar. During my Ph.D., I interacted with and learned from many incredible musical acoustics researchers and instrument builders who have inspired me to begin building guitars and further my interest in the instrument.

When interacting with stringed instrument makers (luthiers), it is clear that there is a divide between the musical acoustics research community and the instrument maker community. Considerable research contributions have been and are being made in both communities, but there seems to be little communication between the communities. I hope to engage in both communities and feel the field can prosper with more discourse. One significant disparity I see is the lack of affordable measurement tools available to the instrument-maker community. Researchers use vibrometers, accelerometers, microphones, and data-acquisition hardware and software that are often too expensive for builders. I have been working on affordable alternatives and hope to further this work in the future.

Guitars are traditionally designed with their geometry and materials first, with an approximate idea of the final sound. Following this design philosophy, luthiers master the craft and are able

to tailor the guitar's sound to their desired outcomes, but ultimately, the final sound is somewhat unknown until the instrument is finished. A long-term goal of mine is to develop methods to design a guitar by its sound, first and foremost, choosing the geometry and materials to achieve this sound. For example, a musician could listen to a virtual synthesis model of an instrument and alter the sound of the model until it matches their ideal sound, which will be set as the desired sound of the instrument. Then, numerical methods combined with measurements of the materials for the instrument could be used to design an instrument that will have the acoustic signature of the desired instrument. Chapter 4 addresses the first part of this problem, developing a method to listen to a virtual instrument and alter its sound to find the desired acoustic response. Chapters 2 and 3 address some of the measurement methods that would need to be used during the construction process. I hope this style of design philosophy could enable new areas of guitar design to be explored.

With all said and done, the main driving force behind my research and interest in the guitar is the desire to learn more about the instrument and its acoustics. Many researchers have published papers and books on the guitar's acoustics, but many aspects are still poorly understood. Learning more about the instrument and pushing the boundaries of guitar design is especially important in helping me justify why I need to buy or make more guitars.

1.2 The American Guitar

The steel-string acoustic guitar is an American development in the guitar tradition and lineage. The steel-string flat-top acoustic guitar is the focus of this thesis, so a brief introduction to its development and history is provided here. For a much more thorough history of the development, the reader is directed to the texts of Turnbull, Schneider, Bacon, Johnston and Boak, and Somogyi, among many others [121, 107, 9, 51, 114].

The steel-string acoustic guitar is one of the most popular instruments in the world but was developed rather recently. The American guitar has a lineage in lute-making, with further developments coming from the classical and flamenco guitars, most closely associated with builders from Spain. In the 1800s, when European instrument makers immigrated to North America, the guitar's design changed significantly. In the European tradition, luthiers learned by apprenticeship and generally followed the design path of their teachers, using intricate details to show their mastery of the craft.

A significantly different mindset was present in 19th-century industrial America. It was uncommon for independent luthiers to build instruments, and what appeared in their place were factories producing instruments. The most notable of these factories, which started in the 1830s and still exists today, is that of C. F. Martin & Company. With factory-produced instruments came changes in their design. Decorative elements were often left out, and the designs were altered to be more friendly to factory production methods. The most notable change introduced by Martin and later developed by the Larson Brothers and others was the introduction of the X-brace. Classical and

flamenco guitars use fan braces that largely run parallel to the neck, while X-bracing uses a large structural X pattern in the middle of the guitar's top plate.

In the late 19th and early 20th centuries, steel strings became more common as they were less expensive to produce and significantly louder. The X-brace proved pivotal as its superior strength held up much better to the increased string tension of steel strings than previous bracing methods such as ladder bracing and fan bracing. The X-brace and steel strings became characteristic of the American steel-string guitar. While other bracing patterns exist, X-bracing is by far the most common.

Most American guitars of the 19th century were relatively small and designed to be played in small rooms and parlors, hence the name “parlor guitar”. In the 20th century, guitar companies began experimenting with larger guitars. In 1916, Martin introduced the Dreadnought model, which is significantly larger than previous guitars but was not a commercial success, so production stopped until the 1930s. In the early 20th century, the banjo was a common jazz instrument, but the tastes soon changed to favor the guitar. Many banjo players switched to guitar but wanted a longer neck more similar to that of a banjo. In 1930, Martin introduced the orchestra model (OM), which had a neck that met the body at the 14th fret, two frets higher than most previous guitars. In 1934, Martin introduced a 14-fret dreadnought model, which became an instant hit and eventually the defacto guitar for bluegrass and folk music.

Factory-produced guitars from companies such as Martin and Gibson dominated the markets until the late 1960s and early 1970s, which saw the rise of the second-wave American guitar builders. Driven by the American folk boom, many individuals began their journeys into guitar building. Independent luthiers such as Jean Larrivée, Richard Hoover, Bill Collings, Linda Manzer, Bob Taylor, Michael Gurian, Ervin Somogyi, and many more emerged. These luthiers and their contemporaries innovated and continue to innovate on the designs of the American steel-string guitar. As opposed to the traditional legacy of many Western stringed instruments, such as the violin and classical guitars, guitarists are generally open to new ideas and different materials and designs. This openness has led to an explosive variety of instruments, each with its place in the musical practice of guitarists.

1.3 The Guitar and its Acoustics

Guitarists' enthusiasm for varying guitar designs and diverse materials provides ample opportunities for variance in the sound and acoustics possible among instruments. All guitars share the same fundamental acoustic properties, but the differences are easily audible. These differences are what musicians care about and what researchers are interested in studying.

This section provides a brief introduction to the acoustics of the guitar. Throughout the thesis, each section will give a more thorough background to the relevant methods and area of focus, so the details will not be as comprehensive in this section. For more comprehensive works relating to

the acoustics of the guitar, the reader is directed to those from the scientific community including works in the Catgut Acoustical Society, Journal of the Acoustical Society of America, International Symposium on Musical Acoustics, and particularly those by Rossing, Fletcher, Jansson, Caldersmith, Richardson, Wright, French, Woodhouse and many more [103, 30, 104, 50, 47, 48, 16, 17, 99, 135, 32, 33, 133, ?]. Additional works from the luthier community including those published by the Guild of American Luthiers and the Association of String Instrument Artisans as well as luthiers Bodganovich, Cumpiano, Natelson, Somogyi, Gore, Siminoff, and many more [75, 122, 114, 37, 39, 109, 21, 13].

A guitar's sound is first generated by plucking the strings. When plucked, Helmholtz motion arises in the string with two traveling waves arising, one traveling toward the bridge and one toward the nut or fretting location [104]. The string energy is transferred to the instrument at the neck and bridge string terminations, with the bridge termination accounting for most of the radiated sound. At the bridge termination, the vibrations will propagate through the bridge and top plate, then to the back plate through the sides and coupling of the enclosed volume of air. The vibrations are propagated through the body and radiated as sound that can be heard.

The characteristic sound of a guitar is a result of the frequency, damping, and shapes of the vibrational modes of the instrument. The frequency and shape of these modes result from the instrument's materials and geometry. Generally, a larger instrument will have lower frequency modes than a smaller one. The guitar top and bracing are typically stated as having the most significant contribution to the guitar's sound. In general, if the relative stiffness of the top is increased, the mode frequencies will increase and vice versa. Conversely, if the relative mass of the top is increased, the mode frequencies will decrease. However, generally, as the top and bracing mass decrease, the stiffness is also reduced. Due to these contrasting factors, different materials, geometry, thickness, and bracing patterns will affect the frequencies and mode shapes of the modes of an instrument and, as a result, the sound. The damping of each mode is related to the geometry, as a larger surface area will be in contact with more air, causing more viscous damping. The damping is also a property of the material, with the internal damping of different woods inherent to their organic structure. Visual examples of mode shapes of a wood board and guitar can be seen in [2.2.2].

All of these parameters can result in different-sounding guitars, but there is generally no "best" sounding instrument, just different instruments. The player's judgment of what makes a quality guitar interests many researchers and builders but is not an easy question to answer because each player will have their preferences. Caldersmith and Jansson found that a guitar with a high initial sound level and a fast initial decay would be ideal for an un-amplified concert hall performance since it is perceived as louder [18]. Meyer conducted listening tests and found correlations between the quality of an instrument and the frequency and damping of the third resonance as well as the average level of various frequency regions [72]. More recently, Merchel et al. found a correlation between the quality of a steel string guitar and a low density and Young's modulus of the spruce top [71]. While these studies and others have looked at the quality of guitars, it is clear that the results are very

dependent on the experiment and preferences of the test subjects.

Perhaps a better question than “what makes a good guitar?” would be “what makes a guitar that is stylistically relevant to a type of music and the preferences of the musician playing it?”. For example, a dreadnought-style acoustic guitar is typically used for bluegrass music. This makes sense as they are typically loud with a short string decay, making them ideal for competing for the sonic space with loud banjos and having note definition while playing fast passages. On the other hand, a small-bodied guitar, which is likely quieter but with strings that ring longer, would be better suited to a slow solo ballad performance. Likely, the development of instruments and the genres with which they are associated are intertwined, and there is no “perfect” instrument for all situations.

1.4 Modal Representation of the Guitar

The vibrational behavior of an object can be described by its “modal” behavior, and this representation will be used extensively in this thesis. The modal model of a vibrating object is formulated in terms of the resonant frequencies, damping, and amplitudes or mode shapes of the object. The time-domain modal representation of the object’s impulse response, $h(t)$, having M vibrational modes, has the form,

$$h(t) = \sum_{m=1}^M \gamma_m e^{2\pi f_m t(i - \zeta_m)}, \quad (1.1)$$

where γ_m , f_m , and ζ_m are the amplitude, natural frequency, and damping ratios of modes $m = 1, 2, \dots, M$ [14, 4].

The modal representation of (1.1) is my preferred representation, but other representations of some of the parameters exist. Brief explanations of the modal parameters and alternatives are given below.

1.4.1 Mode Frequency

The mode frequency is the rate at which the object exhibits vibrational extremes for a given vibration pattern (mode shape). In the form of (1.1), the mode frequency, f_m , is represented in Hertz, or cycles/second, meaning that the particular mode of the object will oscillate f_m times per second. The following sections will refer to f_0 , a particular resonant frequency, rather than f_m . Two alternatives to the representation in Hertz are the “angular frequency”, which is a measure of the angular rate of vibration and is represented as:

$$\omega_0 = 2\pi f_0. \quad (1.2)$$

In signal processing, it is also common to use the normalized frequency and angular frequency, which are normalized by the sample rate as:

$$f_0' = \frac{f_0}{f_s}, \quad (1.3)$$

$$\omega_0' = \frac{2\pi f_0}{f_s}, \quad (1.4)$$

where f_s is the sample rate.

1.4.2 Mode Damping

Damping in a vibrating system is the loss of energy to dissipation. Common sources of damping are internal losses in the material to heat and bending, viscous damping with the surrounding air, and sound radiation. Many variables are commonly used in various engineering practices to represent damping, and some of the more common ones are described below.

Damping Ratio The damping variable used in (1.1) is ζ , known as the damping ratio. The damping ratio is a dimensionless variable that describes how oscillations decay after they are disturbed. The damping ratio for typical physical systems ranges from $0 \leq \zeta \leq 1$ with four distinct regimes:

- *Undamped*: When $\zeta = 0$, the system is said to be undamped, meaning that oscillations occur with no decrease in amplitude. This situation is impossible in reality because there is always some form of damping, but it is possible in simulations.
- *Underdamped*: When $0 < \zeta < 1$, the system is underdamped with the solution being two complex oscillators with decaying exponential envelopes. This is the case of most interest when studying the vibration of musical instruments. When ζ is close to 0, the system will vibrate for a long time, but the vibrations will quickly decay when it is closer to 1.
- *Overdamped*: When $\zeta > 1$, the system resembles the sum of two decaying exponentials with no oscillation.
- *Critically damped*: When $\zeta = 1$, the system is critically damped, sitting on the border of underdamped and overdamped.

The damping ratio is my preferred damping ratio because of the simple relationship to these regimes, so it will be used primarily in this thesis. Since the damping ratio is not used by all and is not the most common variable for damping in audio, alternatives are described below.

Exponential Decay Constant Exponential decay can be represented in the simplest form as:

$$N(t) = N_0 e^{-\lambda t}, \quad (1.5)$$

where $N(t)$ is a function of time, t , and λ is a positive constant known as the exponential decay constant. The exponential decay constant is related to the damping ratio as:

$$\lambda = \zeta \omega_0. \quad (1.6)$$

Exponential Time Constant Related to the exponential decay constant is the exponential time constant, $\tau = 1/\lambda$, representing the time for a system with exponential decay to be reduced in amplitude by $1/e$. The exponential time constant is then related to the damping ratio as:

$$\tau = \frac{1}{\zeta \omega_0}. \quad (1.7)$$

Q-factor The quality factor or Q-factor is often defined as the frequency-to-bandwidth ratio of a resonator as:

$$Q = \frac{f_0}{\Delta f}, \quad (1.8)$$

where f_0 is the resonance frequency in Hz, and Δf is the resonance width, commonly referred to as the full width at half maximum (FWHM). The Q-factor is related to the damping ratio as:

$$Q = \frac{1}{2\zeta}. \quad (1.9)$$

T60 The audio decay time (T60) represents the time in seconds for a signal to decay by 60 decibels (dB). It is used because the time constant, τ , is too short for the signal to become inaudible. It is often used in room acoustics as well as other areas of acoustics. The T60 relates to the decay time and hence damping ratios as:

$$t_{60} = \ln(1000)\tau, \quad (1.10)$$

$$t_{60} = \frac{\ln(1000)}{\zeta \omega_0}, \quad (1.11)$$

where \ln is the natural logarithm [110].

Logarithmic Decrement The logarithmic decrement is found by taking the natural log of the ratio of the amplitudes of two consecutive peaks as:

$$\delta = \frac{1}{n} \ln \frac{x(t)}{(xt + nT)}, \quad (1.12)$$

where n is an integer number of successive peaks, x is the amplitude, and t is time [43]. The damping ratio can be found from the logarithmic decrement as:

$$\zeta = \frac{\delta}{\sqrt{4\pi^2 + \delta^2}}. \quad (1.13)$$

1.4.3 Mode Shape

The mode shape or eigenvector shows the deformation of an object while vibrating at a particular modal frequency. The mode shapes are unique to each object and are governed by the materials and geometry of the object. When observing a single point of an object, a complex scalar can be used to represent the mode shape or amplitude at that exact location. When referring to (1.1), if γ is a scalar, it represents the amplitude at a single location, but γ could also be a vector representing the complex amplitude at multiple points on the object. The mode shape or amplitude values are complex scalars that can be decomposed into their relevant amplitude and phase information.

The mode shapes of musical instruments are important as they show the 2D or 3D vibration patterns of the various modes of the instrument. Single mode shape points or amplitudes are also important when dealing with a single-point measurement of an instrument, such as a bridge impedance measurement where the strings are coupled to the body. Visual examples of modes shapes of a wood board and guitar are shown in 2.2.2.

1.5 Chapter Breakdown

This thesis focuses on methods to study stringed instruments, mainly the guitar. Measurement methods are discussed, along with signal processing methods for analysis and synthesis. Finally, some studies on guitars are presented.

Chapter 2 discusses standard measurement techniques used to study stringed instruments. The concept of admittance measurements with an impact hammer and laser Doppler vibrometer is presented. A scanning laser vibrometer augmentation is described. This augmentation allows for mode shape measurements without an expensive commercial scanning vibrometer. Additionally, low-cost measurement tools aimed at instrument makers are presented. Notably, a device to quickly measure the material parameters of tonewood boards is described.

Chapter 3 focuses on methods to extract relevant parameters from vibration and acoustic measurements. Various modal fitting algorithms are discussed and compared when applied to measurements of musical instruments. When dealing with organic materials such as wood, it is essential to know the material properties of specific samples. An optimization method comparing wood board measurements and finite element simulations is presented, which can be used to predict the material properties of the board.

Chapter 4 presents a signal-processing method to transform the sound from an electric guitar

pickup to resemble that of an acoustic instrument. This method relies on a hexaphonic pickup in the electric guitar and mimics the difference in the physics representing the bridge-to-string interactions between each instrument. The method is parameterizable and provides a new way to study the acoustics of guitars, combining the positives of simulation methods and the realistic playing parameters captured from a physical instrument.

Chapter 5 presents three studies relating to guitar acoustics using methods previously discussed and similar methods. Measurements of guitar tops being carved are presented with a discussion of the modal changes. Measurements of these guitars as they are completed are then presented, showing the construction stages with the most significant modal changes. A third study focuses on the resonator guitar, showing that non-linear modal behavior can be seen at high amplitudes and demonstrating this with synthesis methods.

Finally, Chapter 6 concludes the thesis with thoughts and comments on the previous chapters and areas of interest for future studies.

Chapter 2

Acoustic and Vibratory Measurements of Plucked String Instruments

Acoustic and vibratory measurements of instruments are essential in the study of their resonant structure and when creating synthesis models. The measurement and analysis of string instruments goes back multiple decades, with some prominent people in the field being Neville Fletcher, Thomas Rossing, Carleen Hutchins, Antoine Chaigne, and Jim Woodhouse among many others [131, 104, 19, 30, 42]. Here, I will outline a few standard string instrument measurement methods, best practices, and tools I have developed to aid the measurement process.

2.1 Instrument Measurement Practices and Methods

2.1.1 Location and Mounting

There is no one way to mount an instrument when taking acoustic measurements. When an instrument such as a guitar is played, parts of the instrument are damped by the musician's body [60]. While this may be the most realistic way to measure an instrument, there are many variations on how the instrument may be held, and it is not reproducible or easy to compare to measurements made at different times.

A more common method is to measure the instrument in semi-free conditions, trying to reduce the effect of the mounting on the instrument's vibrations as much as possible. Small instruments like violins are often suspended by the shoulders or scroll using elastic bands, but this becomes impractical with larger instruments like guitars and contrabasses. I have found that the best method for mounting a guitar is to suspend it vertically by the tuning pegs while gently resting the endpin area against foam to reduce any swinging motion that may arise. I have also experimented with mounting guitars horizontally and clamping them at the waist. This results in a position that is

more damped by the mounting structure but closer to a natural playing position. While it is more damped, the sides of an acoustic guitar are generally considered less vibrationally important than the top plate, and they are typically damped in some way during normal playing. The two mounting methods are shown in Fig. 2.1.

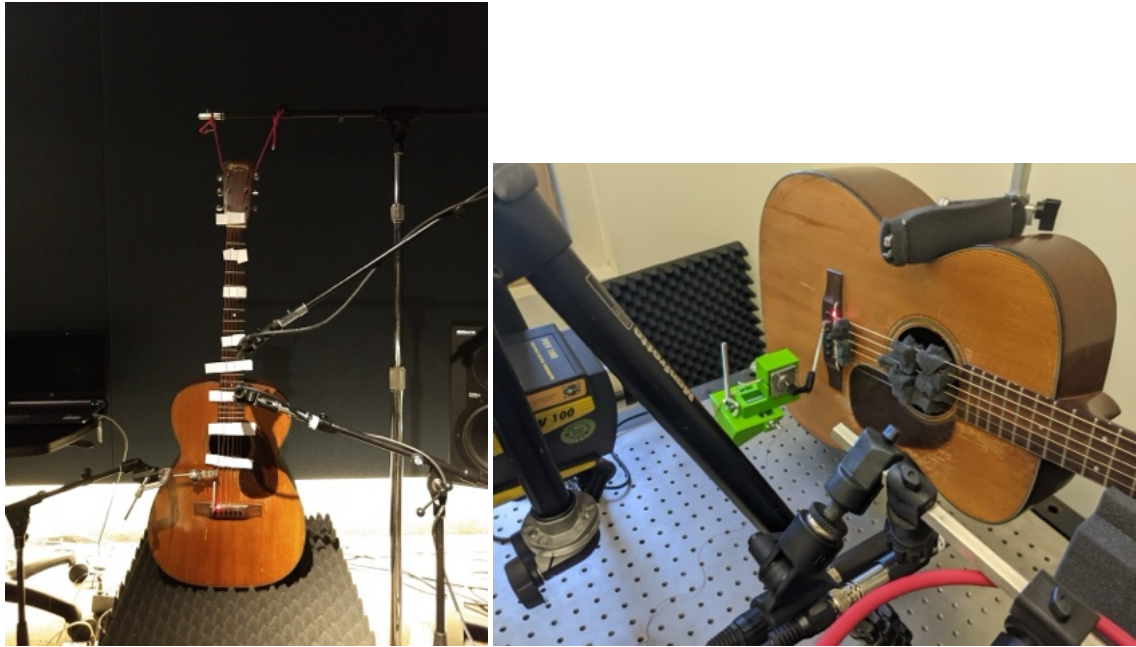


Figure 2.1: Vertical and horizontal mounting of guitars.

While measuring the resonant structure of the body of an instrument, one typically does not want the strings to be in free vibration. One method would be to remove the strings altogether, but the added tension from the strings can change the resonant structure of the instrument, so this is not typically done. More commonly, the strings are tuned to standard pitch and damped with materials such as foam and thick card stock, taking care not to additionally damp the body of the instrument. Other parts of the instrument, such as a loose tuning machine, may need to be damped as well.

2.1.2 Admittance

The most common type of vibratory measurement technique for string instruments is to measure the acoustic input admittance [74, 49, 131, 136]. The admittance is defined in the frequency domain as,

$$\Gamma(\omega) = \frac{V(\omega)}{F(\omega)}, \quad (2.1)$$

where $V(\omega)$ is the velocity and $F(\omega)$ is the force as a function of frequency, ω . The admittance is the inverse of the acoustic impedance. The input and output sensors are assumed to be co-located for an input admittance measurement, which is not physically possible, so they are placed as close as the situation allows.

There are multiple methods to measure the input admittance of an instrument. The most common is to excite the instrument with a force-sensing impact hammer and measure the resulting surface velocity with a laser Doppler vibrometer (LDV). The surface acceleration can also be measured with an accelerometer, which will need to be integrated to calculate the admittance. An LDV is generally preferred over an accelerometer because the accelerometer will mass-load the instrument. However, LDVs are much more expensive than accelerometers, generally on the order of tens of thousands of dollars. Additionally, scanning LDVs exist, which can make multiple velocity measurements over the surface to provide a 2D or 3D measurement.

Rather than a force hammer, a shaker can be used to excite the system. The upsides of the shaker method are that there is more choice in the input signal, and it is possible to do large signal testing such as with variable amplitude sine-sweeps [97]. A force sensor at the tip of a shaker can be used to measure the input force, while an accelerometer or LDV can be used to measure the surface velocity or acceleration. A notable downside to shaker measurements is that the system is mass-loaded by the shaker tip. The tip must also be securely attached to the instrument for anything other than a very low amplitude signal. The preferred method to attach the shaker tip is with epoxy, which is not practical with expensive and rare instruments.

Admittance measurements are most often made at the bridge of a string instrument, as most of the string energy is assumed to be transferred to the instrument at the bridge. However, there is non-zero admittance at the other string termination of the nut or fretting/fingering location [94]. The neck admittance modes primarily result from beam-like neck vibrations.

The instrument's strings will have two-dimensional transverse waves, which can be viewed as propagating in the directions parallel and orthogonal to the top plate of the instrument. If we let the parallel string vibration be v_y and the orthogonal string vibration be v_x , then the bridge admittance can be broken down into four components Γ_{xx} , Γ_{yy} , and $\Gamma_{xy} = \Gamma_{yx}$. Γ_{xx} is measured with the input and output sensors orthogonal to the top plate, Γ_{yy} with the sensors parallel to the top plate, and Γ_{xy} with one sensor parallel and one orthogonal. The string motion orthogonal to the top plate is represented by Γ_{xx} , which has the highest admittance for a typical instrument, so Γ_{xx} is often used to characterize the resonant structure of the instrument for comparison and quality measures. Fig. 2.2 shows a typical admittance measurement in the xx direction with a force hammer and LDV.

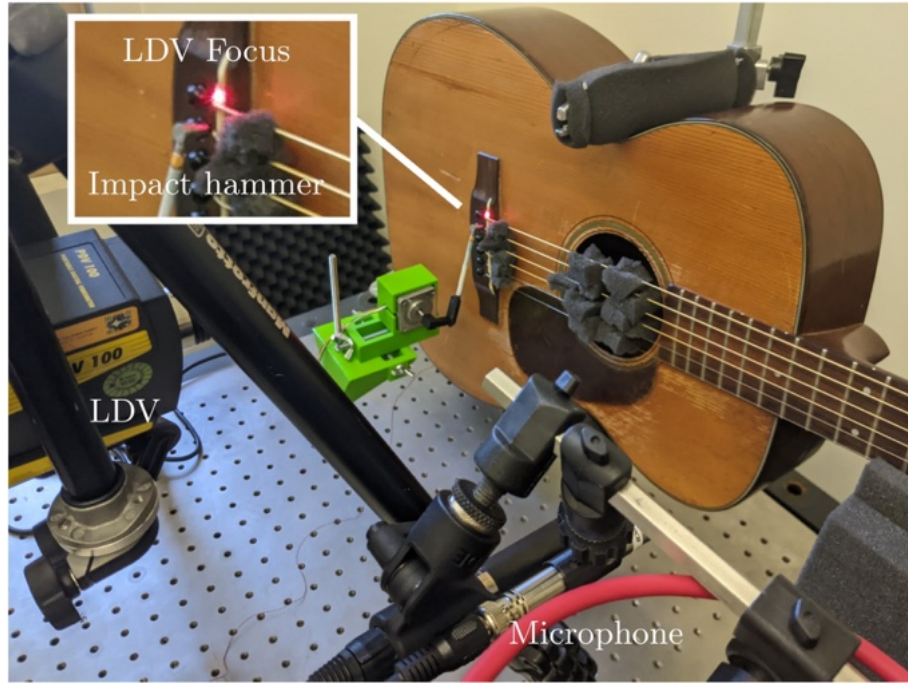


Figure 2.2: Hammer and LDV admittance measurement.

2.1.3 Radiation

The sound radiated by the instrument will share the same set of modal frequencies and damping as an admittance measurement, but the relative amplitudes and phases will be different at each point in space. One or many microphones can be placed around the instrument to measure the radiated sound at those points. There has been a recent surge of interest in microphone arrays to measure the directivity patterns of musical instruments [63, 61, 84]. However, microphone arrays are often large, expensive, and require a near-anechoic environment, so most of the measurements used in this thesis were only recorded with one or two microphones.

2.2 Lab Tools Built for This Thesis

2.2.1 Automated Impact Hammer

It is common to perform hammer tap measurements by hand or to suspend the hammer from a pendulum and manually drop it. However, the measurement equipment can often record human movement close to vibrational measurement setups, causing noisy measurements, so it is ideal for the experimenter to be as far away as possible. I developed a remotely controlled hammer, which can be triggered from afar or programmed to excite the system multiple times. An Arduino controls a

stepper motor with a miniature force hammer mounted via a 3D printed connector. A potentiometer is used to control the speed of the stepper motor to achieve a range of impact forces from the hammer. The mounting system was 3D printed and is easily adjustable. The automated hammer can be seen in Fig. 2.2.

2.2.2 Scanning Vibrometer [96]

While single-point vibrometer measurements are useful for measuring the mode frequencies and damping, the mode amplitude is only measured at that single point. This type of measurement is useful for many applications, such as admittance measurements for synthesis, but sometimes it is desirable to know more details about the mode shapes. For example, if one wishes to track how the modes evolve, it is necessary to know which mode frequencies correspond to which mode shapes so you can be sure to track the exact mode.

There exist multiple ways to make scanning measurements. One common method is known as the “roving hammer” method [108]. In this method, an impact hammer is used to excite the object, while an accelerometer or vibrometer is used to measure the resulting vibrations. Either the hammer or measurement locations are moved to different locations on the object, generally in a grid. Once measurements are made across the object’s surface, they can be reconstructed to show the mode shapes of the measured vibrational modes. While this method can be performed with relatively inexpensive equipment, it has some notable shortcomings. The measurement process is quite laborious, and a dense grid cannot realistically be used because it would be too laborious. Additionally, since either the hammer or measurement location has to be changed for each measurement, some natural variability arises from adjusting the location imprecisely.

An alternative and preferred method for 2D modal scans is a scanning laser Doppler vibrometer such as the Polytec PSV-500 [85]. With this method, the impact hammer is kept in the same position and excited automatically by a control signal from the software running the measurement. The LDV measurement position is moved across the object’s surface, generally using a mirror system to redirect the laser beam. Scanning vibrometer measurements have the advantages of precise measurement location and ease of use since they can be set to run and returned to once the measurement is complete. Because of this ease of use, high-density grids can be used for the measurements. 3D scanning vibrometers such as the Polytec PDV-500-3D also exist which use three scanning laser vibrometer units to measure a 3D surface [86]. The notable downside to scanning vibrometers is the high cost. Commercial scanning vibrometer units generally cost north of \$100 000, and the 3D versions can be closer to \$500 000.

Lacking the budget to purchase a scanning LDV but having access to a single-point LDV (Polytec PDV-100), I designed a system to augment the single-point vibrometer to perform scanning measurements. The cost of this augmentation was under \$200 USD, significantly cheaper than the upgrade to a commercial scanning vibrometer.

2.2.2.1 Design and Construction

In most scanning vibrometer systems, the laser beam is redirected by a pair of mirrors controlled by a galvanometer. The galvanometer is a current-controlled device that can turn the mirror about a rotational axis. Mirror galvanometer systems exist at multiple price points, but the one used for this scanning vibrometer augmentation is at the very bottom, costing \$137 USD at the time of purchase [128]. The mirror galvanometer and control circuits are shown in Fig. 2.3. There are two control circuits, one for each mirror galvanometer associated with the horizontal and vertical directions. Each control circuit takes an input voltage of ± 10 V to turn the mirror $\pm 30^\circ$.

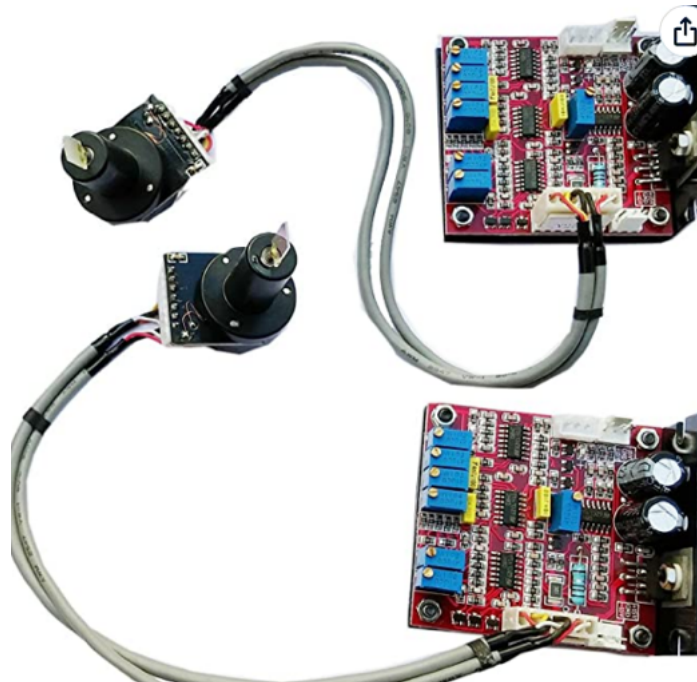


Figure 2.3: Mirror galvanometer and control circuits.

The galvanometer is controlled by a Teensy 3.6 microprocessor, which sends positional arguments over a serial connection [83]. The Teensy 3.6 was chosen because it has two 12-bit digital-to-analog converters (DACs), allowing for 4096 horizontal and vertical positions. The output of the DACs is between 0 – 3.3 V, so additional circuitry needed to be added to provide the necessary control voltages of ± 10 V. Bipolar op-amp circuits were constructed for this purpose [4].

The mirror galvanometer system was mounted directly in front of the Polytec PDV-100 beam. The mounting was 3D printed to hold the mirror galvanometer, control circuits, amplifiers, and Teensy. The bottom of the base is mounted to the PDV-100 with threaded bolts. The 3D printed base, mounted mirror galvanometer, and mounted circuitry are shown in Fig. 2.4.

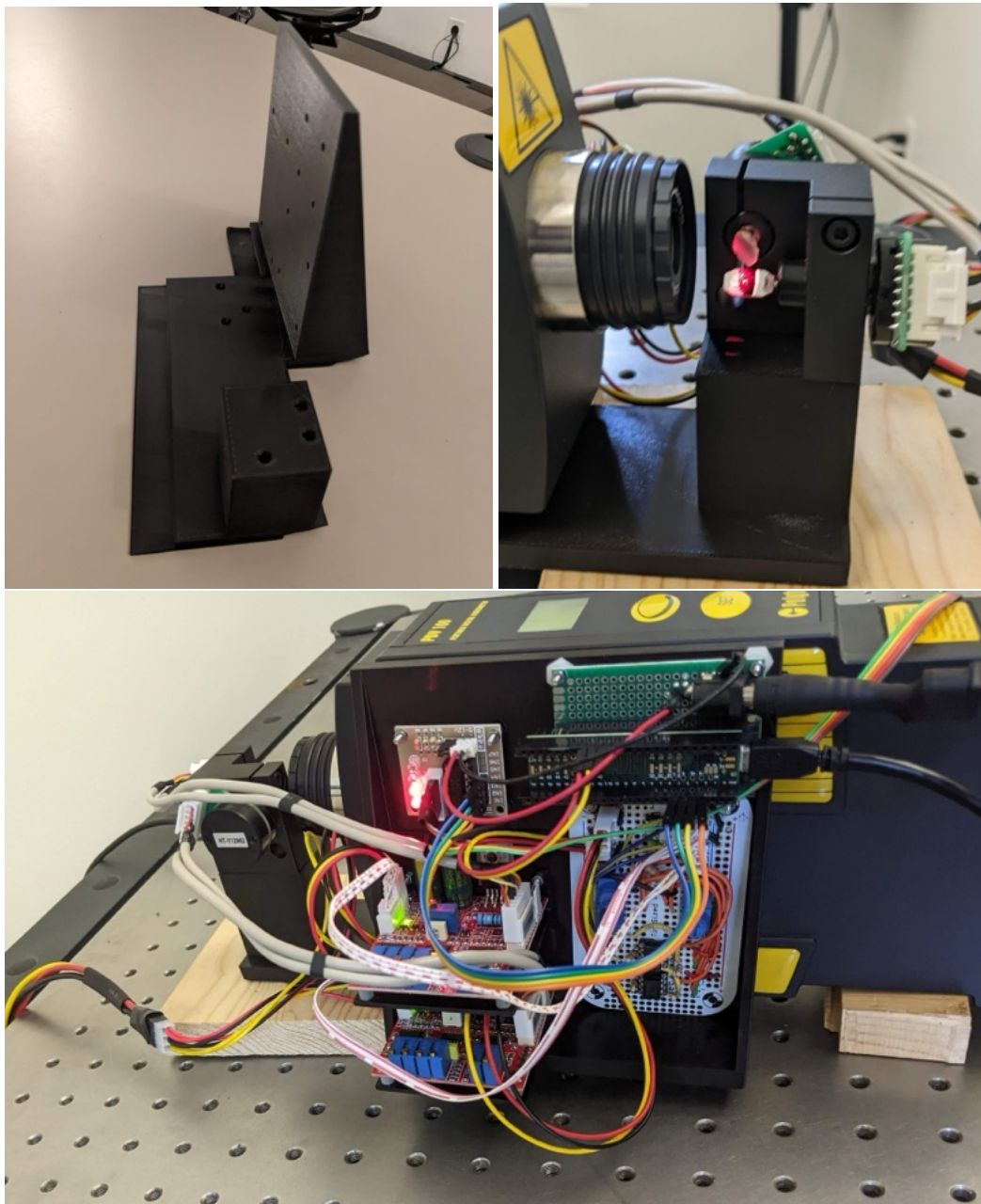


Figure 2.4: 3D printed galvanometer base, mounted mirror galvanometer, and mounted circuitry.

The scanning measurements are controlled with a MATLAB script. The grid density and maximum horizontal and vertical positions are set in the script. Ideally, the system could be set only to scan the object, but at the time of this thesis, it is only set up to scan a rectangular grid. The script then sends serial control signals to the Teensy that are converted to the proper voltage for the

galvanometer control circuits. The scanning system uses the automatic impact hammer described in Sec. 2.2.1. The scanning system moves the measurement point, and the hammer strikes the object while the MATLAB script records both signals. The signals can later be processed to show either the time or frequency information measured as the object vibrates. The complete measurement system set up to measure a violin back plate is shown in Fig. 2.5.



Figure 2.5: Scanning vibrometer setup.

2.2.2.2 Measurements

This section presents a few measurements made with the augmented scanning vibrometer system to demonstrate the type of measurements that are possible.

Time-Domain Wave Propagation Figures 2.6 and 2.7 show the time-domain wave propagation in a whiteboard and thin spruce board. The measurements were made for a study demonstrating a novel transient surface wave imaging method and comparing it to measurements made with a scanning vibrometer [137].

The whiteboard was chosen as it is a primarily isotropic material with high damping. This is

evident when viewing the time-domain wave propagation, as the wavefront spreads evenly in all directions and decays quickly.

The spruce board is meant for guitar building, so it is only 3 mm thick and has less damping than the whiteboard. The spruce board is also orthotropic, which can be seen by the faster speed of sound in the horizontal direction (along the grain) than in the vertical direction (across the grain).

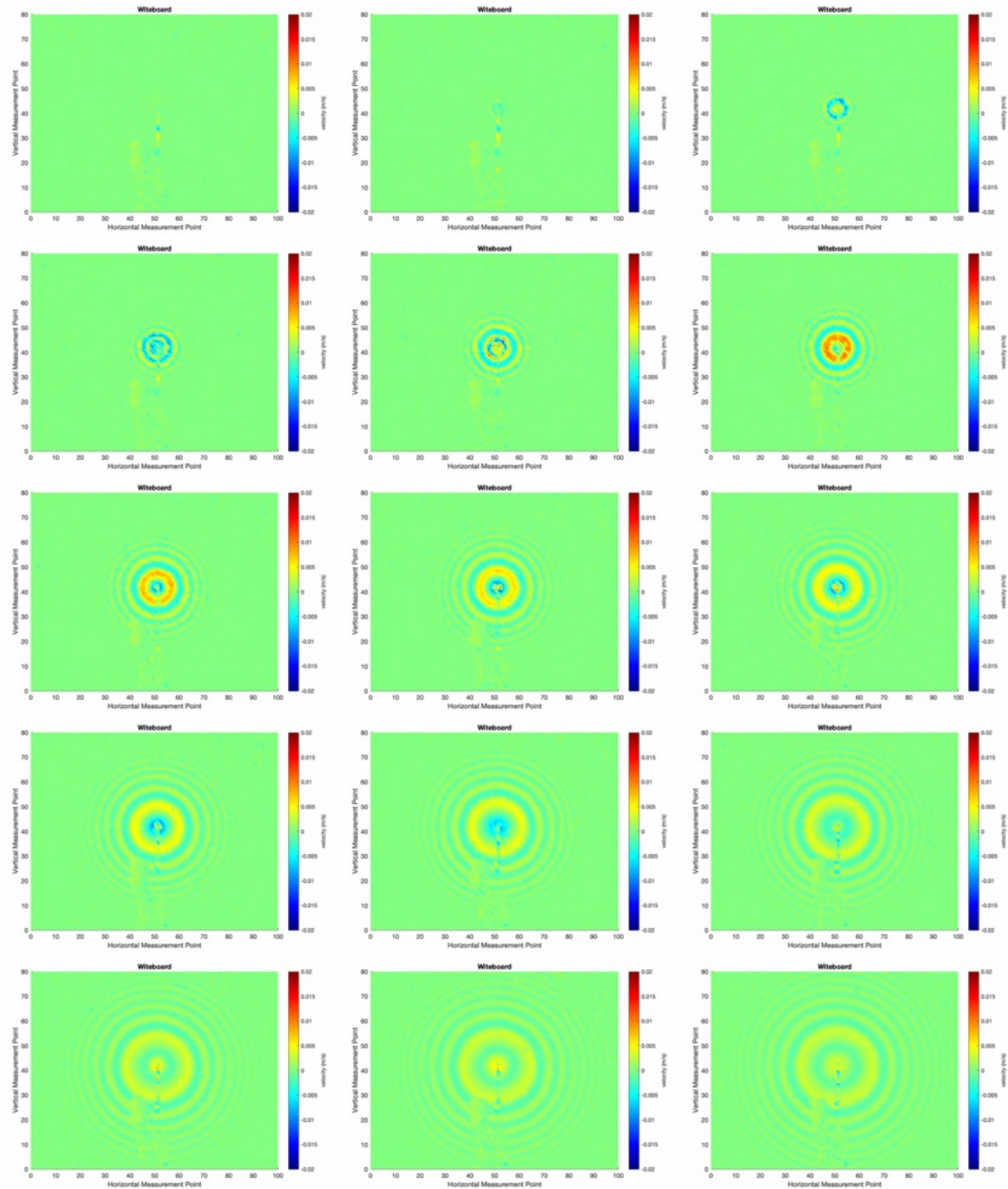


Figure 2.6: Whiteboard time-domain wave propagation.

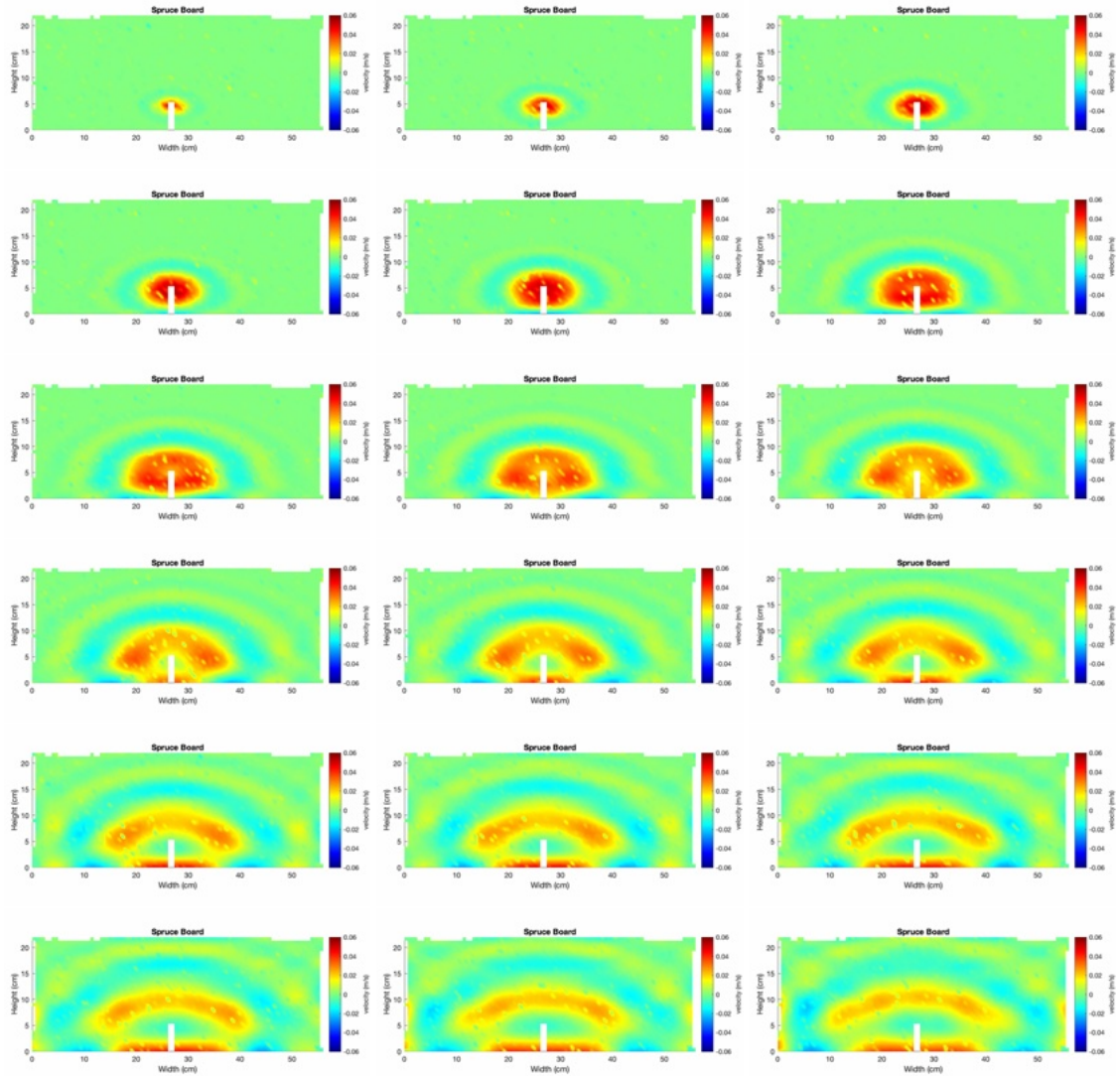


Figure 2.7: Spruce board time-domain wave propagation.

Frequency-Domain Modal Scans If the Fourier transform is taken of the time-domain vibration measurements, the modal shapes of the objects can be viewed. Since the whiteboard is strongly damped, strong mode shapes do not appear. However, multiple mode shapes can be observed in the spruce board scans. Figure 2.8 shows some of the mode shapes observed in the spruce board. The mode shapes were found by first viewing the input admittance (when the hammer strike and vibrometer measurement location are co-located) and picking the significant peaks as shown on the top of Fig. 2.8. Then, for each measurement position, the amplitude of that frequency bin is displayed to show the mode shapes.

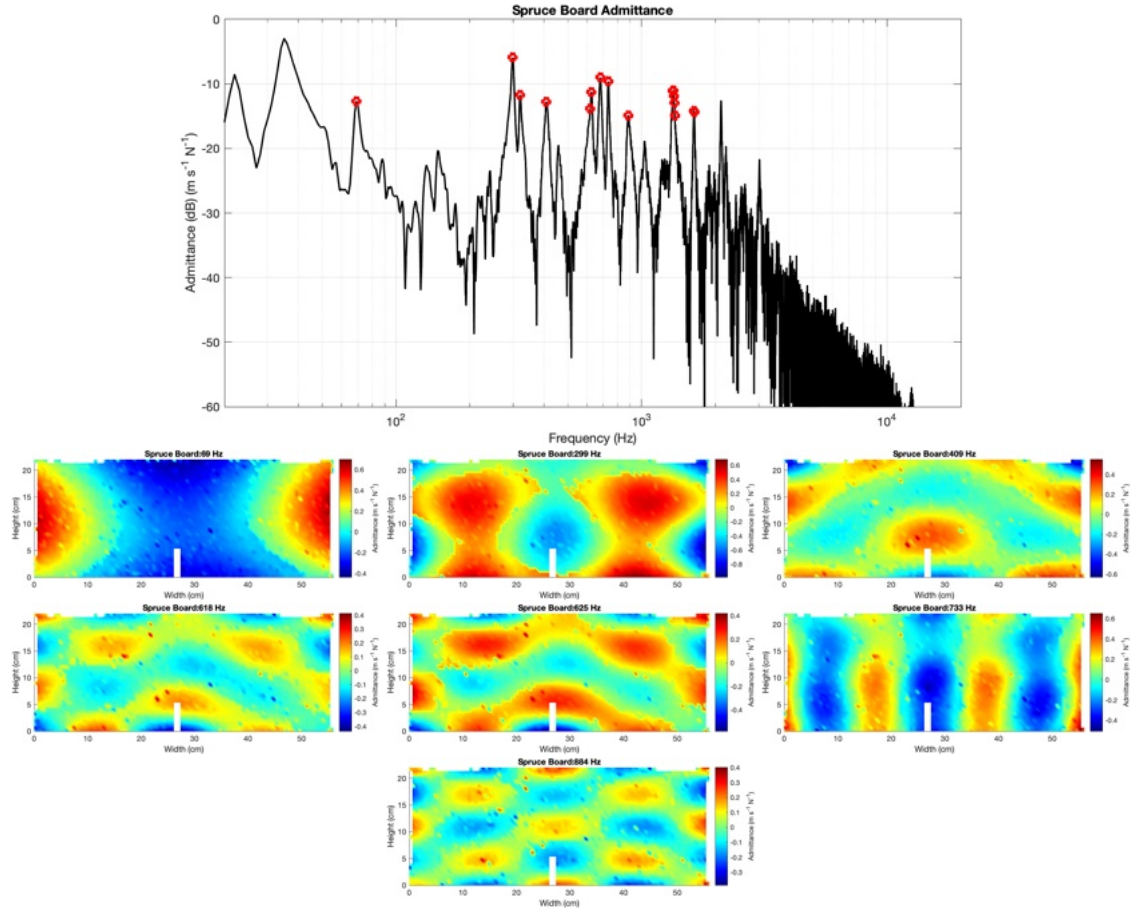


Figure 2.8: Spruce board frequency domain modal scans. The admittance is shown on the top.

Guitar Modal Scan Example To demonstrate a potential use for a scanning vibrometer, scans were made of the front and back of an acoustic guitar. The guitar was excited at the bridge with an impact hammer for all measurements. Measuring both the top and back allows visualization of which modes are strongly coupled or not between the top and back. The measurements were taken of a 1947 Martin 00-18. Figure 2.9 shows the input admittance and top plate scans for three of the strong low-frequency modes. The resonance near 30 Hz is caused by the mounting and is not from the guitar body, so only those resonances above 100 Hz are considered. Figure 2.10 shows the admittance measured at the back, roughly at the vertical and horizontal position of the bridge, and the back plate scans for four of the strong low-frequency modes.

Observing the 101 Hz mode (0,0), the top and back are clearly coupled. Noting that the colors of the back are flipped relative to the top plate because the guitar was flipped, it can be confirmed that this is the out-of-phase breathing mode where the top and back plates move out of phase but at the same frequency. Similarly, the 191 Hz mode can be observed as the in-phase breathing mode.

The 222 Hz mode appears to be a strong resonance in the back plate (0,1) but only weakly coupled to the second strong resonance of the top plate (0,0). Similarly, the 294 Hz mode is clearly observable in the back plate but was not observed in the top plate. However, the 350 Hz mode is strongly observed in both the top and back plates, resulting in in-phase (1,0) in both plates.

A note on the quality of the measurements can also be made when viewing the guitar scans. There are multiple scan points that resulted in noisy data, likely because the vibrometer was out of focus. The focus of the vibrometer depends on the reflectivity of the surface, and the guitar top and back are not ideal candidates. It appears that the back plate is even less reflective than the top plate, which could be explained by the difference in wood of mahogany for the back vs. spruce for the top.

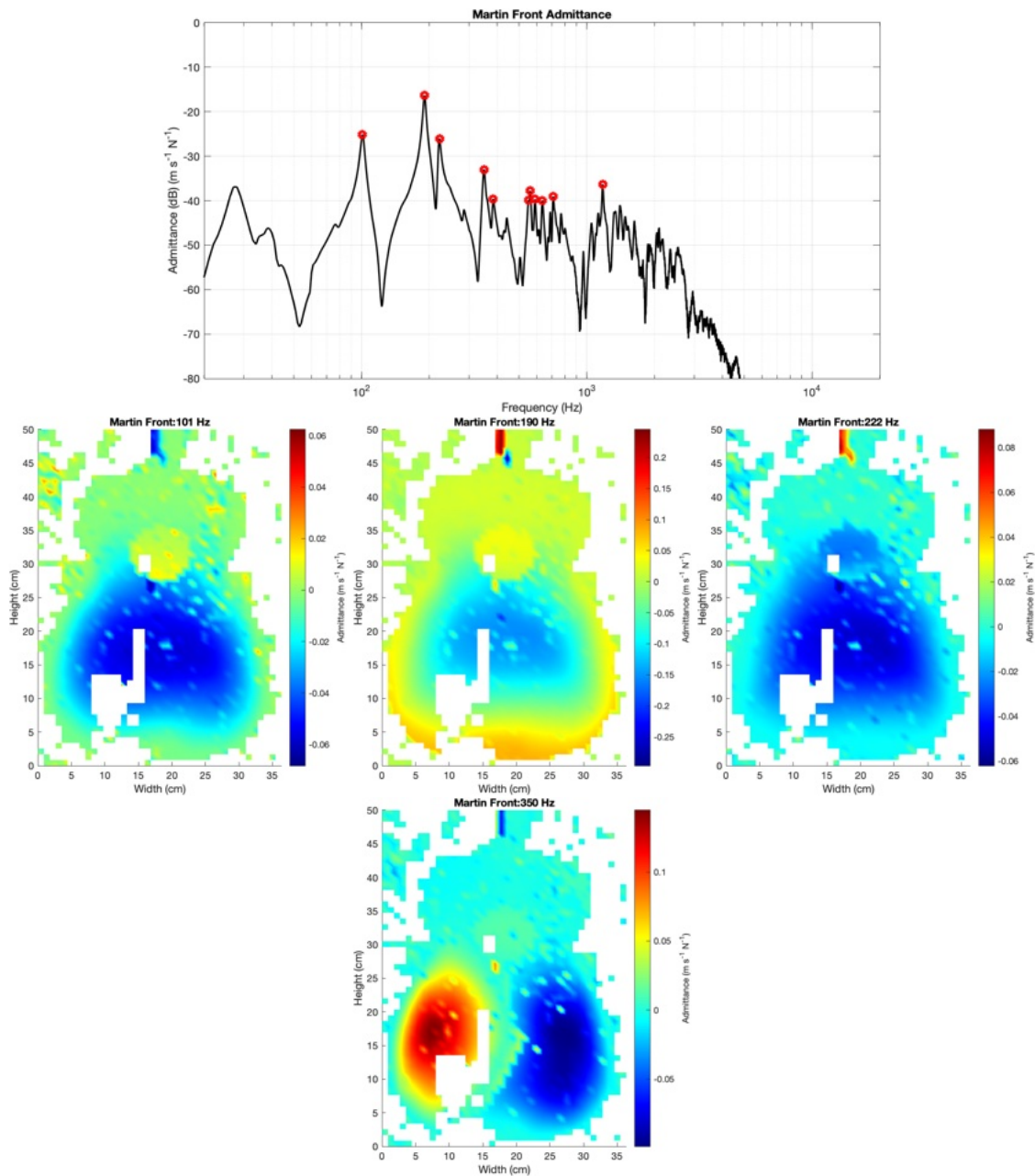


Figure 2.9: Guitar top plate mode scans. The admittance is shown on the top.

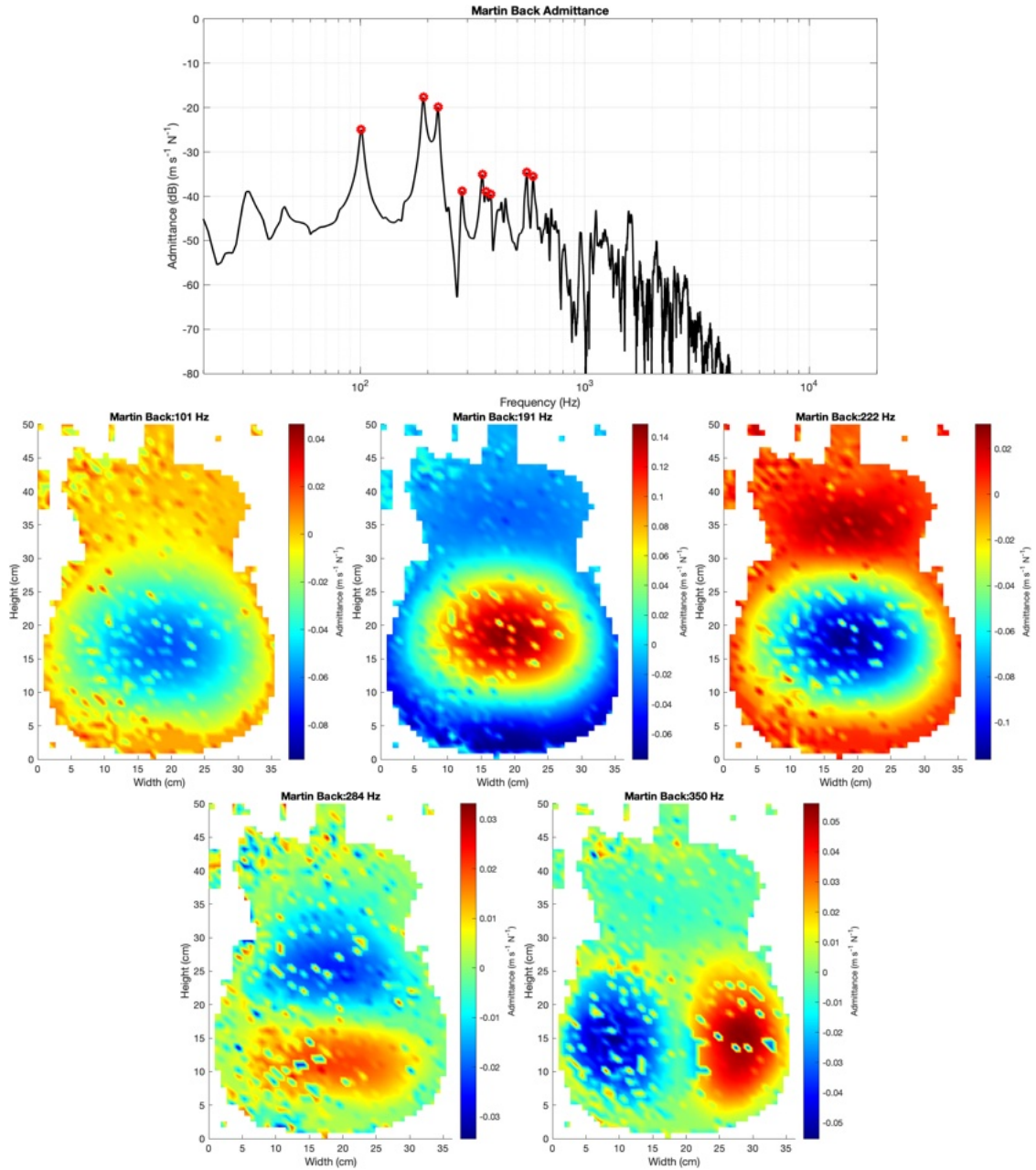


Figure 2.10: Guitar back plate mode scans. The admittance is shown on the top.

2.3 Low-Cost Measurement Devices

One of the main goals of my research is to make it accessible to instrument builders. Instrument builders typically do not have large budgets, so most scientific lab equipment is not accessible. Using this as motivation, I have been working on low-cost alternatives for instrument makers. My collaborations with local luthiers have provided insight into what is useful and practical. Some guidelines are that the tools must be inexpensive, self-contained, and easy to use without manual data processing. This has led me to design 3D printed tools that use inexpensive piezoelectric (piezo) and microphone sensors for the measurement and microprocessors to record and analyze the signals, providing easily understood and useful metrics.

2.3.1 Impact Hammers

The hammer tap method for instrument measurement is ubiquitous among musical acoustics researchers, but the equipment is often multiple thousands of dollars and difficult for untrained individuals to use. I have created 3D-printed force hammers with small piezo sensors in the head to measure the force. The piezo sensor is a Thorlabs PK4DLP1 [119]. It is a 2.5 mm x 2.5 mm x 6.1 mm double piezo stack with a hemispherical tip which is good for a hammer application because the contact area is small. The hammers can be used with a microphone placed nearby to measure the radiation or another small piezoelectric sensor attached to the instrument to measure the surface vibrations. One of these hammers is shown in Fig. 2.11. The time and frequency domain measurement of one of these hammers being used to impact a guitar top with braces is shown in Fig. 2.12.

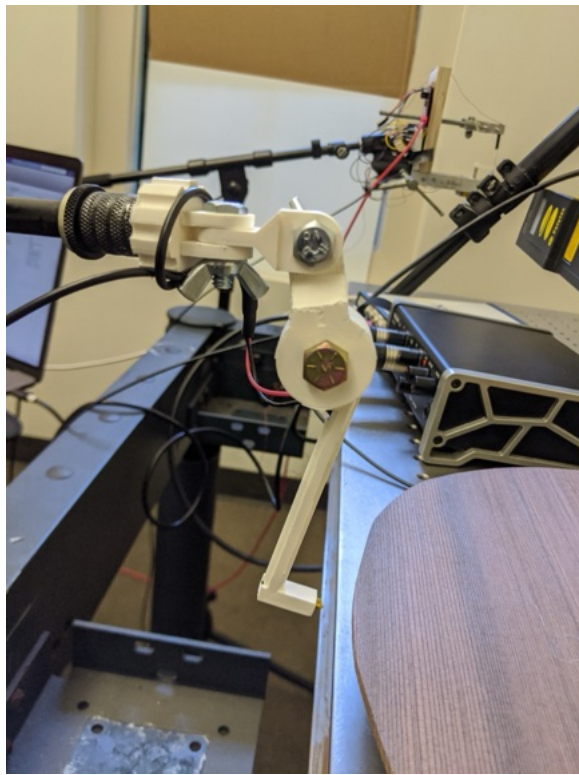


Figure 2.11: 3D printed force hammer.

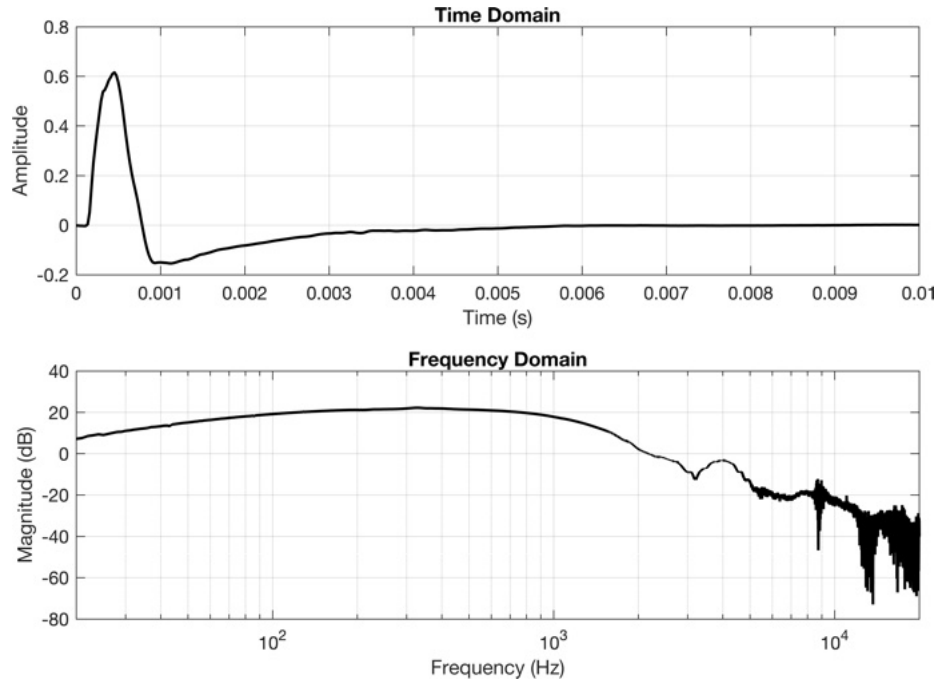


Figure 2.12: 3D printed force hammer measurement.

2.3.2 Vibration Sensors

The same Thorlabs PK4DLP1 piezo stack was used as a surface vibration sensor. With the hemispherical tip removed, it can be adhered to a surface with easily removable PCB Petro Wax accelerometer adhesive [78]. This piezo sensor only weighs 0.5 g, so it does not cause significant mass loading of the object being measured. The sensor being used for surface vibration measurement is shown in Fig. 2.13, and the response of the sensor placed on a braced guitar top struck with the low-cost impact hammer is shown in Fig. 2.14. Using the hammer and vibration sensor, the input force and vibration response are both recorded.

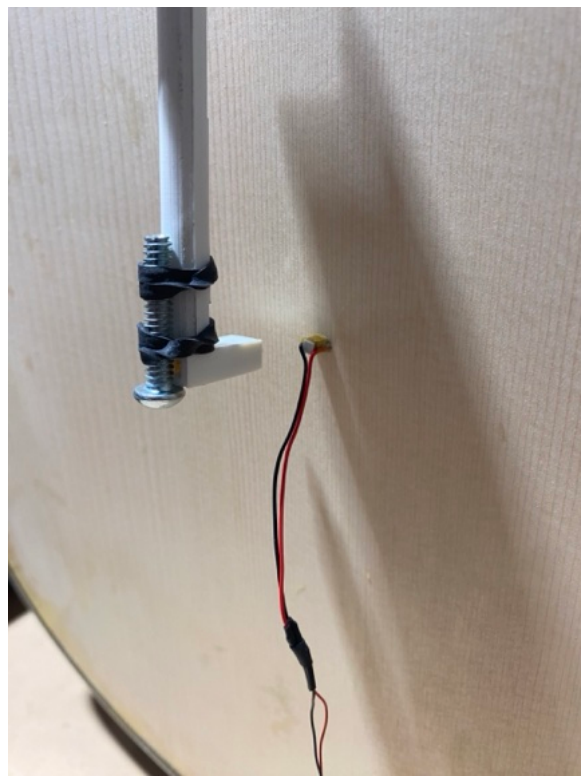


Figure 2.13: Low-cost vibration sensor.

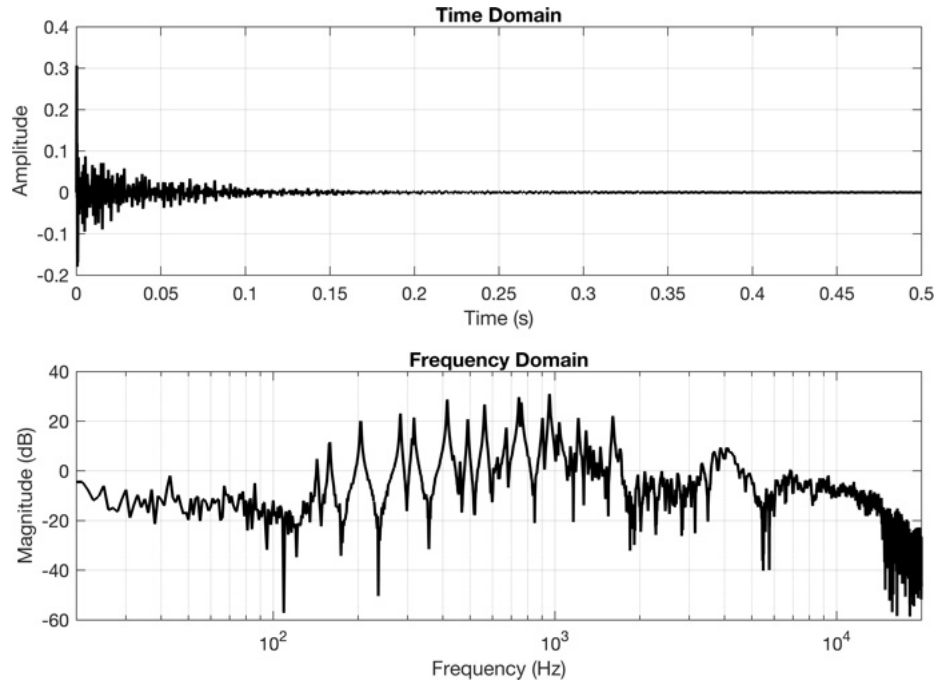


Figure 2.14: 3D printed force hammer measurement.

2.3.3 Wood Speed of Sound Meter

Instrument builders often characterize pieces of unprocessed wood by their stiffness. The most traditional way to measure this is by flexing by hand or with a deflection measurement apparatus. Another way to measure the stiffness is to measure the speed of sound, c , which, in the simple 1D case, is related to the Young's modulus, E , by $c = \sqrt{E/\rho}$, where ρ is the density. There is a device developed by a violin maker called the *Lucchi Meter*, which uses ultrasonic pulses to measure the longitudinal speed of sound across a board of wood. However, this device is quite expensive [120]. I developed a lower-cost alternative that uses a solenoid and piezo sensor to strike a board on one end, while another piezo sensor is attached to the other end. The measured time difference between the two pulses along with the distance, can be used to approximate the speed of sound in the board, giving an indirect measurement of the stiffness in that direction. The speed of sound actuator/sensor is shown in Fig. 2.15

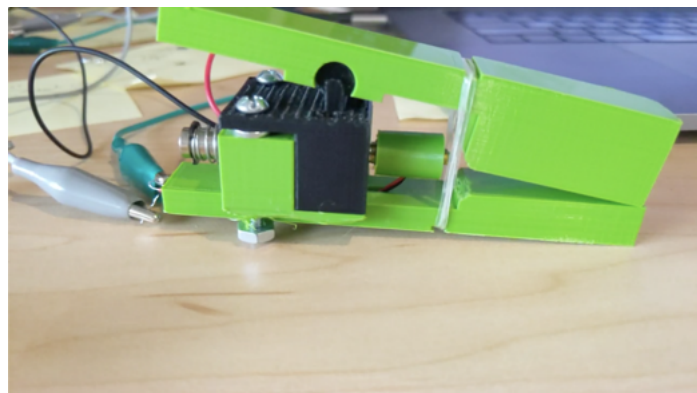


Figure 2.15: 3D printed device to measure the speed of sound in wood.

2.3.4 Wood Measurement Device [93]

When trying to predict how a wood board will behave when used in a musical instrument, it is helpful to know the material parameters of the wood. Since wood is an organic material, there can be significant variations among the material parameters, even among two boards cut from the same tree [127]. Various factors affecting the material parameters are the tree species, the location and elevation where the tree was grown, the age and time period the tree was grown, and even which side of the tree was facing the morning sun. Knowing the variability of wood, it is not possible to simply look up the material parameters of the wood, and efforts must be made to measure them for each individual board.

This project was a collaboration with the Santa Cruz Guitar Company to make a tonewood measurement device that can be used in a guitar shop setting. Due to the practical nature of the device, certain specifications outlined below had to be made:

- The device must be reasonably affordable, less than \$1000 USD.
- Measurements should be quick to take, no longer than a few minutes.
- All measurements must be non-destructive.
- Microphones cannot be used because a quiet room would be needed, which was not available in the guitar shop.
- All data should be stored locally and automatically uploaded to the cloud.

Working within these limitations, some constraints were placed on the boards to be measured. The measurements are only valid for rectangular boards of uniform thickness. A preference was set on measuring softwoods used for guitar tops at the time being, with the possibility of expanding to hardwoods.

Ideally, all material parameters and vibrational information would be measured, but this is not possible, and not all are relevant. The main parameters to extract are described below:

- Young's modulus (E) of the board, in both the longitudinal (along the grain) and transverse (across the grain) directions.
- The radiation coefficient in the longitudinal and transverse directions, which relates the Young's modulus and density as $R = \sqrt{\frac{E}{\rho^3}}$.
- Information about the equalization of the board, essentially, the amplitude of vibration in relative frequency bands.
- Information about the sustain of the board, essentially, the decay time for the different modes or frequency bands.

2.3.4.1 Measurements and Construction

Some parameters of the wood can be directly measured, while some are calculated from those measurements or extracted from vibration measurements. This section describes each parameter and how they were measured or calculated.

The device was constructed primarily out of 80/20 T-slot aluminum bars. 3D printing and laser cutting of acrylic were used for additional parts. The general device is shown in Fig. 2.16.

The device is controlled by software written in Python running on a PC, which communicates with a Teensy 4.0 microprocessor and audio shield over USB with serial commands [82, 81]. The Teensy analog inputs are used for data collection from the various sensors, while the analog outputs control a stepper motor. The Teensy also acts as an audio interface with two inputs for the vibration sensors.

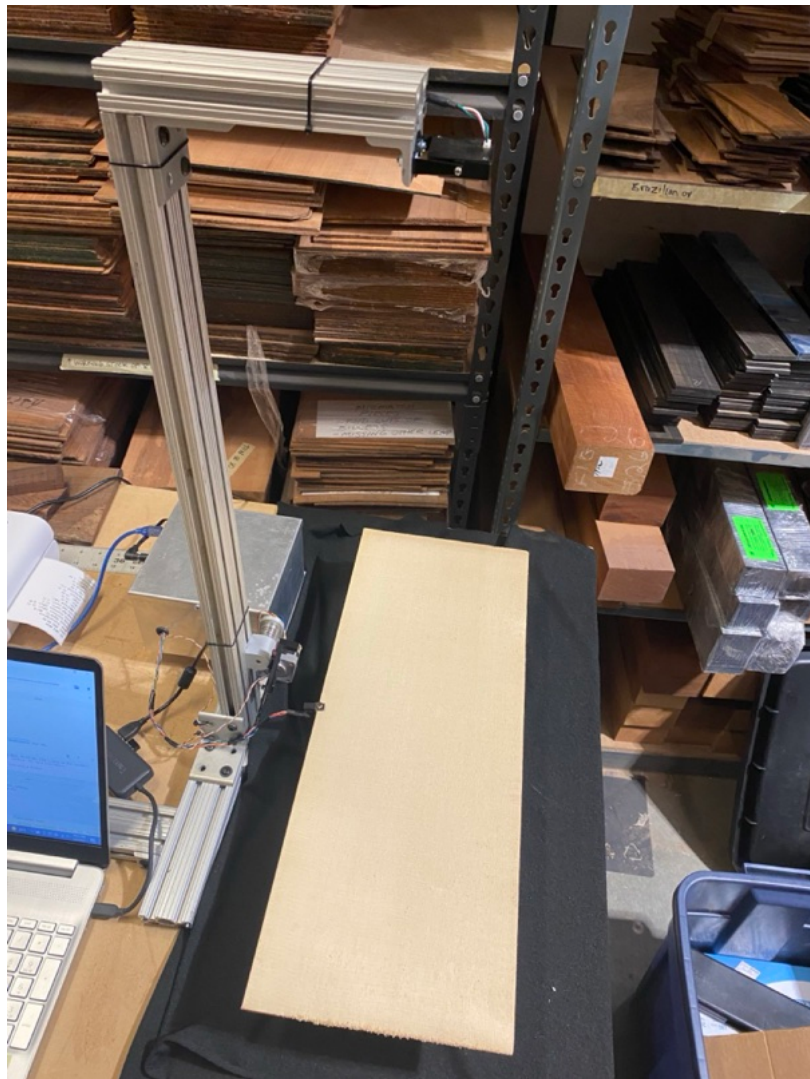


Figure 2.16: Tonewood measurement device.

Mass In order to calculate the density of the board, the mass must be calculated. To do this, the entire mounting of the board is placed on a load cell [45]. The load cell is calibrated to disregard the tare weight out of the mounting hardware. The load cell and mounting hardware are shown in Fig. 2.17.

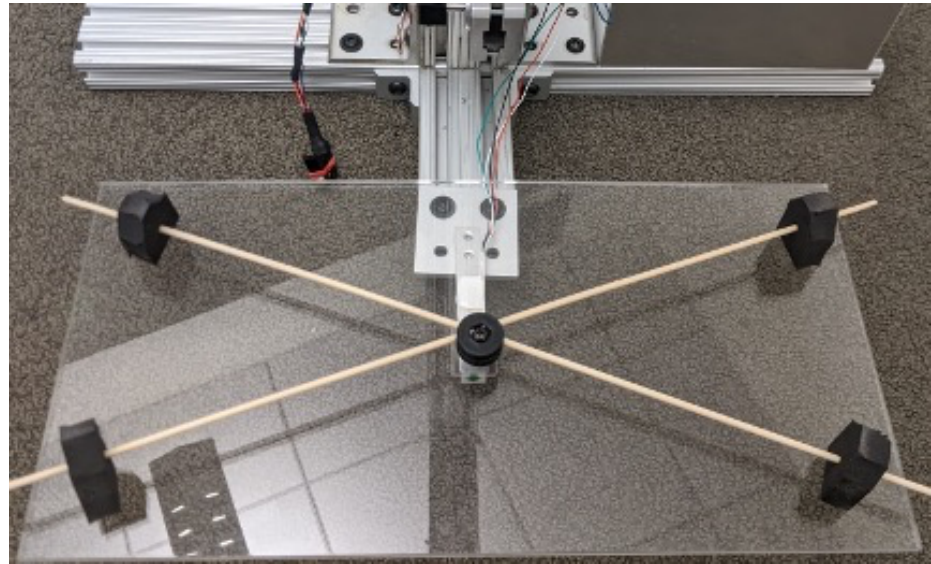


Figure 2.17: Mounting hardware and load cell.

Length and Width The length, width, and thickness need to be measured for the density and Young's modulus calculations. To calculate the length and width, a 4K camera is mounted above the wood board, and a photo is taken [73]. The Python computer vision package OpenCV was used to analyze the image to fit the length and width [41]. A bounding box was fit around the wood board, and the length and width were calculated in pixels, then converted to meters using a calibration. The calibration curves were made by manually measuring multiple boards and knowing their length and width in both pixels and meters. The overhead camera (note, this photo shows an older camera) can be seen in Fig. 2.16, and an example of the bounding box fit with OpenCV is shown in Fig. 2.18.

The thickness is measured with calipers made with a USB thickness gauge [20]. The calipers can be seen in Fig. 2.19. Even if the boards are relatively uniform in thickness, there can be some variability, so ten thickness measurements are made and averaged.

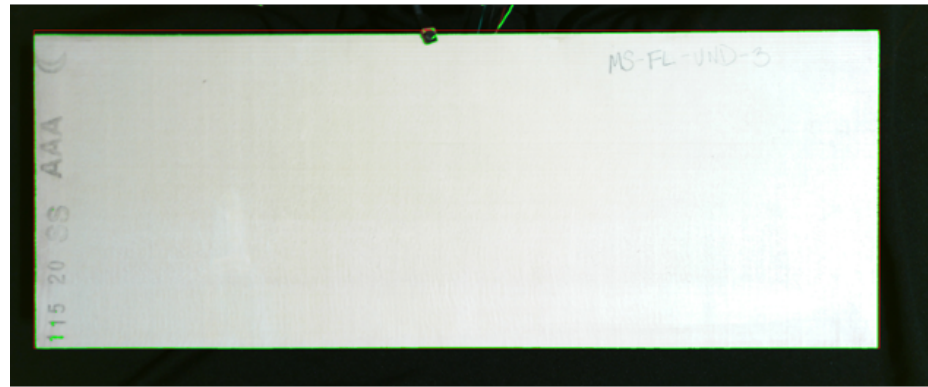


Figure 2.18: Bounding box of board outline.



Figure 2.19: Thickness calipers.

Impact Hammer To excite vibrations in the board, an impact hammer is used. The impact hammer is 3D printed and controlled by a stepper motor. Mounted in the tip of the hammer is a Thorlabs PK4DLP1 piezo stack which is used to record the impact profile [119]. The impact hammer can be seen in Fig. 2.20. The board is struck five times to record multiple impacts.

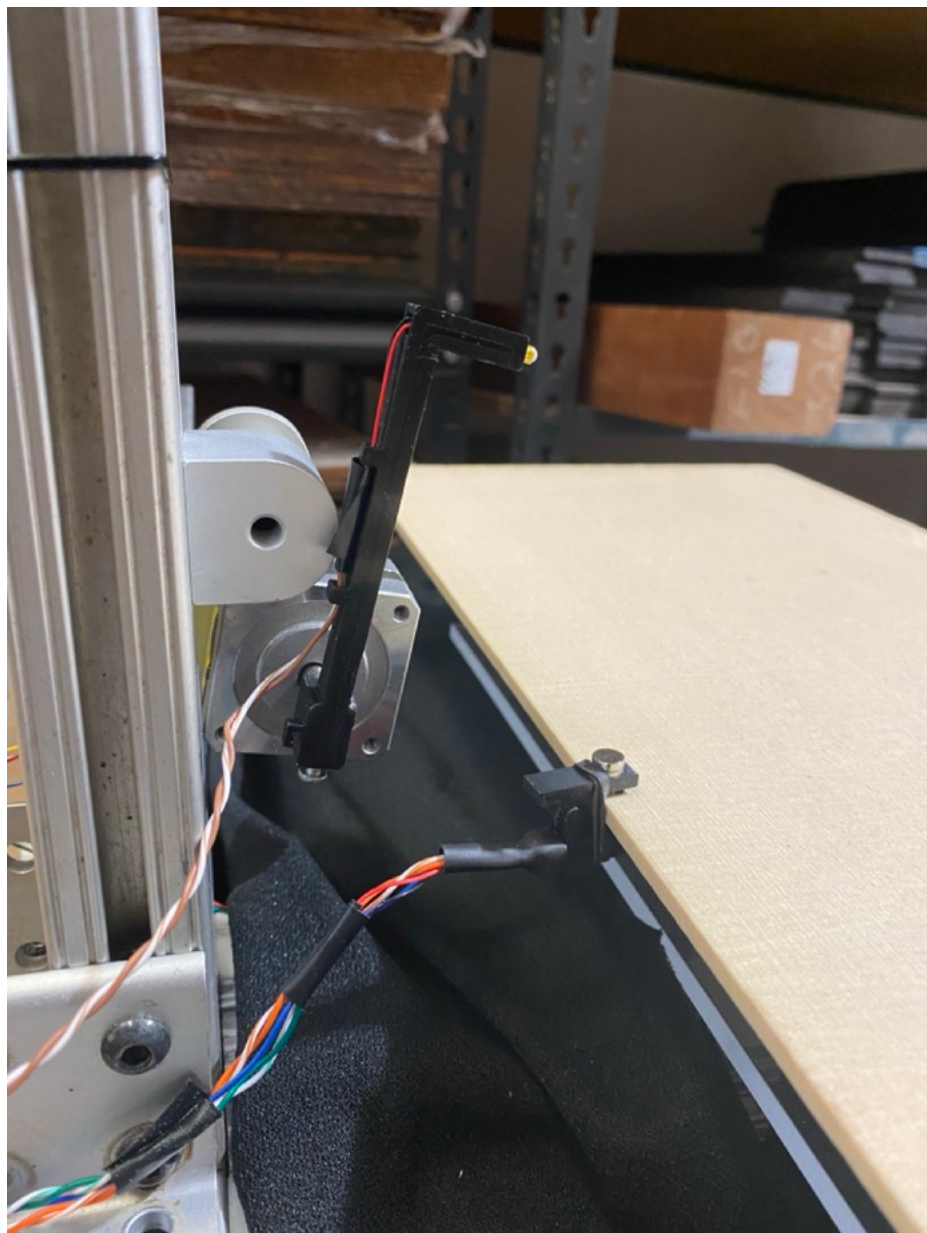


Figure 2.20: Impact hammer and clip-on vibration sensor.

Vibration Response To measure the resulting vibrations in the board once struck, another Thorlabs PK4DLP1 piezo is used. This sensor is housed in a lightweight 3D printed clip and mounted to the board near the impact location, as shown in Fig. 2.20. A piezo sensor was chosen instead of a microphone because it is much more resistant to external noise. Because the impact signal is recorded, it can be deconvolved from the resulting vibrations, making subsequent measurements

comparable.

Wood Mounting The wood board is rested on top of four foam triangles. The board is mounted at the four points where the nodes of the first longitudinal and transverse mode shapes meet, at roughly $0.224L$ and $0.224W$ from each corner [100]. The foam wedges are mounted on thin wood dowels and are able to slide. A rotatable 3D printed part in the center holds the rods together. This mounting was designed to easily adjust the foam mounts for different size boards. The wedges are then mounted on a piece of laser cut acrylic which is connected to the load cell. The mounting hardware can be seen in Figs. 2.17 and 2.21



Figure 2.21: Mounting hardware with a board on top.

Young's Modulus The longitudinal and transverse Young's modulii are calculated using the Impulse Excitation Technique (IET) [100]. If the first flexural frequency, mass, and geometric dimensions are known, the Young's modulus of a thin rectangular object can be predicted using the following equations:

$$E = 0.9465 \left(\frac{m f_f^2}{W} \right) \left(\frac{L^3}{t^3} \right) T, \quad (2.2)$$

$$T = 1 + 6.585 \left(\frac{t}{T} \right)^2, \quad (2.3)$$

where E is the Young's modulus, m is the mass, f_f is the flexural frequency, W is the width, L is the length, t is the thickness, and T is a correction factor.

The first flexural frequency for both the longitudinal and transverse directions are found by taking the first two significant peaks from a Fourier transform of the vibration response measurement, assuming the lowest significant peak corresponds to the longitudinal direction. An example of this measurement is shown in Fig. 2.22. These frequencies are then used to calculate the longitudinal (E_l) and transverse (E_t) Young's modulii.

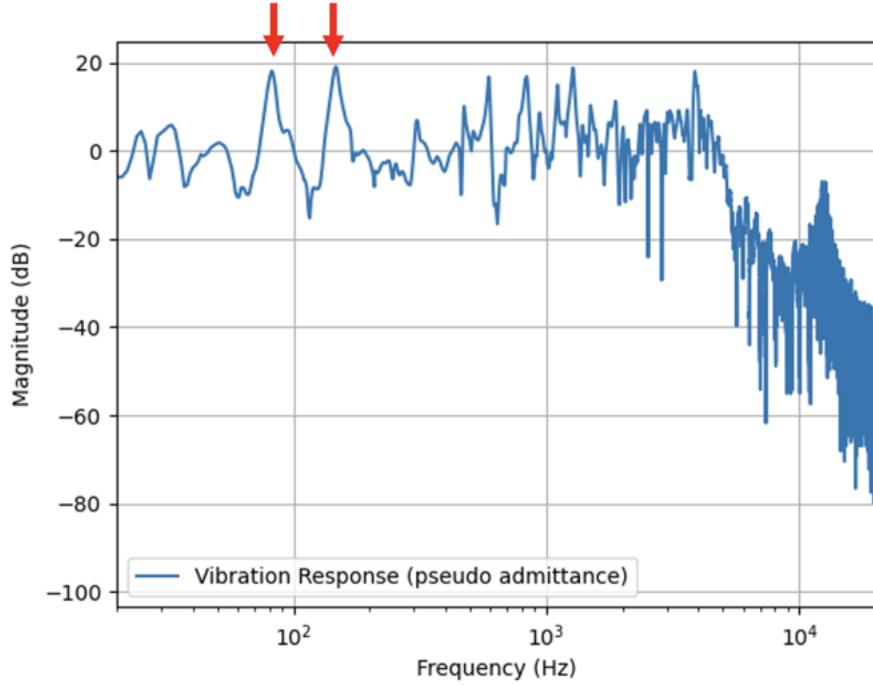


Figure 2.22: Measurement to pick the longitudinal (first arrow) and transverse (right arrow) flexural frequencies.

Derived Parameters The density is calculated as $\rho = \frac{LWt}{m}$ and the radiation coefficient for each of the longitudinal (R_l) and transverse (R_t) directions is calculated as:

$$R_l = \sqrt{\frac{E_l}{\rho^3}}, \quad (2.4)$$

$$R_t = \sqrt{\frac{E_t}{\rho^3}}. \quad (2.5)$$

$$(2.6)$$

Equalization The energy in three bands is analyzed to gather a general idea of the low, middle, and high-frequency balance in the wood. The three bands were chosen as 40-165 Hz (low), 165-800 Hz (middle), and 800-5000 Hz (high). The bands were formed using 2nd-order Butterworth band-pass filters. The signal energy, ε_x in each band is calculated over one second at a sample rate of 44 100 samples/second as,

$$\varepsilon_x = \sum_{n=0}^{N-1} |x_n|^2, \quad (2.7)$$

where x_n is the input signal, and $N = 44\ 100$ in this case. An example measurement can be seen in Fig. 2.23. The three frequency band energy values are shown in dB with horizontal green lines. While the general equalization of the completed instrument will be vastly different from the raw top board, this information may be useful as luthiers learn correlations between properties of raw boards and completed instruments.

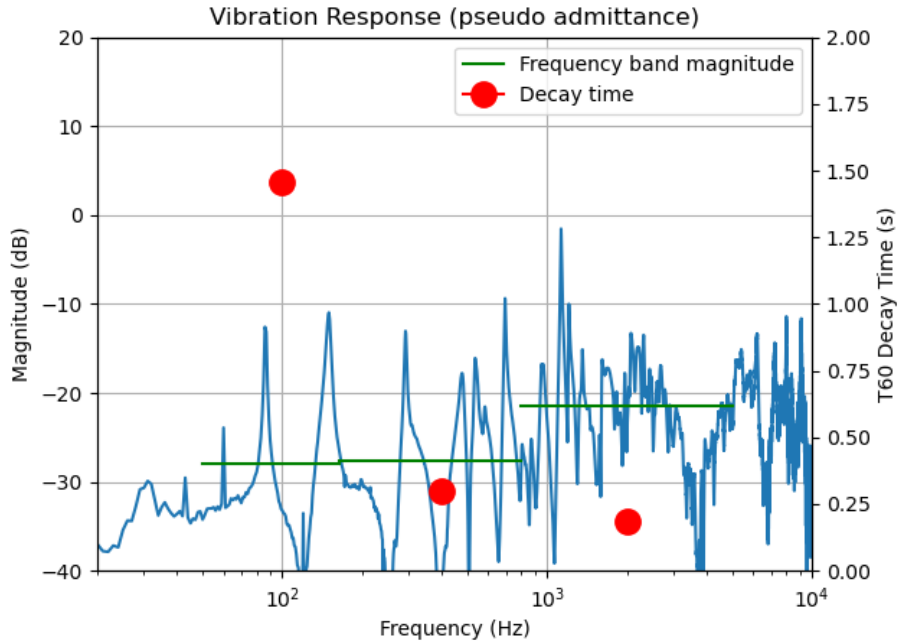


Figure 2.23: Example wood board measurement showing equalization and decay.

Sustain It may be useful to have an idea of the sustain or decay of each frequency range of the board. The same frequency bands as the equalization calculations are used for decay time calculations for the low, middle, and high-frequency ranges. The decay time in each band was found by taking the absolute value of the Hilbert transform of the signal and fitting a line to the result using least squares. The decay time is displayed as the T60 because it is easily understood by a broader range of people than the damping ratio. Additionally, since these measurements are for a specific frequency band of the signal, it makes more sense to talk about the general decay time than, say, the damping ratio. Fig. 2.23 shows the T60 decay times of the three bands with red circles for an example measurement.

Ideally, each mode's amplitude and decay-time or damping ratio would be found, but that is left for a future study. Further methods along this line of work are discussed in Chapters 3 and 5.

2.3.4.2 Wood Measurement Examples

To show some of the measured data and uses for this type of wood measurements, Figs. 2.24|2.27 show transverse and longitudinal stiffness (Young's modulus) as well as radiation coefficient measurements for various wood boards. The stiffness or radiation coefficient is plotted against the density of each board. The types of boards demonstrated here are Adirondack (red) spruce, old-growth Adirondack spruce, figured German spruce, Figured Sitka spruce, Swiss spruce, redwood, and sinker redwood reclaimed from sunken logs.

Viewing tonewood measurements in this way shows the large variance in material parameters among different species and even within the same species. In general, species will cluster together, but there is a significant variation and overlap between species. The spruce examples can be clearly distinguished from the redwood examples, which have significantly lower stiffness values at similar densities. The well-known relationship of the stiffness increasing with increasing density can be observed.

One significant outlier is the Sinker redwood board with a density of around 300 kg m^{-3} , which has exceptionally low stiffness values. The author noted the extreme flexibility of this board when measuring it, which was confirmed by the measurements. If a board such as this was used for an instrument, it would likely lead to structural failure.

From the small subset of boards measured, Sitka spruce was generally the stiffest, while the European spruce boards had the highest radiation coefficients. This is only a small subset of measurements, but knowing the general ranges for different woods can be helpful for an instrument builder when they are picking out woods with specific purposes, which could include consistency or looking for a board at the extremes to achieve a particular sound.

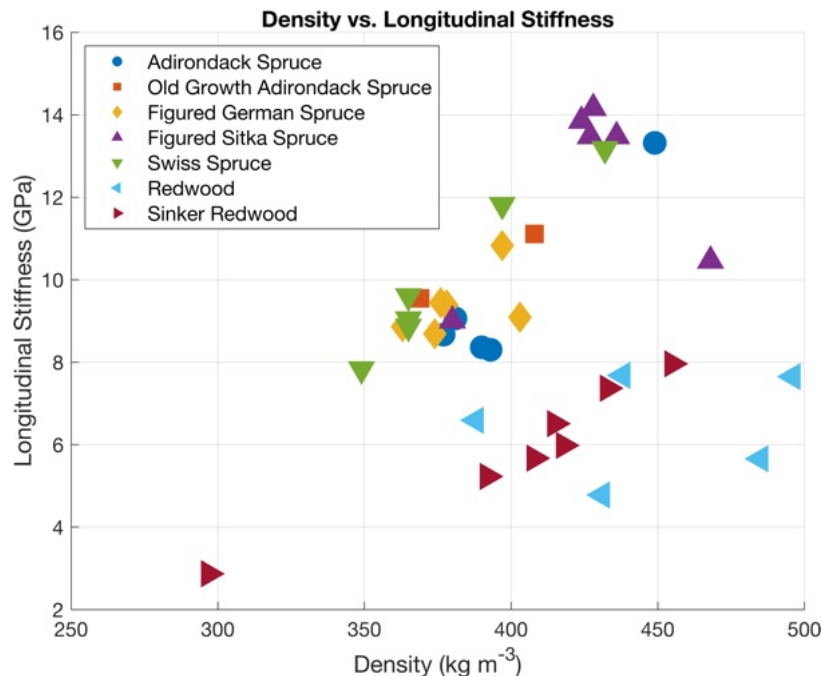


Figure 2.24: Longitudinal stiffness plots for various tonewood boards.

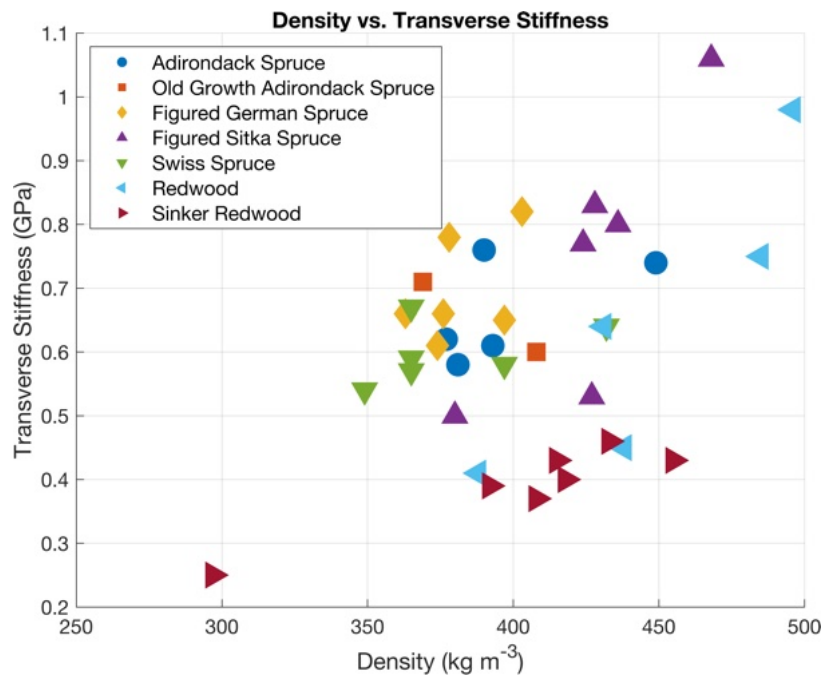


Figure 2.25: Transverse stiffness plots for various tonewood boards.

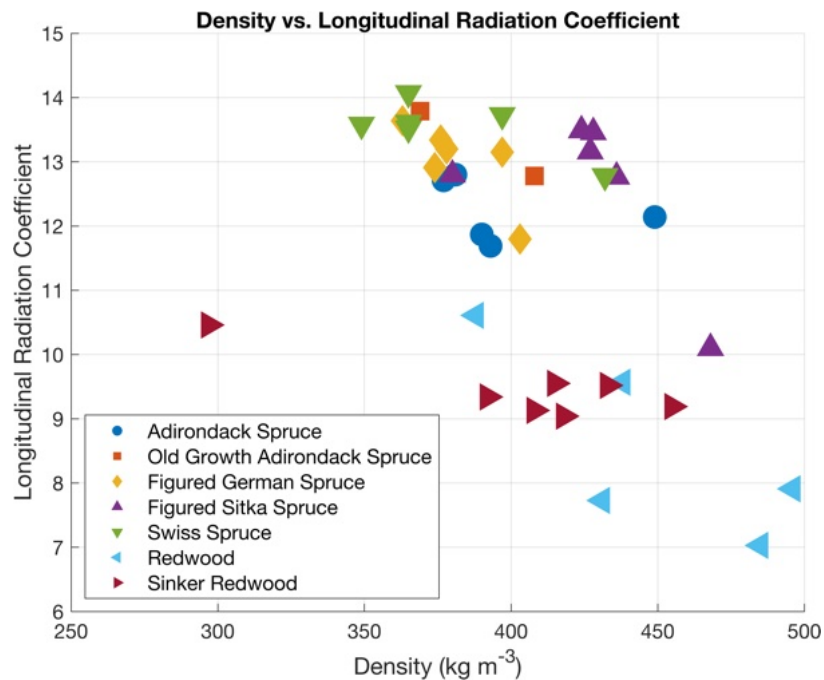


Figure 2.26: Longitudinal radiation coefficient plots for various tonewood boards.

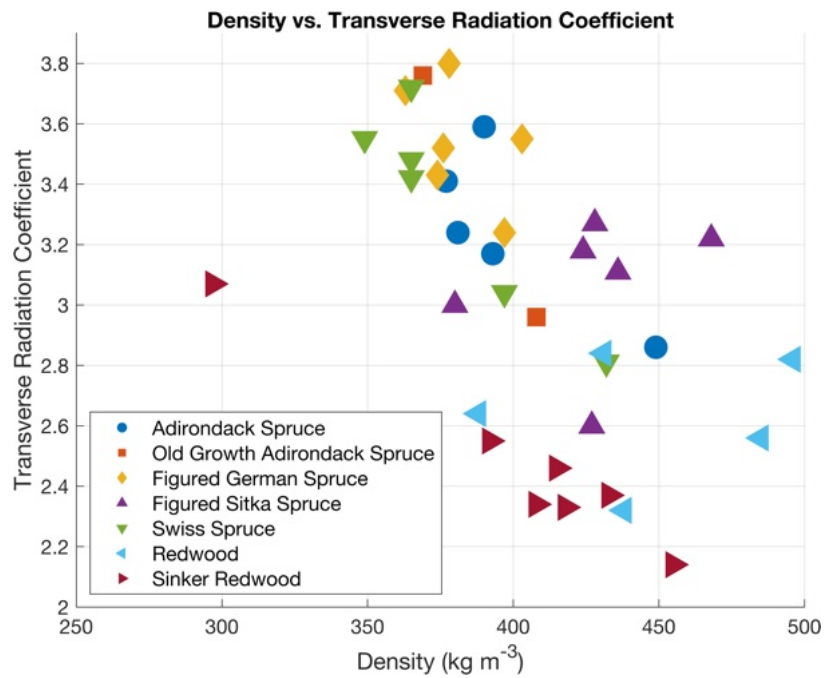


Figure 2.27: Transverse radiation coefficient plots for various tonewood boards.

Chapter 3

Modal and Material Parameter Extraction

Once measurements are taken, generally, some parameter estimations will need to be done to learn more about the measurements. When dealing with vibration measurements, it is common to extract the mode frequencies, damping, and amplitudes. Many methods exist to extract these parameters, and they can work well with high-quality data and supervision from the researcher. However, they do not always perform well when used naively, which would be needed if distributed to instrument makers. This chapter presents a comparison of four common modal extraction methods, demonstrating that they do not work as desired when applied naively to generic data, showing that work needs to be done on more reliable methods.

In Sec. 2.3.4, a device to measure wood material parameters was presented. However, this device does not measure all orthotropic material parameters. This chapter presents an optimization-based method to better approximate the material parameters of an orthotropic wood board.

3.1 A Comparison of Modal Parameter Extraction Methods when Applied to Measurements of Stringed Instruments [95]

Modal testing is a commonly used method to measure the transfer function or frequency response function of musical instruments or their components. Various excitation and measurement tools are used, and the recorded signals are analyzed to estimate the object's modal frequencies, damping ratios, and mode shapes. These modal parameters are used to compare musical instruments, study changes to their geometry and materials, create synthesis models, and verify finite element and other simulation models. An object is typically excited with an impact hammer or shaker, while the resulting vibrations are measured with a microphone, accelerometer, or laser Doppler vibrometer.

However, musical instrument builders don't typically have access to expensive measurement equipment, so more ad-hoc methods may be used. Multiple methods exist to extract modal parameters from the measured transfer function, each with its strengths and weaknesses. This study compares commonly used modal extraction methods when applied to measurements of stringed instruments made with a broad spectrum of excitation and measurement sensors. The methods are evaluated based on generated modal data and then tested with measurements of musical instruments and other objects.

3.1.1 Introduction

When studying the acoustics and sound of musical instruments, it is useful to take vibrational and acoustic measurements. For a struck, plucked, or bowed instrument, such as a marimba bar, guitar, or violin, one can assume the vibrations are small, and the response stays in the linear region. Generally, the modal frequencies, damping, and amplitudes or mode shapes of the structure are of interest. To extract these modal parameters, various algorithms for *mode* or *modal fitting* can be performed [4, 14, 15, 98, 27].

When performing modal fitting on measurements, care can be put into the measurement setup and post-processing, so the algorithms hopefully work reasonably well. Then, you must choose an algorithm and tune the parameters of the algorithm to extract the modal data properly. This is not a trivial task, and each method seems to have shortcomings that are hard to determine before testing each method and parameter space. More sophisticated algorithms, such as those using modal optimization, can be used, but even they typically require a reasonable initial estimate of the modal frequencies, damping, and amplitudes [66, 65].

Modal fitting becomes especially difficult when working with non-ideal measurement conditions or inexpensive sensors. Situations like this are common as instrument builders wish to extract modal data from the instruments they build but may not have access to expensive measurement equipment, a vibration and sound-isolated space, and the tools and software necessary for the mode fitting algorithms [93]. Instrument builders are becoming increasingly interested in acquiring this data, so one motivation for this study is to investigate the reliability, accuracy, and ease of use of some common modal fitting algorithms when applied to musical instruments and similar objects.

This section outlines the initial investigation into testing four modal fitting algorithms. Modal time-domain responses are generated from modal frequencies, damping, and amplitudes to test the algorithms against ground truth results. The generated data includes clean as well as noisy data. Additionally, modal measurements were made with ten guitars, ten other instruments, ten everyday objects, and twenty boards of guitar top wood. The algorithms are briefly described and evaluated on various metrics when applied to the generated and measured vibration data.

Section 3.1.2 outlines the generated and modal data. Section 3.1.3 briefly introduces the four tested algorithms. Section 3.1.4 describes the evaluation criteria used and presents results from the

mode fitting and evaluations. Section 3.1.5 discusses the evaluation, shortcomings, and areas for future study.

3.1.2 Data

To evaluate the algorithms, vibration responses are needed. The vibration response is assumed to be linear, having the response of a set of M damped simple harmonic oscillators. The impulse response is then:

$$h(t) = \sum_{m=1}^M \gamma_m e^{2\pi f_m t(i - \zeta_m)}, \quad (3.1)$$

where γ_m , f_m , and ζ_m are the amplitude, natural frequency, and damping ratios of modes $m = 1, 2, \dots, M$, respectively [14, 4].

The measurements and generated impulse response data are available at <https://ccrma.stanford.edu/~mrau/FA2023/>. Additional information about the instruments and objects, as well as photos, are provided.

3.1.2.1 Generated Data

To evaluate each algorithm, the true values of the mode frequencies, damping ratios, and amplitudes need to be known beforehand, which is not possible with measurements. Impulse responses were generated to be used as synthetic measurements. Each impulse response was formed using (3.1), and is of length 1 second at a sampling rate of 48 000 samples/second.

Impulse responses were generated with $M = [1, 2, 3, \dots, 50]$ modes with 100 examples generated for each. The mode frequencies were chosen randomly between 300 to 10 000 Hz and logarithmically distributed. Damping ratios were randomly chosen between 0.001 and 0.1. Each impulse response had two sets of amplitudes, one with positive-real values, simulating single input/output measurement locations, and one with complex values, simulating different input and output measurement locations [113]. The real and complex parts of each amplitude value were randomly chosen to be between 0.0001 and 1.

To simulate non-ideal measurements, the generated impulse responses were augmented in three different ways. In the first case, white noise having an amplitude of 0.01 was added. In the second case, AC hum was simulated by adding 60, 120, and 180 Hz components at amplitudes of 0.1, 0.01, and 0.001. In the third case, the signals were clipped by enforcing $-0.5 < h < 0.5$.

This resulted in a total of 45 000 simulated impulse responses with known mode frequencies, damping ratios, and amplitudes.

3.1.2.2 Measurements

Ultimately, to test the effectiveness of the algorithms, they need to be evaluated on physical measurements. Four categories of measurements were chosen:

- 10 guitars — 1890s parlour, four dreadnoughts, orchestra model, 00-style, two 000-style, and one classical guitar.
- 10 other instruments — five violins, viola, two cellos, double bass, and one mandolin.
- 10 everyday objects — mug, espresso cup, water pitcher, thermos, frothing pitcher, doorbell, hole saw, coffee tamper, milk pitcher, and a bowl.
- 20 wood top plates for guitars — four German spruce, four Italian spruce, four Sitka spruce, four redwood, and four sinker redwood.

The guitars, other instruments, and everyday objects were measured with lab-quality equipment as well as custom-built low-cost equipment. All measurements were taken with the impact hammer method [14]. The lab equipment consisted of a force hammer for the impact, a laser Doppler vibrometer (LDV), an accelerometer, and a calibrated microphone for the receivers. The low-cost equipment consisted of a 3D printed piezo impact hammer, piezo accelerometer, and inexpensive measurement microphone. The wood boards were measured with a custom-built tonewood measurement device [88].

Five measurements were taken with each object and sensor configuration, resulting in 850 measurements.

3.1.3 Mode Fitting Algorithms

Four modal fitting algorithms are tested. Only brief explanations of the methods are provided, and the reader is directed to the relevant citations for more details on each algorithm. Each algorithm was run in Matlab 2022b on a 2023 Macbook Pro [118].

1. Peak-Picking (pp) - In the frequency domain, significant local peaks are assumed to correspond to a single mode. Each mode is assumed to be a simple harmonic oscillator, and the damping and amplitudes are solved by setting up and solving a system of equations for each mode [117, 14].
2. Least-Squares Complex Exponential (lsce) - The impulse response is compared to a matrix of complex damped sinusoids formed using Prony's method to find the roots that give the mode frequencies and damping. The mode amplitudes are found using least-squares to solve the system of equations corresponding to the basis sinusoids, mode amplitudes, and initial impulse response [117, 5, 14].
3. Least-squares rational function (lsrf) - The transfer function coefficient constraints are expressed in terms of orthonormal rational basis functions on the unit circle, and the mode frequencies, gains, and amplitudes are determined using an iterative scheme [76].

4. Hankel Impulse Response (Hankel) - a Hankel matrix of time-domain impulse response samples is created, and the eigenstructure is analyzed to determine the mode frequencies and damping. The mode amplitudes are found using least-squares to solve the system of equations corresponding to the basis sinusoids, mode amplitudes, and initial impulse response [89]. This algorithm is described in detail in Appendix A

Multiple other mode fitting algorithms exist, but these four were chosen as the first three are reasonably common methods and are implemented in the Matlab Vibration Analysis Toolbox [118], and the author has generally had good experiences with the fourth. All algorithms are tested on 1 second of vibration response recorded at 48 000 samples/second. While better results could be obtained by changing the sample rate, processing the raw data in various ways, and adjusting algorithm parameters, that was not the objective of the study, and each algorithm is evaluated on its performance when implemented in a naive manner.

3.1.4 Evaluation

The generated modal data has a ground truth, so the modal fitting can be evaluated based on the difference between the fit and ground truth. This is not true with the measured modal data, so a qualitative evaluation is provided instead.

3.1.4.1 Evaluation Criteria

The modal fitting of the generated impulse responses was evaluated on six different criteria.

1. The time taken for the modal fitting to run in MATLAB on a 2023 Macbook Pro.
2. The number of Modes fit by the algorithm compared against the true number of modes.
3. Mean absolute error in Decibels of the frequency response when comparing the generated and fit frequency response functions.
4. Mean absolute error between the generated and fit mode frequencies.
5. Mean absolute error between the generated and fit mode damping ratios.
6. Mean absolute error between the generated and fit mode amplitudes.

3.1.4.2 Results

Generated Data Figures 3.1 to 3.6 show the modal fitting evaluations for ten measurements at each of the $M = [1, 2, 3, \dots, 50]$ mode cases. Only the real amplitude with no added noise, AC hum, or clipping is shown for brevity. However, in general, the modal fitting is worse when additional noise,

AC hum, or clipping is added. The graphs of the other cases can be found at <https://ccrma.stanford.edu/~mrau/FA2023/>.

All algorithms are quite fast, with the exception of lsrf. Only pp received a speedup when a lower number of modes was fit. Both the pp and Hankel methods fit a reasonably close number of modes to the true value and underfit the number of modes at higher numbers, while the lsce and lsrf generally fit the same number of modes regardless of the true number of modes. Ideally, the algorithm would fit the correct number of modes, so pp and the Hankel method seem better in this case.

When observing the frequency response error, each algorithm does reasonably well, but the lsrf seems to do better in general. At low numbers of modes, the lsrf appears to fit the mode frequencies but gets worse with a higher number of modes. The other algorithms are all roughly the same, with around 1 Hz of error in the found modes.

The lsce and lsrf appear to fit the damping ratios better than pp and the Hankel method. The Hankel method appears to fit the amplitudes best at low mode numbers but gets worse when more modes are added.

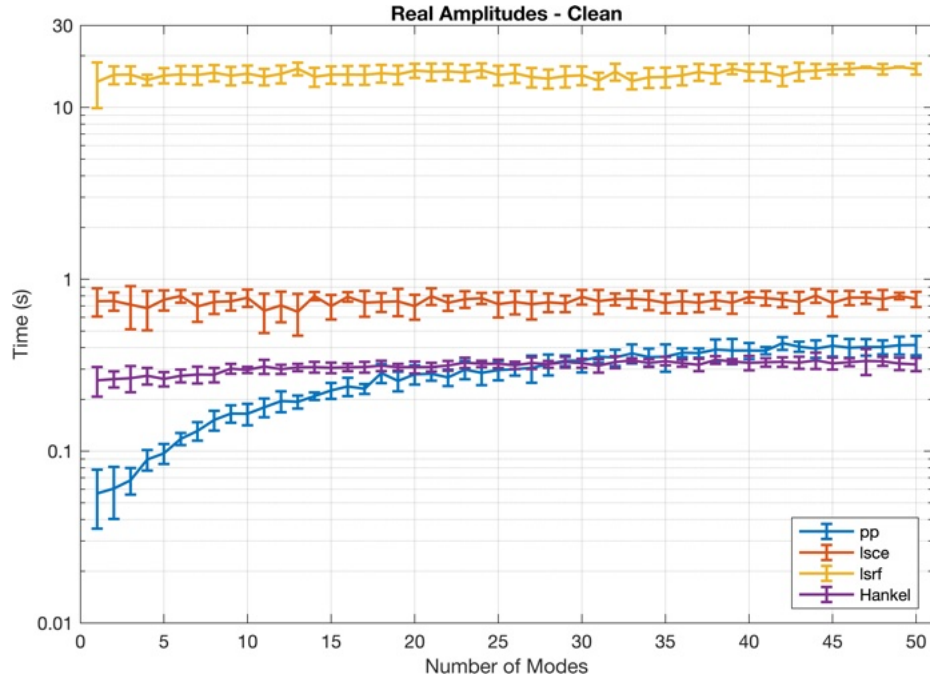


Figure 3.1: Generated fitting time.

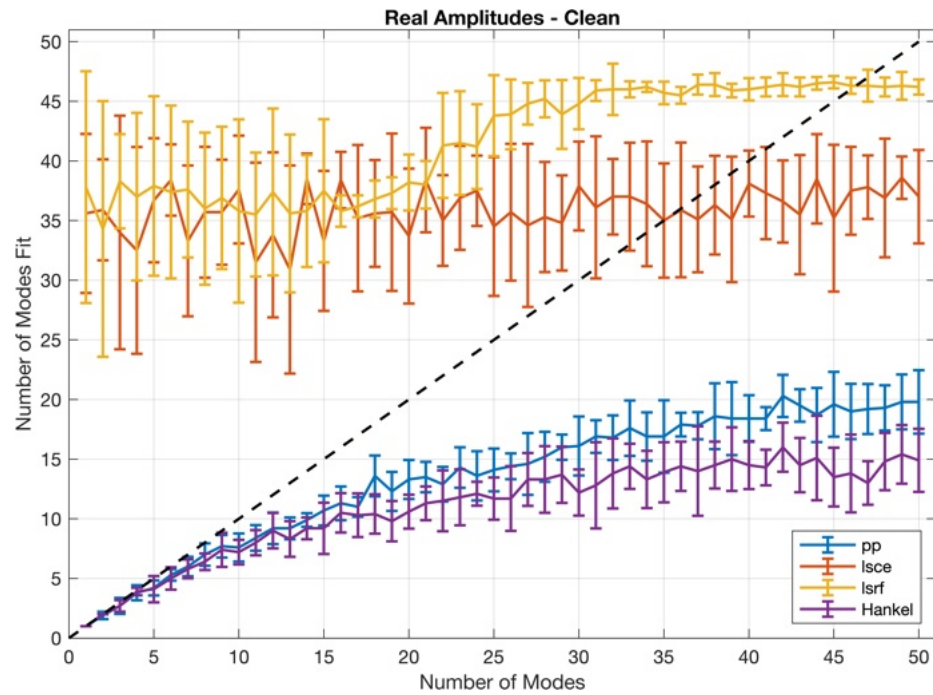


Figure 3.2: Generated number of modes fit.

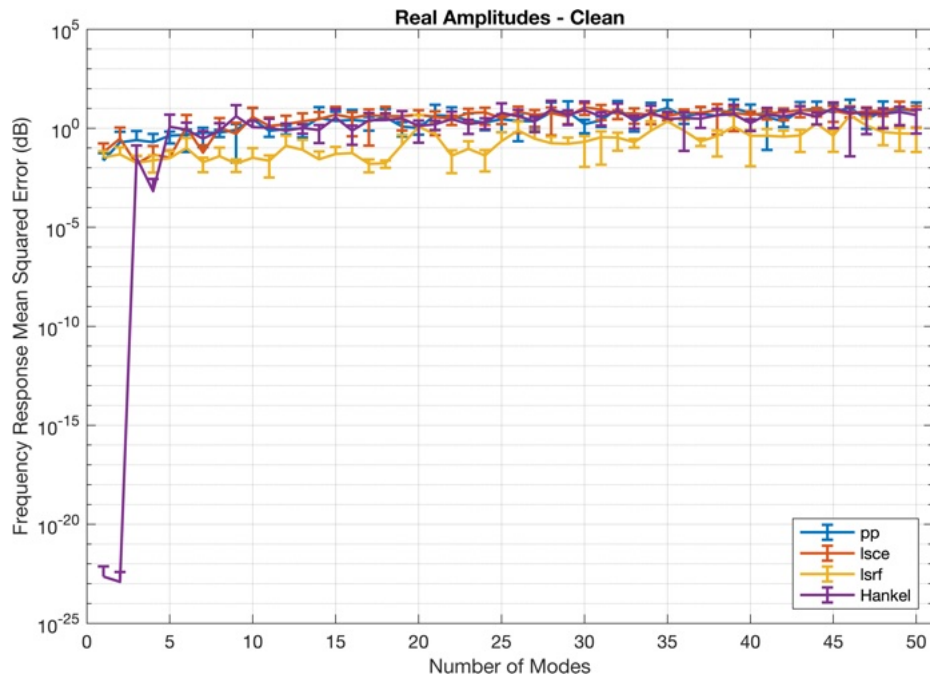


Figure 3.3: Generated fitting frequency response error.

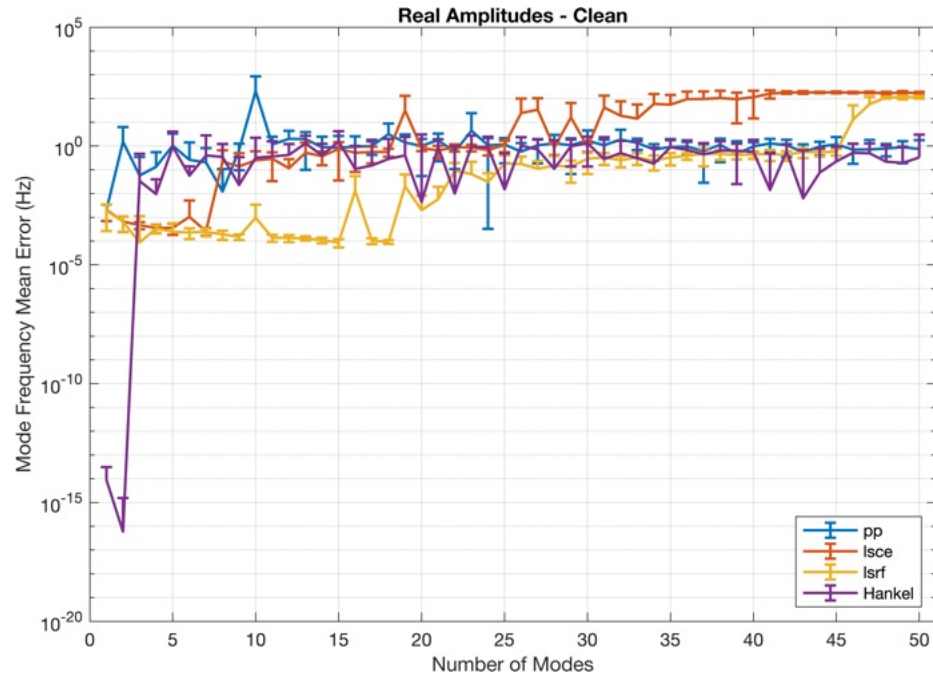


Figure 3.4: Generated fitting mode frequency error.

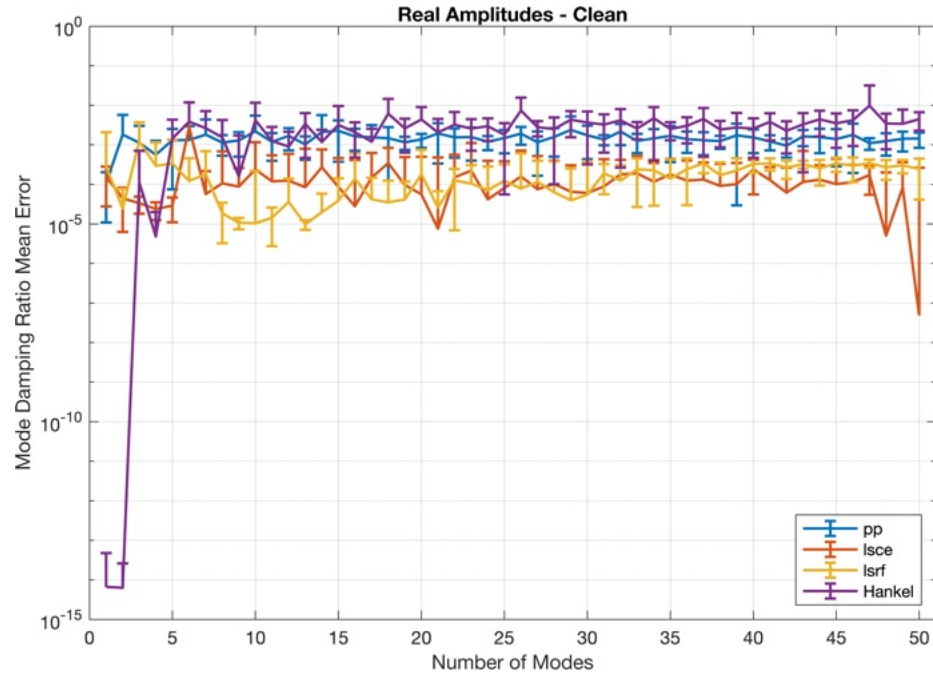


Figure 3.5: Generated fitting mode damping ratio error.

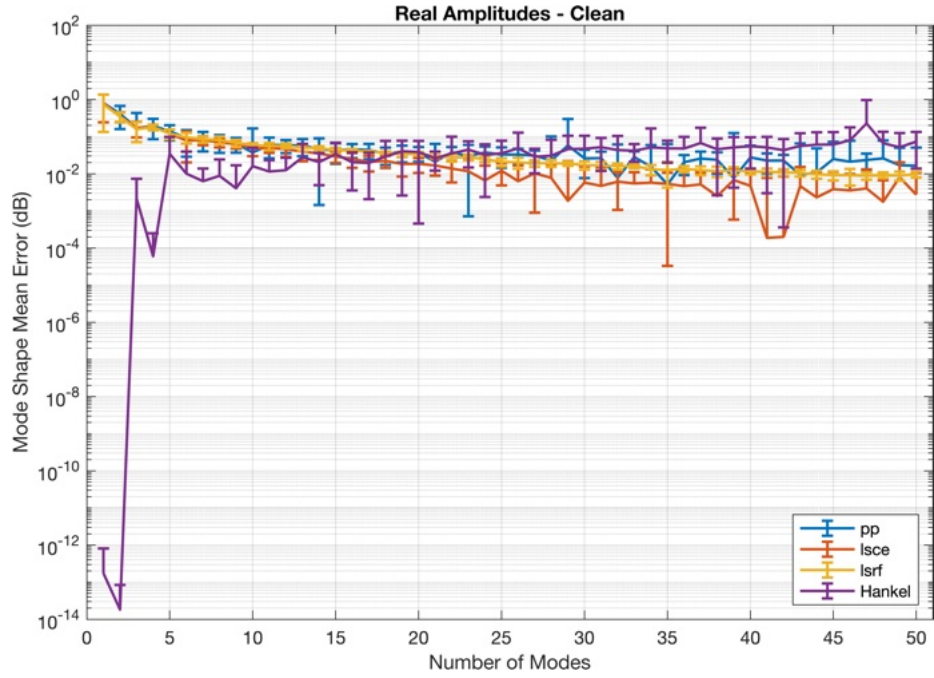


Figure 3.6: Generated fitting mode amplitude error.

Measurements While no concrete evaluation can be performed on the measurements, visual observations can be made when comparing the measured frequency response function to that of the modal fit. Figures 3.7 through 3.11 show admittance measurements of a guitar, upright bass, cello, mug, and wood board. With the mug having fewer modes with low damping ratios, all four mode fitting algorithms do a reasonable job. However, for each of the instrument and wood board examples, none of the algorithms result in what would be considered a good fit. Some are reasonable in certain frequency ranges, but none are perfect. It also appears that no single algorithm works well in each case, with some failing wildly for some instruments and working well for others. In general, it seems that the peak-picking and Hankel methods work the best, but neither is perfect in this naive implementation.

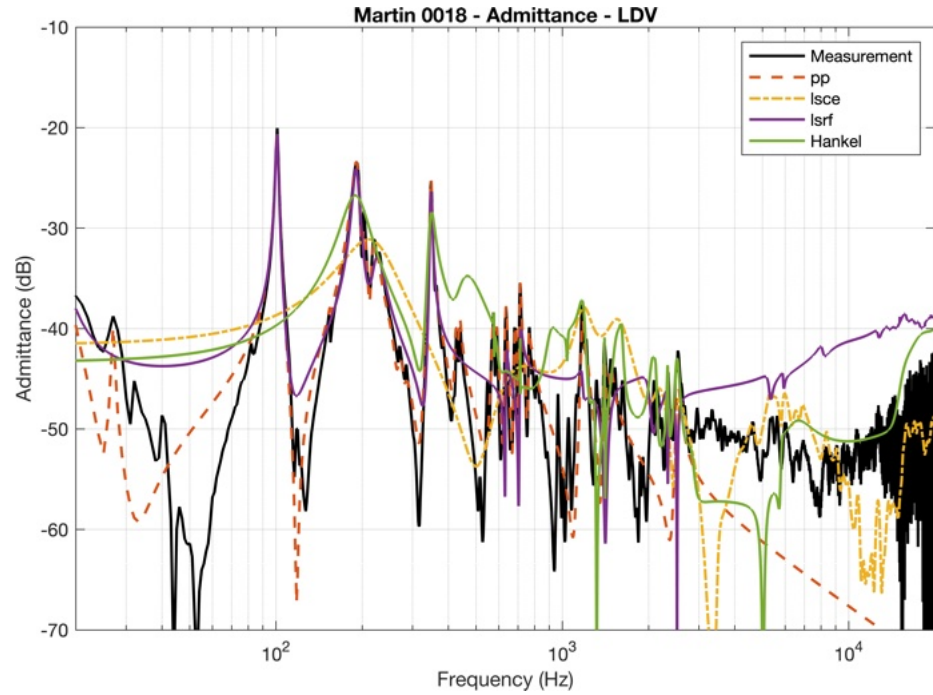


Figure 3.7: Guitar admittance.

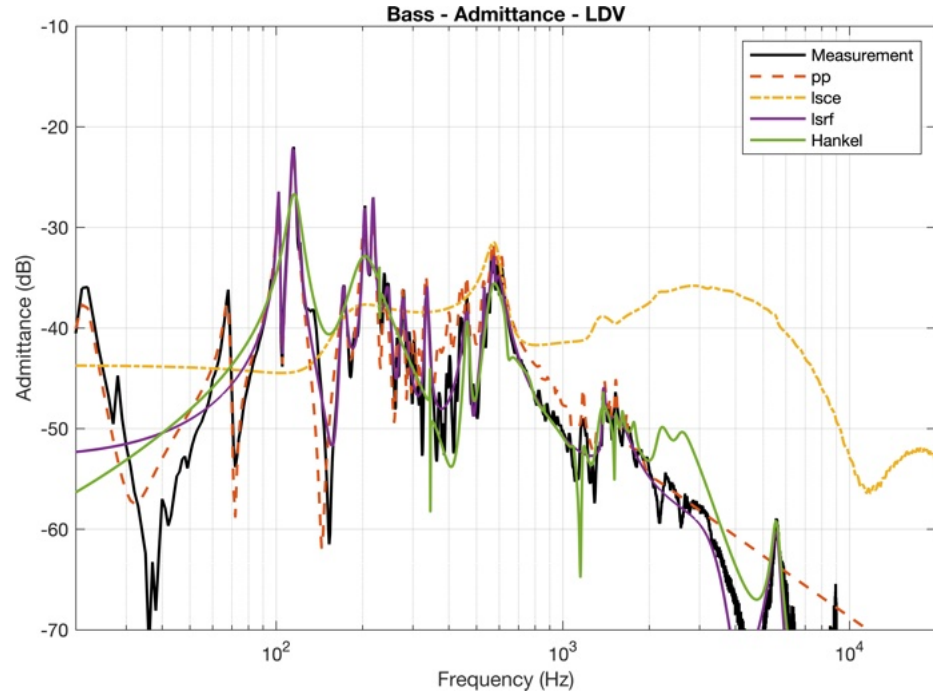


Figure 3.8: Bass admittance.

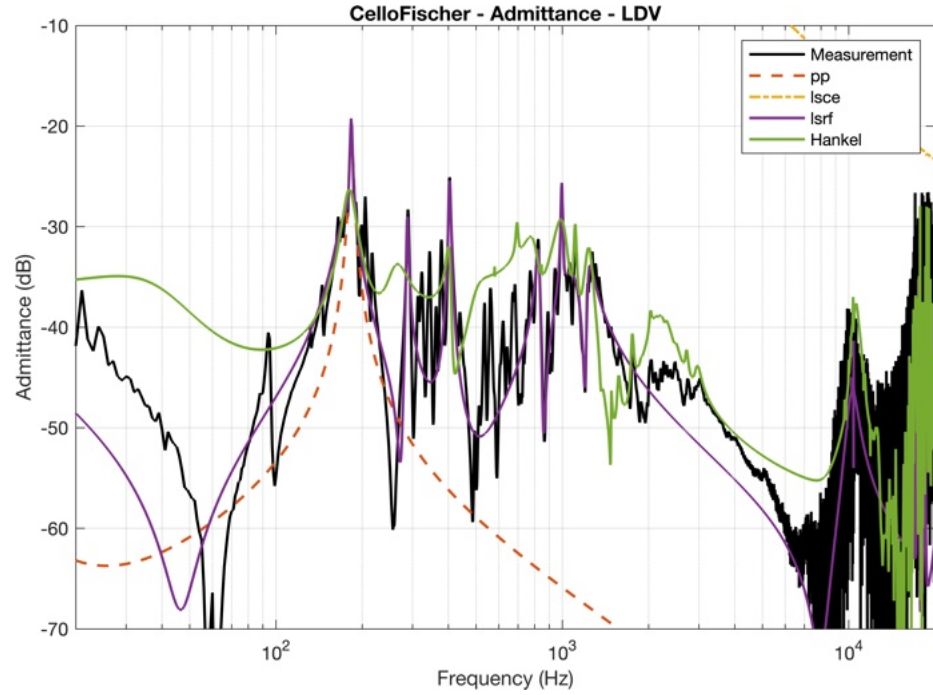


Figure 3.9: Cello admittance.

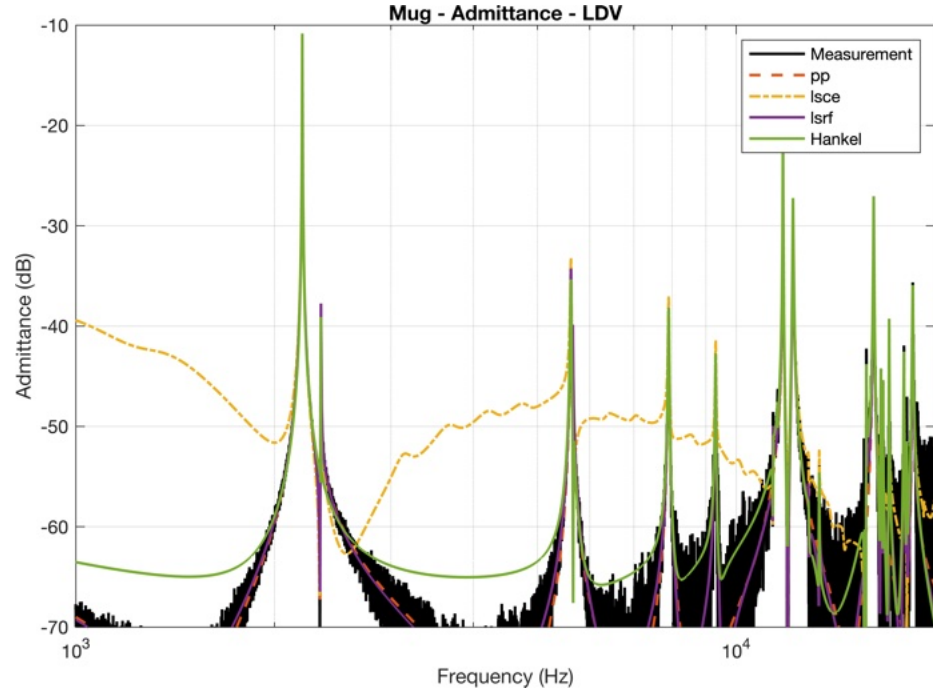


Figure 3.10: Mug admittance.

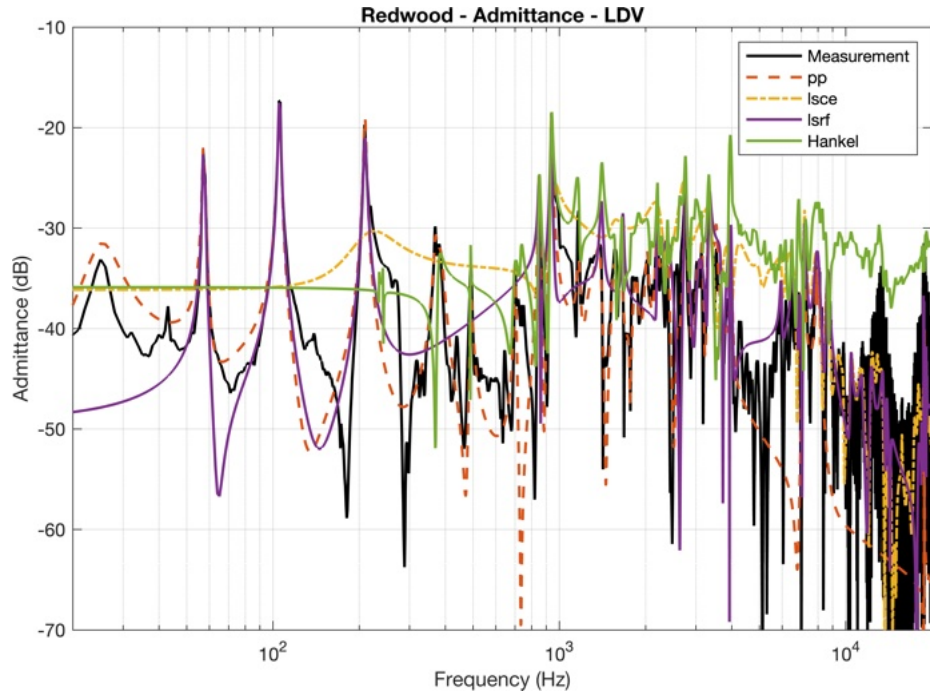


Figure 3.11: Redwood board admittance.

3.1.5 Discussion and Conclusions

This study is not, and was not meant to be, a conclusive investigation of all mode fitting algorithms, but rather serves as a beginning and framework for future studies. However, some conclusions and directions for future investigation can be drawn.

Generated data provides the only true way to evaluate the data, but the modal algorithms tend to perform better on generated data than they do on the measured data. This suggests that physical measurements should always be used as a final check when performing modal fitting.

None of the tested methods perform well enough to be used and trusted in a non-ideal and unsupervised setting, such as when used in an instrument builder's workshop. As shown in Chapters 4 and 5, high-quality modal fits can be achieved with the Hankel Impulse Response method, but it requires a significant amount of hand tuning and fitting based on various frequency bands. More work needs to be done to test different algorithms, and methods to optimize them in a simple and repeatable manner, and verify their reliability [65, 66, 105, 34].

One avenue for future study the author hopes to explore is a machine-learning approach to modal fitting. The generated and measured modal data collected for this study could be used as a training/test set for this machine learning approach. Hopefully, machine learning could potentially be leveraged to provide a lightweight, simple-to-use, and reliable mode fitting approach that can be

used by instrument builders and hobbyists.

3.1.6 Acknowledgments

I would like to thank Samuel Clarke, Daiki Nakajima, Joseph Malinowski, the Santa Cruz Guitar Company, Herbert Myers, and the Stanford Harry R. Lange Collection of Musical Instruments and Bows for graciously lending instruments for this study.

3.2 Wood Material Parameter Extraction and Optimization

The goal of this project is to gain a better understanding of the material parameters of wood used for guitar building. Wood is an orthotropic material, meaning that there are 12 distinct material parameters that differ between species, individual trees, and even the location of the cut of wood from a single tree. In order to accurately model wood, these material parameters need to be known. I propose a method where some of the material parameters are directly measured from a piece of wood and used in a finite element model (FEM), with the non-measured parameters being taken from textbook values. Modal analysis is performed and compared to a vibration measurement of the piece of wood. An optimization scheme is used to better approximate the material parameters by minimizing the difference between the measured and modeled vibration frequency response.

3.2.1 Introduction

It is relatively common to use finite element modeling to study the vibrational response of an instrument such as a guitar and how changes to the geometry can alter the sound. Most of these models use material parameters from textbooks such as the *Wood handbook: wood as an engineering material* [101]. While this yields a model that can be altered to study geometry changes, the model does not represent any physically plausible instrument since the material parameters of wood vary significantly between samples.

If trying to build instruments with the aid of finite element modeling, the material parameters of individual pieces of wood that will be used for the instruments need to be known. It is possible to non-destructively measure some of the parameters but not all of them.

Here, a finite element model is formed for specific pieces of wood (typically a rectangular board), and optimization of the material parameters is used to get a better estimate of the true material parameter values. Initial measurements of some of the material parameters are used in combination with textbook values as the initial design point. The optimization will minimize the difference between a measured vibration response and a modeled vibration response.

3.2.2 Wood Materials

Wood is an orthotropic material, meaning it has independent material parameters in each direction. The directions correspond to the radial, tangential, and longitudinal direction of the tree growth. There are 12 elastic constants which are comprised of 3 Young's modulii, E_x, E_y, E_z , 3 shear modulii, G_{yz}, G_{zx}, G_{xy} , and 6 Poisson's ratios, $\nu_{yz}, \nu_{zy}, \nu_{xy}, \nu_{yx}, \nu_{xz}, \nu_{zx}$. The stress (σ) to strain (ϵ) relationship takes the stiffness matrix form as

$$\begin{bmatrix} \sigma_{xx} \\ \sigma_{yy} \\ \sigma_{zz} \\ \sigma_{yz} \\ \sigma_{zx} \\ \sigma_{xy} \end{bmatrix} = \begin{bmatrix} \frac{1 - v_{yz}v_{zy}}{E_y E_z \Delta} & \frac{v_{yx} - v_{zx}v_{yz}}{E_y E_z \Delta} & \frac{v_{zx} - v_{yx}v_{zy}}{E_y E_z \Delta} & 0 & 0 & 0 \\ \frac{v_{xy} - v_{xz}v_{zy}}{E_z E_x \Delta} & \frac{11 - v_{zx}v_{xz}}{E_z E_x \Delta} & \frac{v_{zy} - v_{zx}v_{xy}}{E_z E_x \Delta} & 0 & 0 & 0 \\ \frac{v_{xz} - v_{xy}v_{yz}}{E_x E_y \Delta} & \frac{v_{yz} - v_{xz}v_{yx}}{E_x E_y \Delta} & \frac{1 - v_{xy}v_{yx}}{E_x E_y \Delta} & 0 & 0 & 0 \\ 0 & 0 & 0 & 2G_{yz} & 0 & 0 \\ 0 & 0 & 0 & 0 & 2G_{zx} & 0 \\ 0 & 0 & 0 & 0 & 0 & 2G_{xy} \end{bmatrix} \begin{bmatrix} \epsilon_{xx} \\ \epsilon_{yy} \\ \epsilon_{zz} \\ \epsilon_{yz} \\ \epsilon_{zx} \\ \epsilon_{xy} \end{bmatrix}. \quad (3.2)$$

An approximation can be made that the Young's modulii are not independent and follow the relationships:

$$\frac{v_{yz}}{E_y} = \frac{v_{zy}}{E_z}, \quad (3.3)$$

$$\frac{v_{zx}}{E_z} = \frac{v_{xz}}{E_x}, \quad (3.4)$$

$$\frac{v_{xy}}{E_x} = \frac{v_{yx}}{E_y}, \quad (3.5)$$

which reduces the problem to having 9 independent variables [26].

3.2.3 Measurements

For comparison to the FEM model, there needs to be vibration measurements of real wood boards. To excite vibrations in the boards, an impact hammer with a force sensor is used. This allows for the force of the impact to be recorded to normalize the measurements. The resulting vibrational velocity is measured with a laser Doppler vibrometer. Ideally, the board would be mounted in free-free conditions, but this is not possible, so two different mounting layouts are used. To isolate the first flexural vibration modes in the along and across-grain directions, the board is mounted on four small foam supports at the nodal lines. Similarly, to isolate the first torsional mode, the board is mounted on 5 foam supports at the nodal lines. These mountings will be referred to as the flexural and torsional mountings. Finite element simulations of the three vibrational modes of the board are shown in Figure 3.14. A measurement with the force hammer is shown in Figure 3.12.



Figure 3.12: Wood measurement.

From the vibration measurements, three notable modal frequencies are obtained. The first two prominent flexural mounting mode frequencies are related to the Young's modulii along and across the grain while the first prominent torsional mounting mode frequency is related to the Shear modulus relating the along and across grain directions. A Fourier transform of the vibrational velocity signal for each measurement can be used to find these prominent mode frequencies. The frequency

peaks are picked by taking the max value in a range and performing quadratic interpolation. The relevant frequency domain velocity plots with the chosen mode frequencies for a sample of Italian spruce are shown in Figure 3.13.

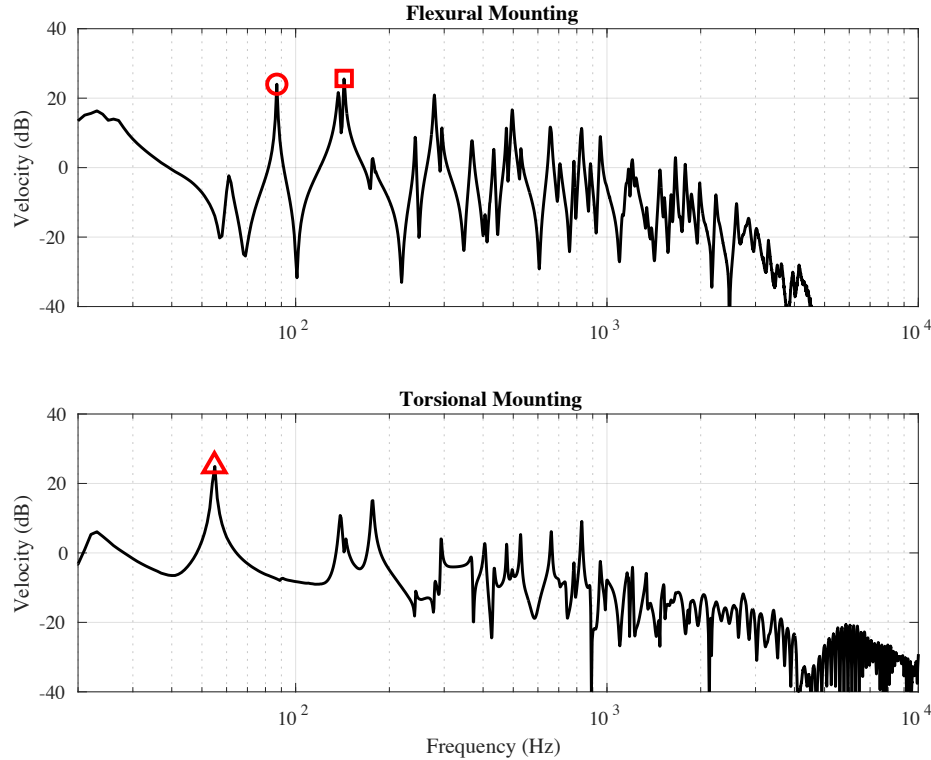


Figure 3.13: Flexural (top) and torsional (bottom) mounting velocity vibration. The circle, square, and triangle mark the first and second flexural mode frequencies and the first torsional mode frequency respectively.

Estimates of the Young's modulii along and across the wood's grain, E_y , and E_x , and the shear strain, G_{xy} , relating the along and across grain directions can be obtained using the impulse excitation technique [100]. For a rectangular bar, the impulse excitation technique approximates the Young's

modulus, E, and Shear modulus, G, as:

$$E = 0.9465 \left(\frac{mf_f^2}{W} \right) \left(\frac{L^3}{t^3} \right) T, \quad (3.6)$$

$$T = 1 + 6.585 \left(\frac{t}{L} \right)^2, \quad (3.7)$$

$$G = \left(\frac{4Lmf_t^2}{Wt} \right) R, \quad (3.8)$$

$$R = \left[\frac{1 + \left(\frac{W}{t} \right)^2}{4 - 2.521 \frac{L}{W} \left(1 - \frac{1.991}{e^{\pi \frac{W}{t}} + 1} \right)} \right] \left[1 + \frac{0.00851 W^2}{L^2} \right] - 0.060 \left(\frac{W}{L} \right)^{\frac{3}{2}} \left(\frac{W}{t} - 1 \right)^2, \quad (3.9)$$

where m is the mass, W is the width, L is the length, t is the thickness, f_f is the flexural frequency, f_t is the torsional frequency, and T and R are correction factors. The length, width, thickness, and mass of the board were measured with a measuring tape, calipers, and a digital scale.

3.2.4 Modeling

For the numerical modeling, a mesh first needs to be created from the geometric measurements of the wood board, and then modal analysis needs to be performed. Gmsh is used to create meshes of the wood boards [36]. An open-source finite element package, FEniCS, is used for the modal analysis [6, 106]. The finite element model is orthotropic and parameterized by a vector of the three Young's modulii, three independent Poisson ratios, and three shear modulii. Along with the mesh and density, this is sufficient information to perform modal analysis on the model. Quadratic elements are used with a relatively coarse element size since many solves will need to be done in the optimization process. Each solve takes about 0.5 s on a 2016 Macbook Pro. The first two flexural and first torsional mode shapes solved for in an example test board are shown in Figure 3.14.

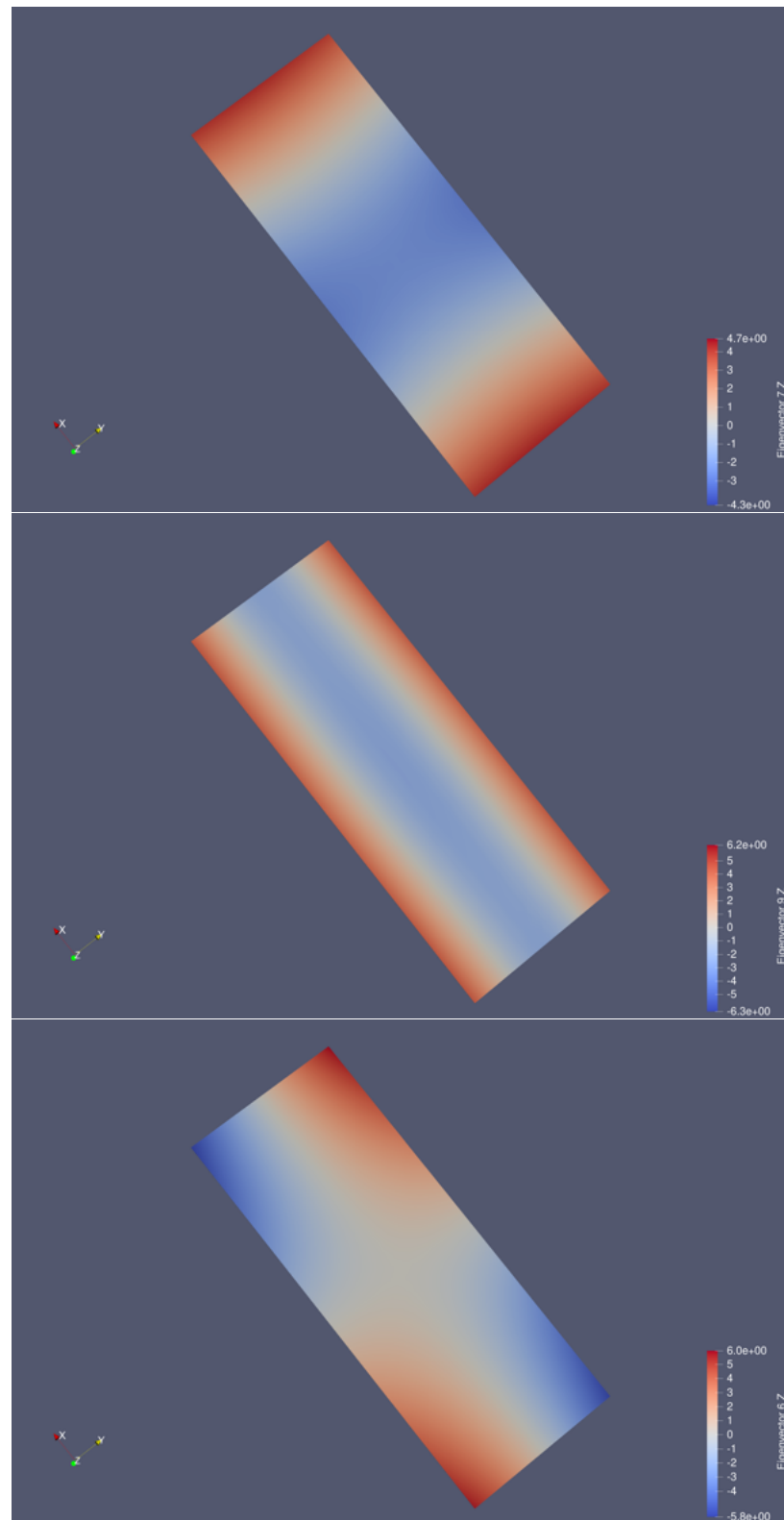


Figure 3.14: First flexural mode (top), second flexural mode (middle), and first torsional mode (bottom).

3.2.5 Optimization

An optimization problem is formulated to optimize the material parameters outlined in Section 3.2.2 to minimize the error between a measured and modeled vibration response of a specific wooden board. The mean squared error (MSE) between the measured and modeled vibrational frequencies of the first two flexural and first torsional mode frequencies are used as the function evaluation to be minimized. The optimization problem is thus:

$$\min_{E_x, E_y, E_z, v_{xy}, v_{xz}, v_{yz}, G_{yz}, G_{zx}, G_{xy}} g(f), \quad (3.10)$$

$$f = [f_{f1}^m, f_{f2}^m, f_{t1}^m, f_{f1}^s, f_{f2}^s, f_{t1}^s], \quad (3.11)$$

$$g(f) = \sqrt{\frac{1}{3} ((f_{f1}^m - f_{f1}^s)^2 + (f_{f2}^m - f_{f2}^s)^2 + (f_{t1}^m - f_{t1}^s)^2)}, \quad (3.12)$$

where f_{f1}^m , f_{f2}^m , and f_{t1}^m , are the measured flexural and torsional frequencies, and f_{f1}^s , f_{f2}^s , and f_{t1}^s , are the simulated flexural and torsional frequencies.

The initial guess parameters for E_y , E_x , and G_{xy} are obtained using the impulse excitation technique as described in Section 3.2.3, while the initial guess for the rest of the parameters are taken as textbook values [101].

For this optimization problem, there is no access to gradient information, so a gradient-free method must be used. I choose to use the Nelder-Mead method since it is gradient-free and should be able to make progress relatively quickly by adapting the simplex size [56]. The optimization was implemented in Python and used SciPy for the optimization algorithm [123], [125]. In theory, this problem could be treated as a constrained optimization problem since the material parameters cannot be negative, but in practice, I did not run into any issues, and the algorithm never approached non-physical design points, so I kept it as an unconstrained problem for simplicity.

3.2.6 Results and Discussion

As a test case for the optimization formulation, I used a board of Italian spruce. The board was 56.6 cm long, 21.8 cm wide, 5.0 mm thick, and had a mass of 160.5 g. The initial material parameter guess was derived from a combination of those calculated using the impulse excitation technique on a vibration measurement and textbook values for Englemann spruce [3.2.2]. I could not find textbook material parameters for Italian spruce, so Englemann spruce was used as a substitute, highlighting the need for a method like this to approximate wood material parameters from vibration measurements alone.

The initial material parameter guesses as well as the optimized material parameters are shown in Table 3.1.

The optimization was run for 200 iterations and took about 2 minutes to run. The mean squared

| | E_x (GPa) | E_y (GPa) | E_z (GPa) | ν_{xy} | ν_{xz} | ν_{yz} | G_{yz} (GPa) | G_{zx} (GPa) | G_{xy} (GPa) |
|---------------|----------------|----------------|----------------|------------|------------|------------|-------------------|-------------------|-------------------|
| Initial Guess | 12.1 | 0.747 | 0.714 | 0.422 | 0.462 | 0.530 | 0.120 | 1.45 | 0.737 |
| Optimized | 12.1 | 0.748 | 0.709 | 0.428 | 0.475 | 0.529 | 0.122 | 1.46 | 0.692 |

Table 3.1: Wood material parameters before and after optimization.

error between the measured and simulated mode frequencies is plotted against the evaluation iteration in Figure 3.15.

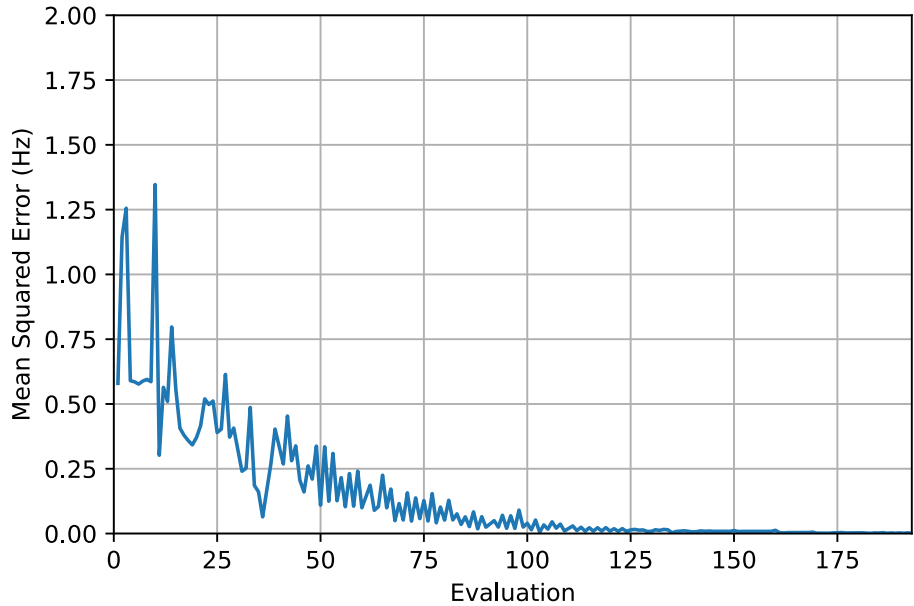


Figure 3.15: Mean squared error between the measured and simulated mode frequencies vs iteration number of the optimization.

This test case shows that the optimization methodology clearly works to get a better estimate of the wood material parameters to more closely match the measured and simulated mode frequencies of the three modes taken into account. While the initial guess was already pretty good, the optimization reduced the mean squared error to very close to zero. The MSE was reduced to 0.0009 Hz for this example, a very small error that is imperceptible when considering the pitch discrimination of humans. Noting the small error, fewer iterations could be used to save computation time.

Future work for this project includes testing with more wood boards to confirm that the methodology will generalize. Additionally, I would like to test more optimization algorithms and see if the number of function evaluations can be reduced since each one is computationally expensive.

Chapter 4

Electric-to-Acoustic Pickup Processing

For the past century, the development of the guitar and guitar-centric music has been intertwined with the development of amplification and effects processing. The effects and amplifier used with an electric guitar are as significant as the instrument itself, and the application for electronic processing of acoustic instruments has been of interest more recently. While much of the processing concerns effects such as reverb, distortion, and compression to alter the sound in musical ways, my research focuses on manipulating the sound to reproduce a “more acoustic” sound from instrument pickups.

When an acoustic string instrument is recorded in a studio, microphones are typically placed around the instrument to capture the radiated sound at various locations. This is often not possible during live performances due to feedback from the sound amplification system. The alternative approach is to use a contact pickup to amplify the instrument. Contact pickups significantly reduce the chance of feedback occurring, but they typically produce a less desirable sound.

Acoustic instrument contact sensors can be equalized, often in an attempt to make them sound more similar to the instrument’s acoustically radiated sound. Commercially available acoustic instrument equalizers are limited in use and require trial and error to achieve a desirable sound. If an instrument’s body is approximated as a linear and time-invariant system, a transfer function between various measurement locations can be defined, which will allow digital signal processing (DSP) techniques to force a signal captured at one location to sound more similar to a signal captured at a different location.

Such DSP equalization has been studied previously by Karjalainen et al. [54, 52, 53]. This work focused on the case of an acoustic guitar with an electret film pickup and aimed to find a transfer function, which was the spectral ratio of microphone and contact sensor transfer functions:

$$Q(\omega) = \frac{P(\omega)}{X(\omega)}, \quad (4.1)$$

where $Q(\omega)$ is an equalizer transfer function, $P(\omega)$ is the acoustic radiation transfer function measured with a microphone, and $X(\omega)$ is the transfer function through a contact sensor. They found transfer functions by first using an impact hammer to excite an impulse and second by playing musical information through both sensors and deconvolving the contact sensor signal from the microphone signal. They constructed filters based on both of these methods using FIR and IIR structures. It was concluded that the deconvolution method paired with an FIR filter of order 500 or higher with an additional digital resonator tuned to the mode of the guitar's top plate produced the most desirable sound.

A similar problem of interest is the processing of a less-resonant instrument to sound like a more resonant instrument, for example, making an electric guitar sound like an acoustic guitar. The equalization is relatively similar to the pickup-mic matching case and can be applied with an impulse-response method. However, less-resonant instruments will have a high bridge impedance, resulting in strings that decay for longer than highly-resonant instruments with a low bridge impedance. My recent work has addressed this problem by applying a time-varying filter fit to represent the continued string scattering as the string continually encounters the bridge. The method is described below and can be found in [89].

A signal processing method to impart the response of an acoustic string instrument to an electric instrument, which includes frequency-dependent string decay alterations, is proposed. This type of processing is relevant when trying to make a less resonant instrument, such as an electric guitar, sound similar to a more resonant instrument, such as an acoustic guitar. Unlike previous methods, which typically only perform equalization, our method includes detailed physics-based string damping changes by using a time-varying filter, which adds frequency-dependent exponential damping. Efficient digital filters are fit to bridge admittance measurements of an acoustic instrument and are used to create equalization filters as well as damping correction filters. The damping correction filters are designed to work in real-time as they are triggered by onset and pitch detection of the signal measured through an under-saddle pickup to determine the intensity of the damping. A test case is presented in which an electric guitar is processed to model a measured acoustic guitar.

4.1 Introduction

Acoustic string instruments are desirable for their characteristic sound radiation, but they are not always practical for live performance situations due to difficulties in accurately amplifying the sound and avoiding feedback. This led to the development of dedicated electric adaptions of the instrument, which radiate very little acoustic sound and rely on amplification in all instances. The electronic instruments are commonly built with heavier materials, such as solid blocks of dense wood, to reduce vibrations in comparison to the acoustic counterparts, which are typically built with thin pieces of wood. The material choices have a profound effect not just on the loudness and equalization of the

radiated sound but also on the length of time the strings will ring. These effects are readily apparent when comparing an acoustic guitar to a solid-body electric guitar. These sonic differences make each guitar suitable for certain instances and styles of music. However, it can be desirable to process the pickup signal of one instrument to make it sound more similar to a microphone signal of the same instrument or a completely different instrument altogether.

String instrument pickups have advantages over microphones in live-playing scenarios but often do not sound like an accurate representation of the acoustic instrument, so it would be desirable to have a pickup that sounds like a well-placed microphone. A method was developed by Karjalainen et al. to use simultaneous impulse-response measurements of the pickup and microphone signals of an acoustic string instrument and use frequency-domain deconvolution to produce an impulse response which can be used to process the pickup signal with convolution to better match that of the microphone signal [53]. The author has also worked on similar methods using more detailed measurement methods and an efficient modal structure to perform the processing [90]. This type of pickup processing is gaining popularity in the commercial market, and there are multiple products that use related methods, notably the LR Baggs Voiceprint DI [11] and the Audio Sprockets ToneDexter [115].

The use of acoustic instrument pickups is an option for live performance, but they can still have issues with feedback and have the potential for damage in extreme playing conditions such as outdoors. An alternative is to use an electric instrument with processing to make it sound like an acoustic instrument. This type of processing also provides the option to make it sound like various different instruments. Karjalainen et al. have worked on methods to process an electronic string instrument to sound like an acoustic instrument using a similar method to their work discussed previously for equalization while supplementing it with digital signal processing methods to simulate the increased harmonic beating, sympathetic vibrations, and control of decay and sustain seen in acoustic instruments [52].

Penttinen et al. expanded this research to morphing between the virtual acoustics of multiple virtual instruments [80, 79]. Maestre et al. also worked on processing of an electric violin to sound more like an acoustic instrument with a focus on the spatially radiated sound [63].

The proposed method makes notable extensions and improvements on the previous methods for processing electronic string instruments to replicate acoustic instruments. Rather than a single electromagnetic or piezoelectric pickup for all the instrument's strings, a pickup with individual piezoelectric string sensors located at the bridge is used. In the case of a guitar, this is a hexaphonic pickup. This allows independent processing on each string with no comb filtering resulting from the location of a pickup not located at a string termination. Detailed vibration and acoustic measurements are made on both the electric and acoustic instruments involved in the processing which allows for accurate modal fitting of the impulse responses. The same modal frequencies and damping can be used to model the admittance and radiation with their respective modal amplitudes.

A notable improvement is made to address the different string damping. String-to-bridge reflectance scattering filters are fit by comparing the string impedance and measured bridge impedance of the body. These filters mimic the physical interaction of the string and bridge on a real instrument that is responsible for the frequency-dependent string decay. The filters are applied to the electronic pickup signal in a time-varying manner, such that they accurately model the frequency-dependent string decay. Frequency-warped finite impulse response (FIR) filters are used to efficiently model this time-varying filtering, which, when applied in a warped frequency domain, allow for a shorter FIR filter with more resolution in the low frequencies, where the most prominent modes appear [40].

While processing an electric instrument to sound like an acoustic instrument as an audio effect is of interest to many musicians, I am particularly interested in this processing as a tool to study how the sound is altered by varying modal parameters of an instrument in a realistic playing situation. Building multiple instruments with different designs and materials is expensive and time-consuming, so methods to study material and design changes with synthesis and modeling are desirable. There have been multiple studies that use physical synthesis models of instruments to study the perceptual threshold of modal alterations in synthesized instruments [132, 35]. While string instrument sounds can be synthesized quite accurately, it is difficult to accurately capture realistic playing parameters and transfer them to the synthesis model [59, 58]. This method forgoes this problem by allowing the user to play a physical guitar, which can be altered in real-time to check how different modal parameters of a virtual guitar affect the sound and suit their playing style. The desire is that this method can be used to help musicians decide what type of instrument will suit their playing style and sound preferences in an instrument, leading to better-informed purchasing or building decisions.

Sec. 4.2 discusses the proposed signal processing method. Sec. 4.3 presents a test case of the method used to process an electric guitar to match a specific acoustic guitar, as well as an altered version of that guitar. Finally, Sec. 4.4 discusses the results and applications.

4.2 Processing Method

The motivation for the proposed digital signal processing method comes from the physics of a string instrument. Fig. 4.1 (a) shows the block diagram of a simple single-polarization string model with an acoustic instrument, and Fig. 4.1 (b) shows a similar block diagram for an electric instrument with a correction filter added to process the output to sound more similar to that of the acoustic instrument. These diagrams will be referenced to help motivate the proposed method.

When a string is plucked, left and right going transverse traveling waves are started on the string. In Fig. 4.1, the transverse traveling waves are represented by the delay, $z^{-N_0/2}$ where $N_0 = f_s/f_0$ is the number of samples for one complete cycle of the wave motion with frequency, f_0 , and sample rate, f_s . When the traveling waves interact with a string termination such as the nut, bridge, or a fretted note, the wave scatters, with some of the energy being reflected back to the string and

some of it being transmitted. At the bridge termination, this string energy will be transmitted through the bridge and transferred to radiated acoustic energy by the instrument body, which, in the case of an acoustic instrument, is designed to be an efficient radiator. However, with finite energy being input to the string, if there is efficient acoustic radiation, the reflected string energy will be low, resulting in a short string decay. This is contrary to how a solid body electric instrument functions with inefficient acoustic radiation, resulting in a long string decay. The proposed method uses digital filters that model the string-bridge reflection scattering (reflectance) and the transmitted energy through to the radiated sound [111]. In Fig. 4.1, $P_N(z)$ represents the scattering filter at the nut while $P_{B,a}(z)$ and $P_{B,e}(z)$ represent the scattering filter at the bridge of the acoustic and electric instrument respectively.

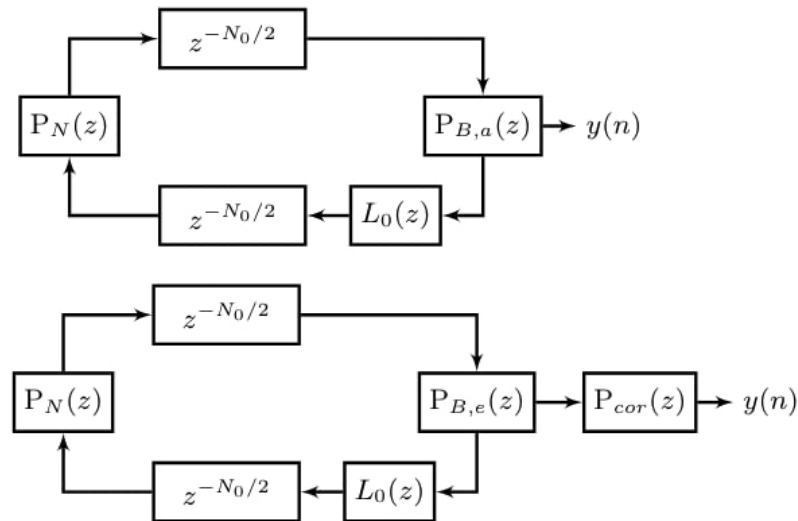


Figure 4.1: Single-polarization string model for (a) an acoustic instrument, and (b) an electric instrument with a reflectance correction.

A string traveling wave will propagate at speed $c = \sqrt{T/\epsilon}$, where T is the string tension, and ϵ is the linear mass density of the string. If the string is of length L , every $t_s = c/(2L)$ seconds, a pulse will return to its original position, encountering both of the string termination points in the process. Making reference to Fig. 4.1, t_s is equivalent to N_0 in samples. With an acoustic instrument, the impedance of the bridge is generally much lower than that of the nut or a fretted note, so the problem can be simplified by treating the nut or fretted termination as rigid, meaning that the bridge termination is responsible for the string decay time. The neck vibrations will also result in a low impedance and short string decay [94] but will be ignored in this study as a simplification. A wave pulse on the string will repeatedly hit this bridge termination every t_s seconds. This behavior is approximated by modeling the bridge scattering reflection termination as a filter, which is varied

to have the behavior of being repeatedly applied every t_s seconds or N_0 samples.

Referencing Fig. 4.1, if we want to achieve an acoustic sound from an electric instrument, the string traveling waves recorded by the electric instrument pickup are known and are used as input to be processed. If the same set of strings is used, the string-loss filter, $L_0(z)$ can be assumed the same. If we assume the nut scattering is perfectly rigid, we are left only to correct for the bridge scattering. The electric instrument includes $P_{B,e}(z)$ in the feedback loop, and we need to process the output signal with $P_{B,a}(z)$ at each N_0 samples to replicate it being placed in the feedback loop. This is achieved using the correction filter,

$$P_{cor}(z) = \left(\frac{P_{B,a}(z)}{P_{B,e}(z)} \right)^Q, \quad (4.2)$$

which is updated at each N_0 samples, where Q is the number of pitch periods that have occurred.

The method relies on a set of time-varying reflectance filters which need to be reset each time a new note is played on the instrument, so onset detection is needed. The filters need to be updated every t_s seconds, which depends on the period of the note being played. The length can be determined if we predict the fundamental frequency of the note. The reflectance filters will be used to process the incoming pickup signal to match the damping, while a radiation filter will be used to achieve the desired equalization at a virtual listening position. Both of these filters can be designed from modal properties fit to measurements of an acoustic instrument or designed to mimic any desired theoretical instrument. The processing needs to be applied independently on each string as the reflectance filters depend on the string impedance of each individual string. A simplification is made to only treat 1D string vibration in the plane orthogonal to the top plate of an instrument. This simplification was done as it is the polarization responsible for the majority of the radiated sound and because string instrument pickups typically only measure the polarization in this direction.

The processing can be broken up into four steps: transient detection, pitch detection, damping correction filtering, and sound radiation filtering. A block diagram of the processing algorithm is shown in Fig. 4.2

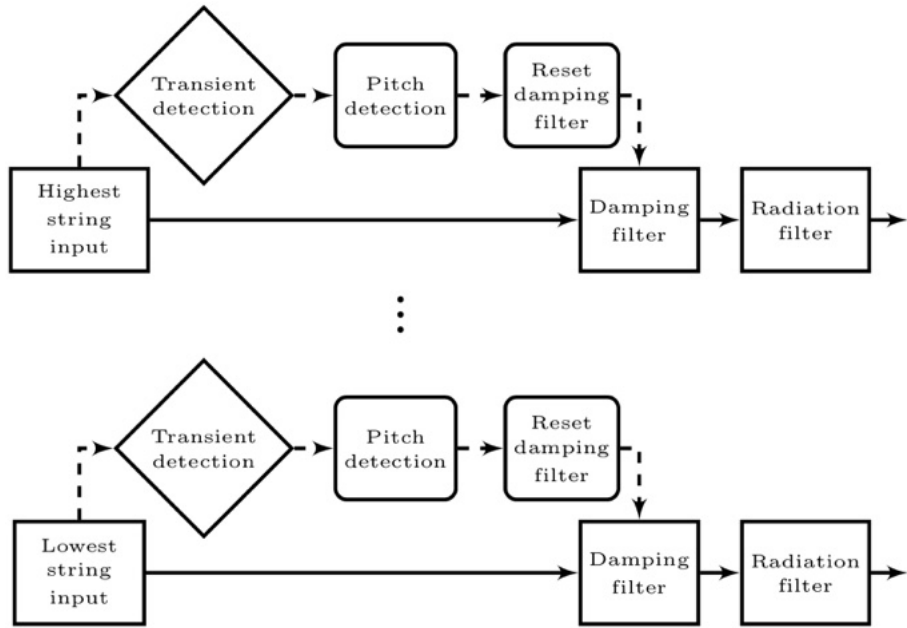


Figure 4.2: Signal processing block diagram.

4.2.1 Transient Detection

For transient detection purposes, the pickup signal is first high-pass filtered with a fourth-order Butterworth filter having a cutoff frequency of $15f_c$, where f_c is the fundamental frequency of the open note frequency for that string. The high-pass cutoff frequency was empirically chosen to reduce the chance of high-frequency oscillations triggering the onset detection. A short-term root-mean-squared (RMS) detector with a time constant of $\tau = 200$ ms is used to capture the overall level of the signal. The RMS detector for a signal $x(n)$, $n = 0, 1, \dots$, is implemented as

$$\begin{aligned} \lambda_{RMS}(n) &= (a_1 \lambda_{RMS}(n-1)^2 + b_0 |x(n)|^2)^{\frac{1}{2}}, \\ a_1 &= e^{\frac{-1}{\tau f_s}}, \\ b_0 &= 1 - a_1, \end{aligned} \quad (4.3)$$

where λ_{RMS} is the approximate RMS level and f_s is the sample rate.

A leaky peak detector with an attack time of $\tau_a = 1$ ms and a release time of $\tau_r = 20$ ms is used to closely follow the peaks in the signal. The peak detector is implemented as

$$\lambda_p(n) = \lambda_p(n-1) + (1 - e^{\frac{-1}{\tau f_s}})(|x(n)| - \lambda_p(n-1)), \quad (4.4)$$

where λ_p is the approximate peak level, initialized as $\lambda_p(0) = 0$, and $\tau = \tau_a$ if $x(n) > \lambda_p$, or $\tau = \tau_r$

otherwise. Both level estimates are low-pass filtered to smooth the signal and reduce the chance of transients being incorrectly detected. They are filtered with a fourth-order Butterworth filter with cutoff frequencies of 100 Hz for the RMS level and 200 Hz for the peak level. A transient is determined to occur if $\lambda_p > \lambda_{RMS}$ and $\frac{d\lambda_p}{dt} > 0$, i.e., when the peak level is increasing and crosses the RMS level.

Robust transient detection relies on the choice of parameters to match a specific instrument and playing style. The time constants, τ , τ_a , τ_r , were heuristically chosen such that for typical guitar playing, the leaky peak detector closely tracks the signal, and RMS level tracks the overall level. One of the most common problems with this type of transient detection is detecting multiple transients at a note onset due to the rapid variation of the peak detection. The low-pass filters helped to smooth the level estimates and reduce the occurrence of false transients.

4.2.2 Pitch Detection

Detecting the pitch of the incoming pickup signal is relatively straightforward because the signal is monophonic, has a high signal-to-noise ratio, and is in a known range. The main difficulty is making the pitch estimation fast enough to detect it in one period and during the initial transient. However, the main purpose of pitch detection is to set the time-varying filter to alter the string decay time. Therefore, if one period is missed at the start of the transient, it is likely not perceptually relevant. Additionally, since the signal will continue, successive estimates of the pitch can be made to capture any variations, such as the increase of the pitch after a strong pluck due to the tension modulation nonlinearity.

The normalized correlation function [8] is used to estimate the pitch, referred to as f_0 . The pitch is estimated with a constant window length, which can be adjusted to a longer window for lower-pitched strings. For example, with a guitar, a window length of 2048 samples could be used for the low E string, with a window length of 1024 samples for all other strings. A window overlap of half the window length is used for successive estimations. The playable pitches on each string are known, so the pitch estimation can have bounds to guarantee it represents a note on the string in question. When the pitch is not yet known, such as during the start of the transient, the pitch estimate is set to be that of the lowest possible note playable on the string. Additionally, if the pitch estimate is outside the playable range of the string, it is deemed an erroneous estimate, and the pitch is set as that of the lowest note playable on the instrument. This decision helps to reduce the errors that can arise by applying the time-varying filter at the wrong time.

The pitch estimate sets the time in samples at which the reflectance filter needs to be updated as $N_0 = f_s / f_0$.

4.2.3 Damping Correction

The damping correction filter represents the scattering reflectance at the string-to-bridge interface of an instrument. In the Z-domain, this can be represented as

$$P(z) = \frac{R_B(z) - R_S}{R_B(z) + R_S}, \quad (4.5)$$

where $P(z)$ is the reflectance, $R_B(z)$ is the bridge impedance, and R_S is the string impedance calculated as $R_S = \sqrt{T\epsilon}$ [111].

The bridge admittance, $\Gamma(z)$ for an arbitrary set of modes can be constructed as a parallel filter bank of resonant peaking filters. Given the mode center frequencies, f_m , damping ratios, ζ_m , and amplitudes, γ_m , the filter bank can be constructed for $m=1,\dots,M$ modes as

$$\Gamma(z) = \sum_{m=1}^M \Gamma_m(z), \quad (4.6)$$

$$\Gamma_m(z) = \gamma_m \frac{1-z^{-2}}{1+a_{m,1}z^{-1}+a_{m,2}z^{-2}}, \quad (4.7)$$

where $a_{m,1} = -2r_m \cos(\omega_m)$, and $a_{m,2} = r_m^2$, with $r_m = \exp(-\omega_m \zeta_m)$ being the pole radius, $\omega_m = 2\pi f_m / f_s$ the natural frequency, and f_s the sampling rate [12, 66]. These modal parameters can either be arbitrarily chosen if simulating a hypothetical instrument or fit to a bridge admittance measurement of a physical instrument. The bridge impedance is the inverse of the admittance, $R_B(z) = 1/\Gamma_B(z)$, so the reflectance is determined given the string impedance R_s .

The bridge reflectance can be expanded to form the series bank of second-order filters,

$$P(z) = \prod_{m=1}^M P_m(z), \quad (4.8)$$

$$P_m(z) = \frac{(1-R_s \gamma_m) + a_{m,1}z^{-1} + (a_{m,2} + R_s \gamma_m)z^{-2}}{(1+R_s \gamma_m) + a_{m,1}z^{-1} + (a_{m,2} - R_s \gamma_m)z^{-2}}. \quad (4.9)$$

The bridge reflectance is found using (4.7) to calculate $R_B(z)$, and substituting this parallel filter bank in (4.5). This expression is reduced by factoring out the respective denominators of R_B , resulting in a series filter bank, similar to a filter bank of notch filters.

Since this method of electric instrument processing is often concerned with solid-bodied instruments, which typically have a high bridge impedance, it may be possible to ignore any resonant structure of the electric instrument in the processing. However, if the electric instrument has a significantly low enough bridge impedance, the response of this instrument should be factored into the processing using inverse filtering to reduce its effect. If we let the scattering reflectance filters for the electric instrument be $P_e(z)$, and that of the acoustic instrument be $P_a(z)$, then the combined

reflectance correction filter response is

$$P_{\text{cor}}(z) = \frac{P_a(z)}{P_e(z)}. \quad (4.10)$$

The filtering of $1/P_e(z)$ could result in an unstable filter if the fitting is not an exact match to the electric instrument, which can happen with slight variation in the modes due to temperature, humidity, or playing conditions, so limits should be placed on this filter to prevent it from going unstable. A choice was made to set an artificial limit of P_{\max} to avoid the potential for instability. The electric instrument reflectance, $P_e(z)$, was rearranged according to Appendix A.1, so that the individual biquad filters are controlled by a gain, $g_{P,e,m}$, which is between 0 and 1 [3]. If $P_{\text{cor}}(z) > P_{\max}$ at the notch frequencies of $P_e(z)$, their respective gains were recalculated as

$$g_{P,e,m}^* = P_{\max} \frac{|P_a(e^{j\omega_m T})|}{g_{P,e,m}}, \quad (4.11)$$

where $g_{P,e,m}^*$ are the new gains, and $|P_a(e^{j\omega_m T})|$ is the acoustic instrument reflectance magnitude evaluated at the electric instrument mode m . Let $P_{\text{cor}}^{\text{limits}}(z)$ be the combined reflectance filter with the new electric instrument gains $g_{P,e,m}^*$, resulting in a stable filter.

The correction can be applied efficiently as a bank of series second-order infinite impulse response (IIR) filters, but since it has to be repeatedly applied in the processing, the filter order would be increased at each N_0 samples relating to the pitch period. Implementing the time-varying damping filter as an IIR filter provides a challenging filter design problem, so a choice was made to implement it as an FIR filter. While choosing to switch to an FIR implementation after taking care to formulate the problem as an IIR structure may seem strange, there are multiple reasons why it was done. The processing method is designed to work with a measured admittance as well as a hypothetical admittance. If using a measured admittance, the entire process could be undertaken with FIR filters, but this is not the case if the modal structure is being arbitrarily chosen. Additionally, the IIR implementation allows the user to easily vary specific modal parameters to adjust the sound. Another advantage of the IIR implementation is that the IIR filters can be designed such that they are positive-real, guaranteeing stability of the acoustic instrument reflectance, which is not always the case for a measured FIR admittance. Similarly, since only a small number of the electric instrument modes are measured, we can correct for any instability that may arise by the filtering of $1/P_e(z)$, which would be more difficult if conducted only with FIR filters.

If we refer to the FIR reflectance filter as $\rho_{\text{FIR}}(z)$ which is the impulse response of the filter $P_{\text{tot}}^{\text{limits}}(z)$, and Q is the number of pitch periods which have occurred, we can represent the repetitive FIR filter as

$$\rho_{\text{FIR},Q}(n) = \mathcal{F}^{-1}(\mathcal{F}(\rho_{\text{FIR}}(n))^Q), \quad (4.12)$$

where $\rho_{\text{FIR},Q}(n)$ is the new filter to be applied beginning $N_0 Q$ samples after the transient is detected.

\mathcal{F} and \mathcal{F}^{-1} are the Fourier and inverse Fourier transforms.

Since there are many prominent low-frequency modes, a long FIR filter would be needed to represent the reflectance. Instead, a frequency-warped FIR (WFIR) filter can be used to reduce the filter length while maintaining the accuracy of the low-frequency modes [40]. The warping is performed by replacing the unit delay, z^{-1} , with a first-order all-pass filter,

$$\zeta^{-1} = \frac{z^{-1} - \alpha}{1 - \alpha z^{-1}}, \quad (4.13)$$

where α is the warping factor.

Modes near DC are warped by a factor of $\frac{1+\alpha}{1-\alpha}$ while modes near the Nyquist frequency are warped by a factor of $\frac{1-\alpha}{1+\alpha}$. Hence, choosing a larger warping factor will increase the resolution of the low-frequency modes while decreasing it for the high-frequency modes.

This architecture can be used with a unit impulse $\delta(n)$ as input, and $h(n) = \rho_{\text{FIR}}(n)$ to get the frequency-warped impulse response, $\rho_{\text{WFIR}}(n)$. The same filter architecture can be used to process a signal with the frequency-warped impulse response, and warp back, but using the negative warping constant, $-\alpha$. The incoming instrument pickup signal is processed in this way with $h(n) = \rho_{\text{WFIR}}(n)$. In the implementation, the frequency-warped reflectance, $\rho_{\text{WFIR}}(n)$, only needs to be calculated once. It can then be converted to $P_{\text{WFIR}}(z)$ using a Fourier transform, while $\rho_{\text{WFIR},Q}(n)$ is calculated at each $N_0 Q$ samples in the same manner as in (4.12).

The frequency-warped processing is applied using $\rho_{\text{WFIR},Q}(n)$, which is updated at each pitch period. The filter coefficients are directly updated at each pitch period. Ideally, the coefficients would be updated in a more gradual fashion, but since the updates are small, it works reasonably well in the meantime, with no obvious artifacts attributed directly to the abrupt updates.

4.2.4 Sound Radiation

The admittance in (4.7) represents the modal structure of the instrument. This modal structure can also be used to process the output sound to mimic the radiated sound equalization. The mode frequencies and damping will stay the same, but a new set of mode amplitudes, $\gamma_{m,r}$, are needed to represent the sound amplitude radiated to a specific point in space. These mode amplitudes can be complex to account for phase differences at the measurement location. This filtering can be implemented efficiently as a parallel bank of first-order complex resonators with the difference equation [70]:

$$y_m(n) = \gamma_{m,r} x_m(n) + e^{\omega_m(i - \zeta_m)} y_m(n-1). \quad (4.14)$$

The output of this filter is complex, but a real signal can be obtained by taking the real part of the output.

4.3 Test Case: Measured Guitar

As a test case of the proposed processing method, two guitars were used, referred to as the electric and acoustic guitars. The electric guitar is a Les Paul model with a piezoelectric hexaphonic bridge pickup [10]. The body of this guitar is constructed of solid mahogany and maple, so it has a high bridge impedance. The acoustic guitar is a 1940s Martin 00-18 which has a much lower bridge impedance due to the light and thin spruce top plate. Both instruments were strung with the same set of acoustic guitar strings. The electric guitar has a scale length of 62.9 cm while the acoustic guitar has a scale length of 63.2 cm. The difference in scale length means the tension of the acoustic guitar strings, and string impedance will be slightly higher. Since both guitars were strung with the same set of strings, the string damping contributions from viscosity in the surrounding air and the bending stiffness can be ignored [134].

4.3.1 Measurements

Bridge input admittance measurements were taken on both guitars by striking the bridge near the lowest string, normal to the guitar's top plate. A force-sensing impact hammer (PCB 086E80) was used with a remote-controlled driver to strike the bridge. A Polytec PDV-100 laser Doppler vibrometer (LDV) was used to measure the surface velocity at a point as close as possible to the striking point of the hammer. The measured driving-point force and velocity were used to compute the admittance in the frequency domain as $\Gamma(z) = V(z)/F(z)$, where F and V are the force and surface velocity. Measurements were only made in the direction normal to the instrument top, and the processing for this test case is simplified to only process one dimension of the string motion. A calibrated microphone (PCB 738A06) was placed 20 cm away from the 12th fret of the guitar to record the sound radiation during the hammer strikes. Both guitars were measured the same way and were mounted on their side with foam used to damp the strings. The measurement setup can be seen in Fig. 4.3.

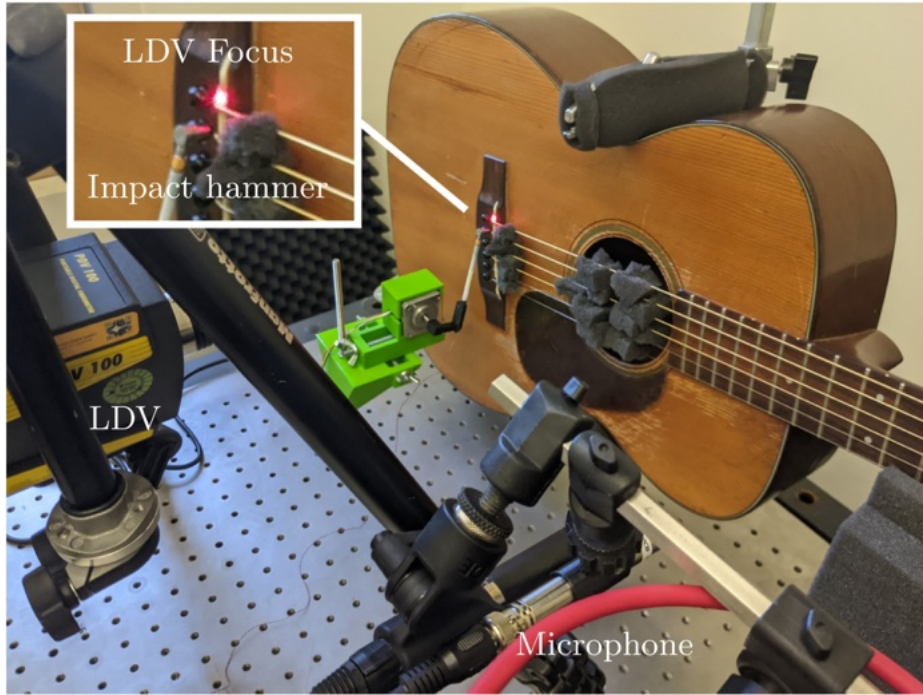


Figure 4.3: Bridge admittance measurement setup for the acoustic guitar.

4.3.2 Mode Fitting

Mode fitting was performed on the bridge admittance measurements to estimate the mode frequencies, damping, and amplitudes. Modes were fit assuming the system has the damped harmonic oscillator behavior given by the impulse response of (4.7) [14]. The mode fitting was done using a method by Abel et al. which involves analysis of the eigenstructure of a Hankel matrix of admittance impulse response samples [1]. The M largest singular values of this decomposition can be viewed as the singular values associated with the signal space as opposed to the noise space. The order M was chosen as the lowest number of modes which visually produced a good fit in the frequency domain. A brief overview of this method is provided in Appendix A.2.

The mode fitting method gave better results when performed in separate frequency bands, allowing the impulse response to be downsampled by different factors. For the acoustic guitar, the mode fitting was performed in three frequency bands: 60-300, 300-920, and 920-6000 Hz. The frequency bands were chosen visually to have transitions between prominent modes. The admittance impulse response was downsampled by a factor of 10, 8, and 3 for each frequency band to increase the frequency resolution in the lower end of the frequency band, and a downsampled impulse response of 512 samples was used. Modes with frequencies outside the desired frequency band were discarded, and the remaining modes were combined for the final fit. The mode fitting was only performed up

to 6 kHz as the signal became noisy at high frequencies, and individual modes were not able to be resolved. As a simple approximation, the high frequencies were approximated with a first-order high-pass filter having a cutoff frequency of 6 kHz. This approximation breaks the assumption that the system is comprised of modal resonators, but provides a tolerable approximation of the unknown high-frequency behavior.

Since the mode fitting was done in separate bands and the high-pass filter was added, the mode amplitudes needed to be recalculated. Positive-real mode amplitudes, $\boldsymbol{\gamma}_a = [\gamma_{a,1} \dots \gamma_{a,M}]^\top$, for the admittance were found by creating a basis of the modal impulse responses and high-pass filter,

$$\mathbf{B}_a = \begin{bmatrix} e^{\omega_1(i-\zeta_1)\theta} & \dots & e^{\omega_{M_a}(i-\zeta_{M_a})\theta} & h_{hp}(0) \\ \vdots & \ddots & \vdots & \vdots \\ e^{\omega_1(i-\zeta_1)(N-1)} & \dots & e^{\omega_{M_a}(i-\zeta_{M_a})(N-1)} & h_{hp}(N-1) \end{bmatrix}, \quad (4.15)$$

where h_{hp} is the high-pass filter impulse response, M_a is the number of modes fit, and N is the number of samples in the impulse response. Least squares was then used to solve the system,

$$\mathbf{h}_a = \mathbb{R}(\mathbf{B}_a)\boldsymbol{\gamma}_a, \quad (4.16)$$

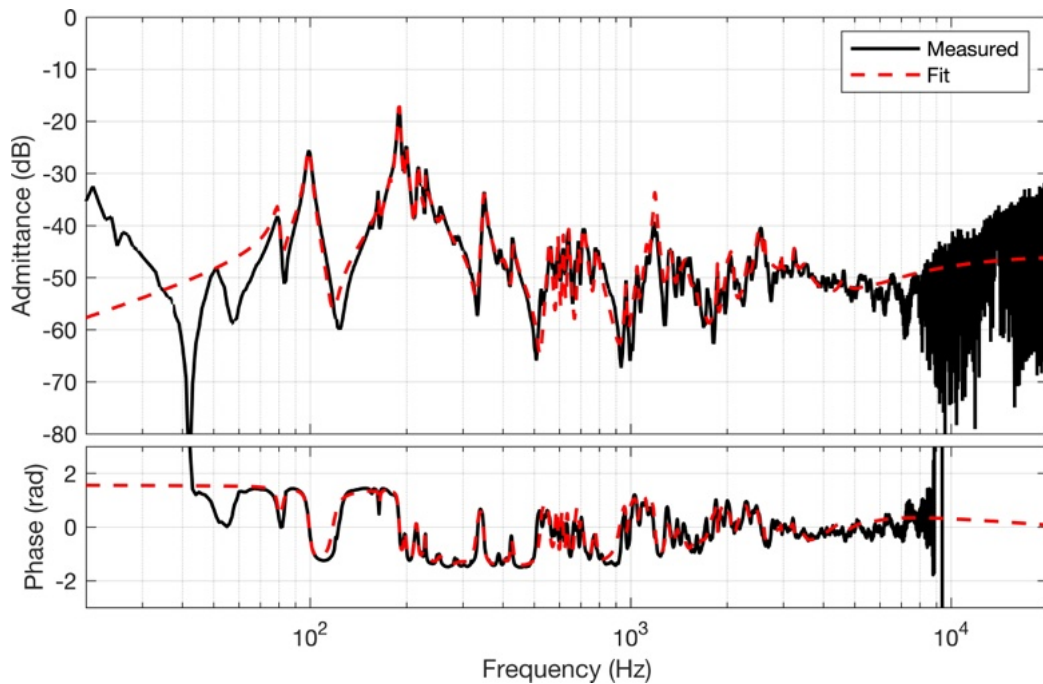
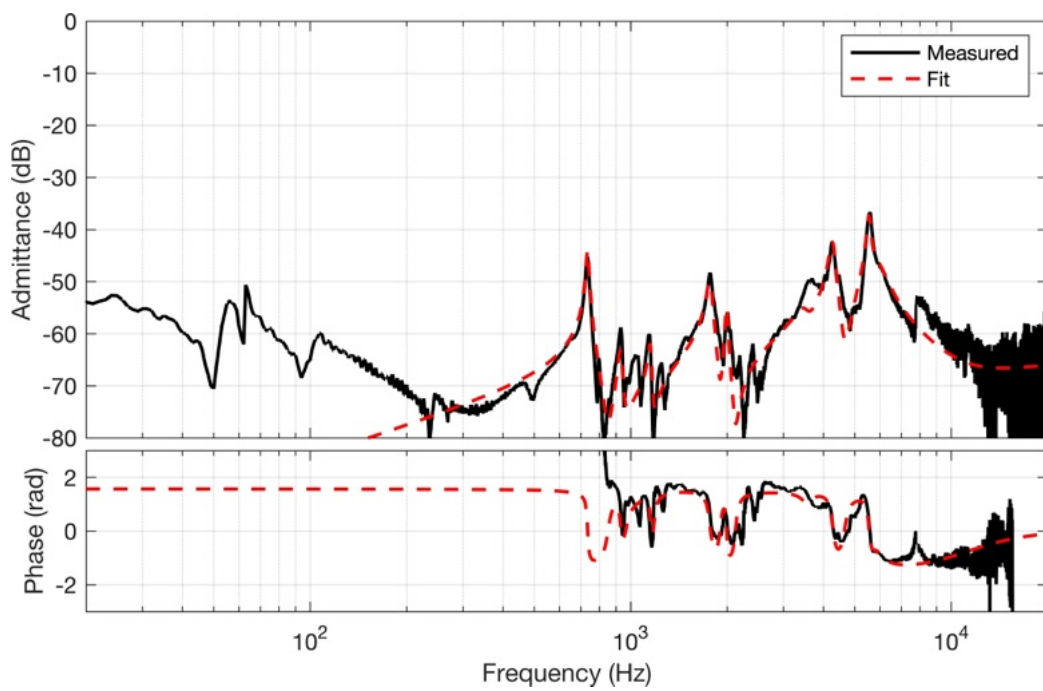
where $\mathbf{h}_a = [h_a(0) \dots h_a(N-1)]^\top$ is the measured acoustic guitar admittance. Fig. 4.4 shows the measured and fit admittance for the acoustic guitar with $M_a=50$ modes.

The acoustic guitar has a complex modal structure due to the thin wood pieces used for the construction and the resonant cavity, as well as a much higher overall admittance. However, the electric guitar has a low overall admittance with only a few strong modes, likely corresponding to the bending modes of the neck. The low number of modes means that the electric guitar admittance can be fit accurately with a lower model order than with the acoustic guitar.

To fit the electric guitar, frequency bands of 300-2200 and 2200-6000 Hz were used with down-sampling factors of 8 and 2. The high frequencies were fit with a first-order high-pass filter having a cutoff frequency of 8 kHz. The mode amplitudes were then calculated by solving the system,

$$\mathbf{h}_e = \mathbb{R}(\mathbf{B}_e)\boldsymbol{\gamma}_e, \quad (4.17)$$

formed in the same manner as with the acoustic guitar, where, \mathbf{h}_e , \mathbf{B}_e , $\boldsymbol{\gamma}_e$ are the admittance impulse response, modal basis, and modal amplitudes for the electric guitar. Fig. 4.5 shows the measured and fit admittance for the electric guitar with $M_e=11$ modes.

Figure 4.4: Mode fitting of the acoustic guitar admittance using $M_a = 50$ modes.Figure 4.5: Mode fitting of the electric guitar admittance using $M_e = 11$ modes.

4.3.3 Reflectance Filter

The method described in Sec. 4.2.3 was used to create reflectance filters. The strings used were light gauge (12-53) phosphor bronze acoustic strings, and the impedance was calculated from known measurements of the linear mass density and tension of the string [22]. A separate reflectance filter is calculated for each string as the string impedance differs. The reflectance filters for the low E string of the electric and acoustic guitars, as well as the combined reflectance filters with and without limits calculated using (4.10) and (4.11) are shown in Fig. 4.6. The maximum reflectance was chosen as $P_{\max} = 0.999$. The combined reflectance filter magnitude is shown to be unstable as it is greater than 1 at some frequencies, but the combined reflectance with limits does not go above 1.

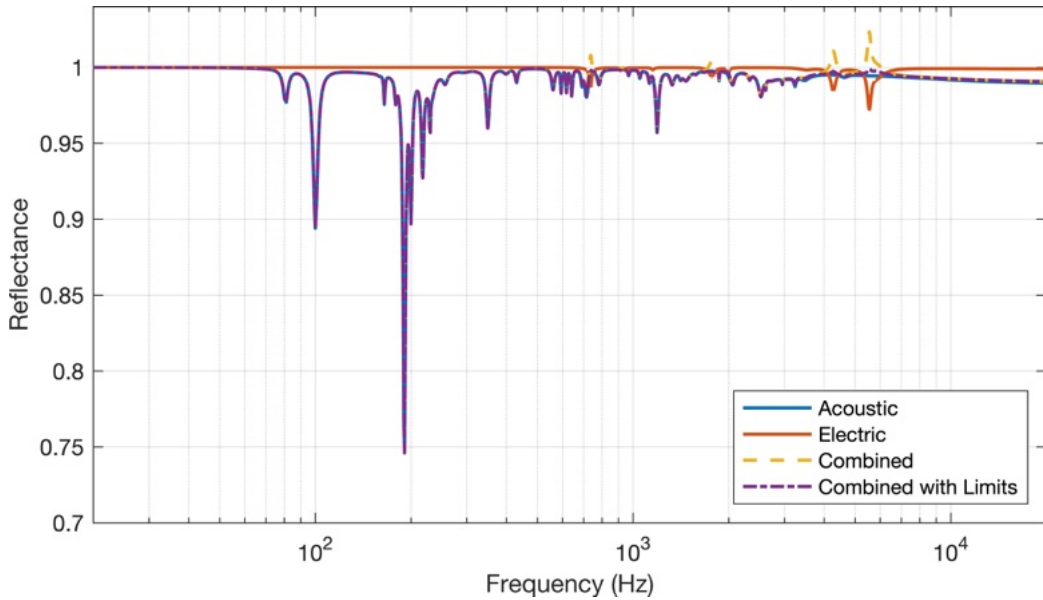


Figure 4.6: Reflectance of the acoustic and electric guitars as well as the combined reflectance with and without limits.

To achieve a shorter FIR filter, a frequency-warped approach was taken. Since there are many prominent modes in the low frequencies, a warping factor of $\alpha = 0.75$ was used, which effectively zooms in on the low modes by a factor of 7. A frequency-warped filter of length 2048 was used as it was the shortest filter that still provided a good match to the original reflectance filter. Fig. 4.7 shows the frequency response of the length 2048 warped reflectance filter along with a length 2048 linear-frequency filter and the original reflectance. The linear-frequency filter has ringing in the low frequencies caused by the impulse response truncation, which causes the response to exceed a gain of one, creating stability problems. While using a warped FIR filter allows for a shorter filter, care should be taken to avoid ringing if the filter is too short.

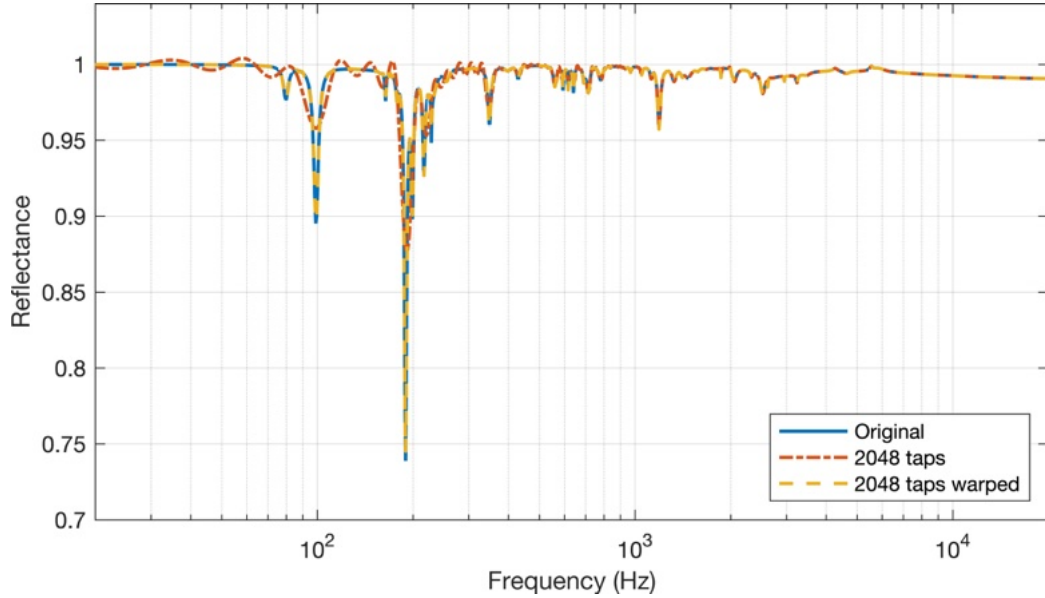


Figure 4.7: Comparison of the original reflectance with a 2048 tap FIR and frequency-warped FIR filter.

4.3.4 Radiation Filter

The sound radiation at the microphone location can be efficiently implemented as a modal parallel IIR filter bank. Since the radiation measurements are much noisier than the admittance measurements, the same set of modal frequencies and damping for the acoustic guitar admittance is used for this IIR filter bank. However, unlike with the admittance, which has in-phase modes, the radiation modes can have phase differences. The phase differences can be accounted for by fitting complex mode amplitudes, $\boldsymbol{\gamma}_r$. The fitting is performed in a similar manner as in Sec. 4.3.2 by performing least squares to solve the system,

$$\mathbf{h}_r = \mathbf{B}_a \boldsymbol{\gamma}_r, \quad (4.18)$$

where, \mathbf{h}_r , \mathbf{B}_a , $\boldsymbol{\gamma}_r$ are the radiation impulse response, modal basis, and modal amplitudes for the acoustic guitar. Fig. 4.8 shows the measured and fit radiation for the acoustic guitar with $M_a = 50$ modes. While the fit is not perfect in the high frequencies, this is acceptable as human hearing is not sensitive to individual modes at high frequencies [139].

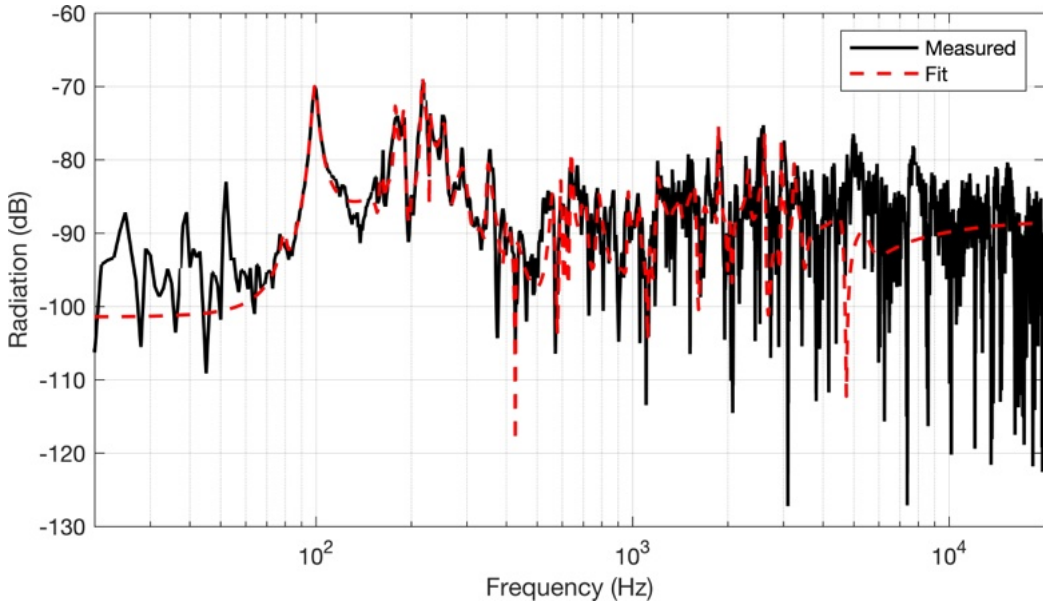


Figure 4.8: Radiation filter for the acoustic guitar with $M_a = 50$ modes.

4.3.5 Sound Processing

The filters designed for the reflectance and radiation were used to process the piezoelectric hexaphonic pickup of the electric guitar. The time integral of the voltage measured across the piezoelectric pickup is proportional to force, which is what we want to measure [126]. Ideally, a charge amplifier would be used to convert the pickup signal to be proportional to force, but I did not have a 6-channel charge amplifier. Instead, the pickup signal was read directly from a sound card and numerically integrated with the leaky integrator filter,

$$G(z) = \frac{1}{1 + a_1 z^{-1}}, \quad (4.19)$$

where $a_1 = -0.998$.

4.3.6 Evaluation

Spectrograms of an open low E string pluck through the unaltered electric guitar pickup, integrated pickup, pickup with only the radiation filter, and fully processed pickup are shown in Fig. 4.9, along with a pluck of the same note on the acoustic guitar. Fig. 4.10 shows similar plucks for the 3rd fret of the high E string. Audio examples can be found online [87]. These two plucks were chosen for display as they represent the range of results, with the 3rd fret high E pluck being a close match and the open low E pluck displaying clear errors.

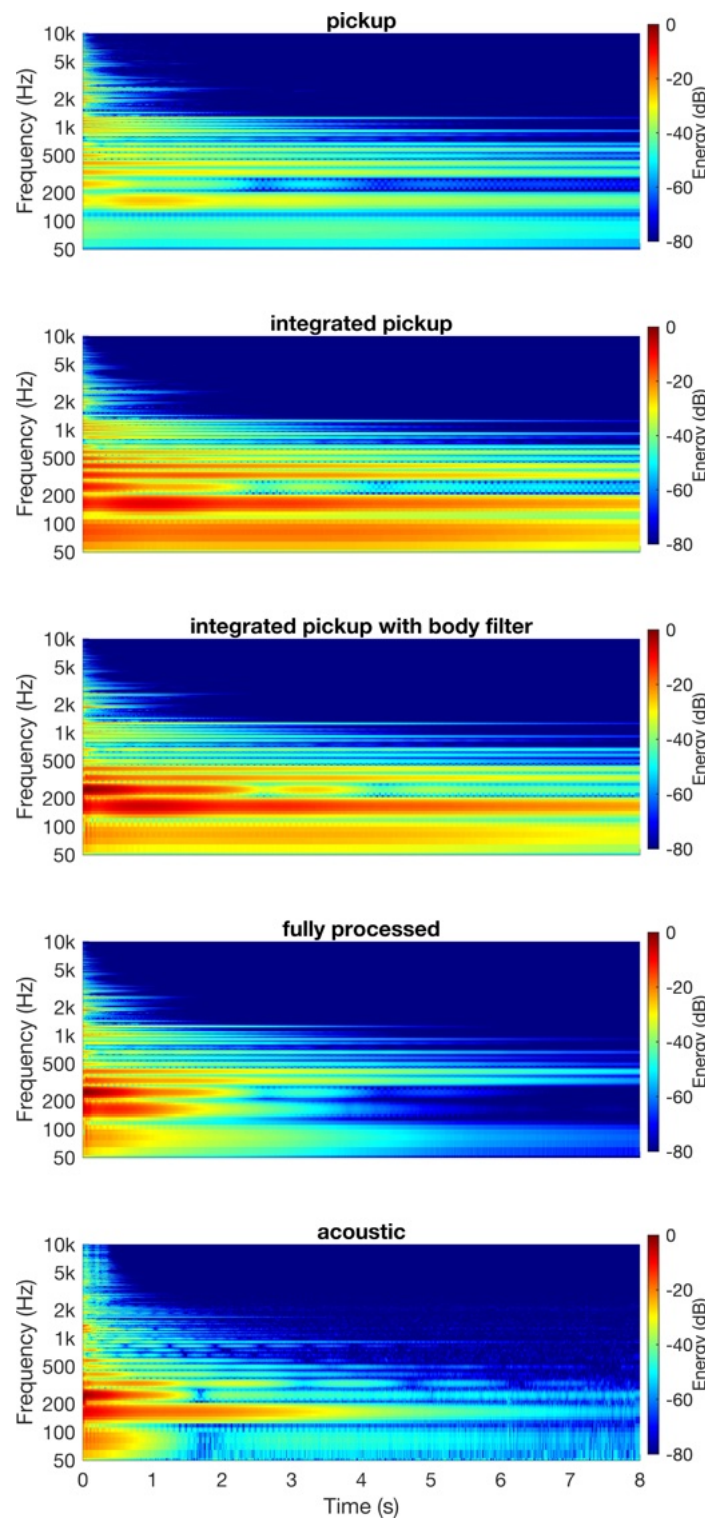


Figure 4.9: Open low E string pluck comparison.

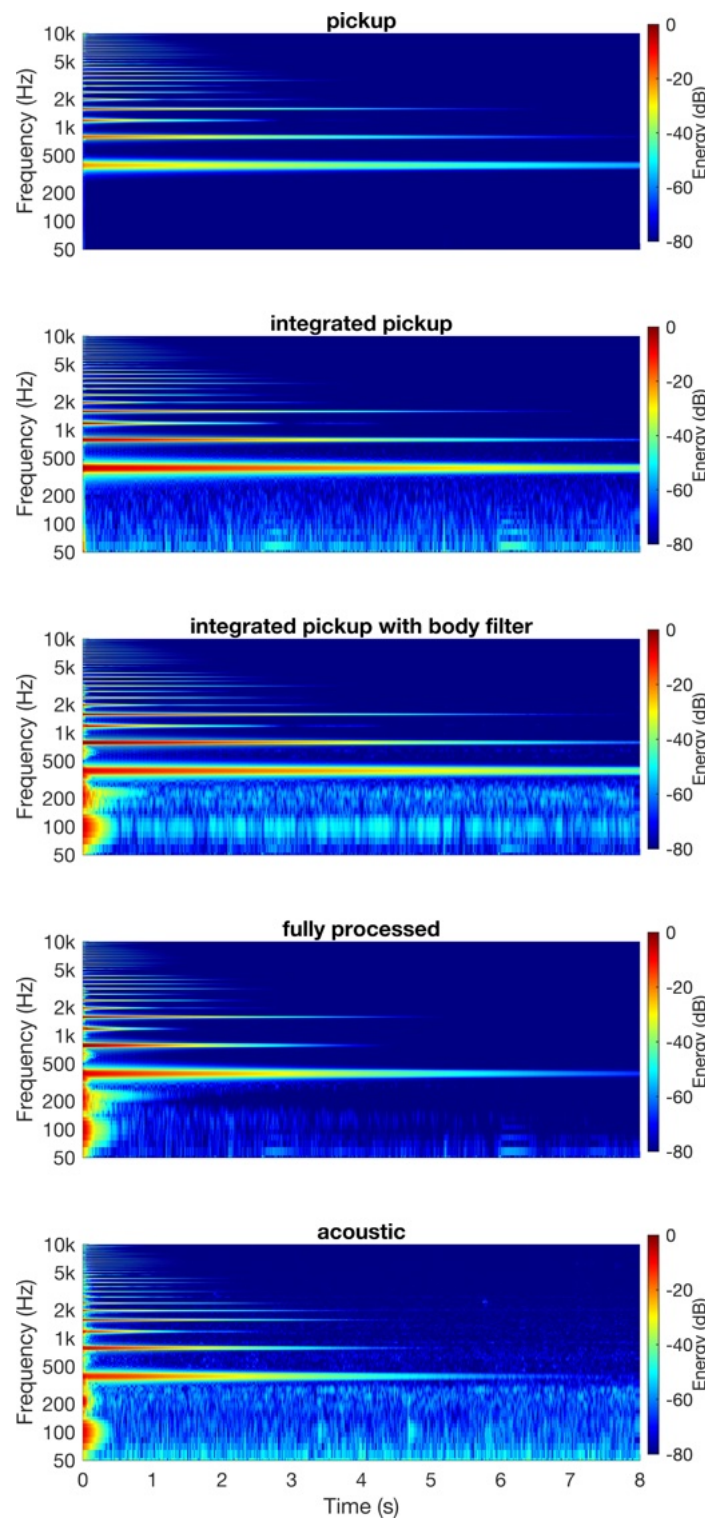


Figure 4.10: 3rd fret high E string pluck comparison.

Fig. 4.11 shows the time for the first 10 harmonics to decay by 60 dB (T_{60}) for the pickup, processed pickup, and acoustic plucks of the same open low E and 3rd fret high E notes. It is apparent from viewing the spectrograms and T_{60} plots that the string decay of the fully processed plucks is much closer to the acoustic plucks than without the damping correction. The 3rd fret high E string pluck is visually and auditory quite similar and a large improvement on the pickup with only a body filter.

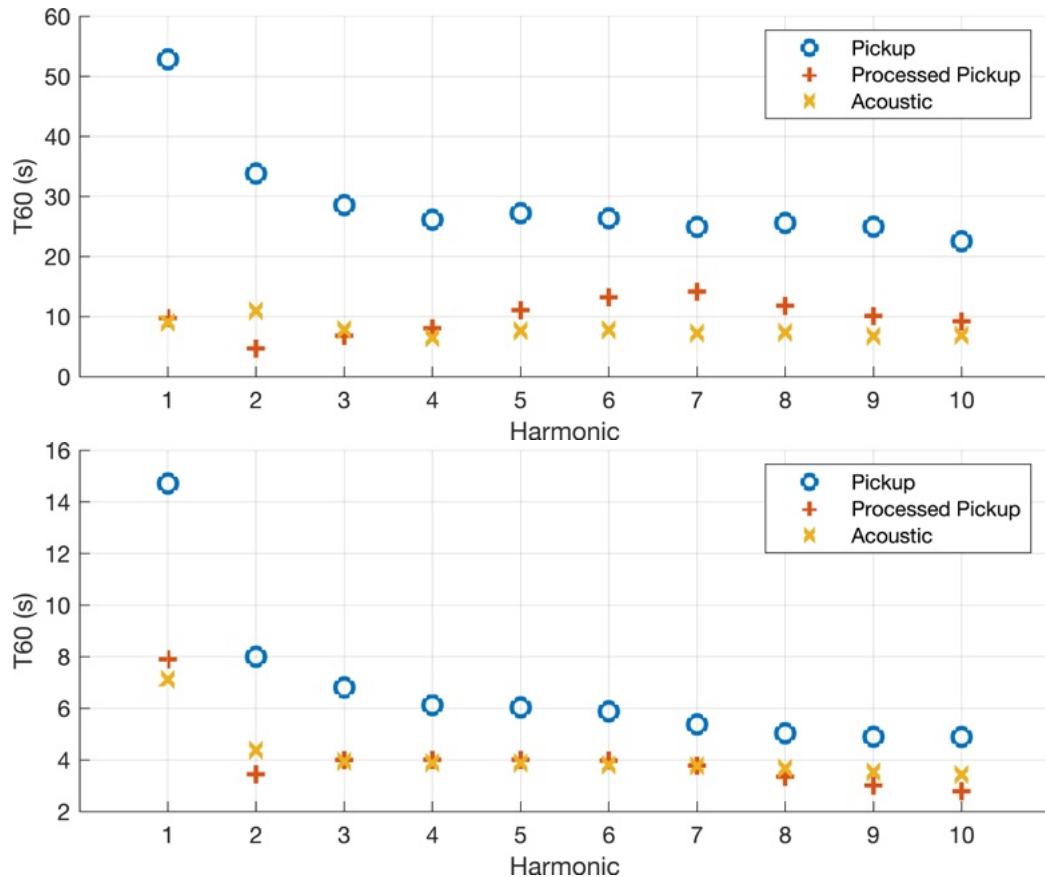


Figure 4.11: T_{60} of the first 10 harmonics of the (a) open low E, and (b) 3rd fret high E strings.

The processed open low E pluck looks overall more similar to the acoustic pluck than without the damping correction, however, there are errors that can be seen and heard. Many of the harmonics of the acoustic pluck display a two-stage decay and beating, notably the fundamental, 3rd, and 4th harmonics. These effects are caused by the two-dimensional motion of the string and how it is coupled to the bridge in directions parallel and perpendicular to the top plate, and become more pronounced at higher amplitude plucks and are audible. Since the processing method assumes 1D string motion, these effects cannot be captured. Additionally, some harmonics display too much or too little damping, such as with the 2nd and 5th harmonics, likely due to errors in the mode fitting.

The response of the body radiation filter is visible in the high E string plucks, notably, the two resonances near 100 and 200 Hz, below the fundamental frequency of the string. The body impulse response can be heard in the acoustic pluck and is necessary for the pluck to sound like it is coming from an acoustic instrument. The body response is also acting to change the equalization of the electronic instrument to be closer to that of the acoustic instrument.

In addition to the individual plucks shown, a strummed chord sequence can be found at the project website, and some informal observations will be given here. The integrated pickup on its own does not sound at all like an acoustic instrument and purely sounds like an electric guitar with a piezoelectric bridge pickup. The electric guitar with the body filter sounds more similar in timbre to an acoustic guitar, but it sounds very muddy as the string decay matches that of the electric instrument. A few high-pitched ringing frequencies become apparent, suggesting that there may be some resonances due to the pickup, which are being exaggerated by the body filtering. The fully processed guitar sounds more similar to an acoustic guitar as the string decay is much closer. The sound is not an exact match to the raw acoustic recording, but it would likely not be recognized as an electric guitar, perhaps rather an acoustic guitar with some recording issues. The acoustic guitar was recorded in a different room and with different equipment than the admittance measurements, so an exact match of the sound is not expected, but are rather looking for a form of processing that gets closer to approximating an acoustic instrument.

4.3.7 Altered Guitar

One of the driving motivations behind this method is to create a tool to hear how altering specific modal parameters of an instrument will change the perceived sound in a realistic playing situation. Since this method is implemented with a modal architecture at the core, it is easy to manipulate the modal parameters of the virtual instrument. For example, if a guitarist is unsatisfied with the sound of their instrument in a particular range, alterations could be made to the instrument to adjust the modal structure. However, these adjustments are often irreversible, and the guitarist would not know if they are satisfied with the changes until they are completed. This processing could be used to allow the guitarist to hear an approximation of how the instrument will sound with the proposed changes before they are made to the physical instrument.

Another application is when designing an instrument from scratch. Typically, the builder has to infer what sound will be desired by a musician and build an instrument to achieve this sound. This method would allow a musician to choose a hypothetical frequency response of an instrument, and the builder could use a combination of computational modeling and their prior experience to construct an instrument having a similar frequency response.

To demonstrate how this method could be used to virtually reshape the sound of a known instrument, an altered version of the modeled acoustic guitar was created by shifting all the mode frequencies higher by a factor of 1.5. The mode damping and amplitudes were left unchanged.

Fig. 4.12 shows spectrograms of the unshifted processed guitar as well as the mode-shifted version of the same low E pluck. It can be observed that not only is the equalization different, but the frequency-dependent harmonic damping has also changed.

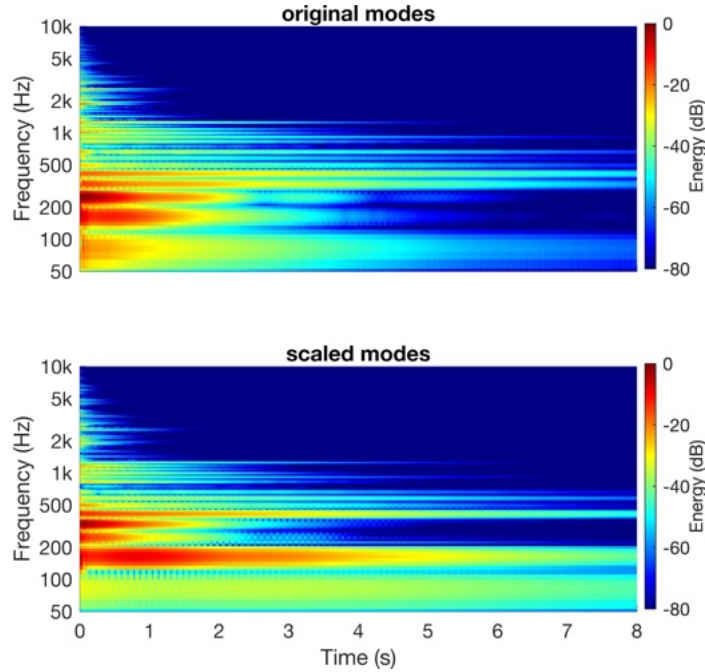


Figure 4.12: Pluck comparison with the measured and mode frequency scaled processing.

4.4 Discussion and Conclusions

A method for processing an electric instrument pickup to replicate the sound of an acoustic instrument is presented. The method does a reasonable job of replicating the equalization and frequency-dependent damping of a measured acoustic guitar as a test case. The basic architecture of the processing works, but multiple improvements could be made to the individual components.

The transient detection is reasonably accurate but still produces false positives occasionally. Notable errors with transient detection can occur during note onsets when multiple transients can be detected. An example of this is when the second or third period of the transient has a higher peak level than the first period, causing multiple transients to be detected. This type of error could be addressed in a naive manner by forcing a minimum amount of time, after which a second transient could occur, or by further refining the transient detection method. Additionally, the transient detection was tuned to work well for typical guitar playing but did not test edge cases such as extremely fast playing or multiple plucking styles such as with the flesh or nail of a finger.

The pitch detection is quite simple and can result in some errors, particularly in the transients.

During transients, if the pitch is not detected, it is set to the lowest pitch possible on the string. This error results in too little artificial string damping being applied, but the decision was made that too little damping is better than too much which can be caused by an erroneous high pitch estimate. If a single note is left to decay, the pitch detection will eventually fail as the guitar signal approaches the noise floor. If the pitch cannot be detected, the artificial string damping will be incorrect, however, since the note has likely decayed to perceptual silence, it is not a problem. A more complex pitch detection method would likely improve the performance of the pitch estimation.

The reflectance correction filter is directly updated at each pitch period, and while there don't seem to be extreme artifacts, a more formal investigation should be made into the variation of the filter coefficients.

The mode fitting in the example is a reasonable approximation but could be improved by optimizing the modal parameters [67, 66]. At high frequencies, measurement limitations make it impossible to approximate the modal structure, so a simple high-pass filter was used to approximate the high-frequency admittance. While the majority of audible sound from a guitar is below this range, and humans are less sensitive to errors at high frequencies, perhaps a more sophisticated high-frequency approximation such as a statistical model of the high-frequency modes could be used [91].

The mounting of the measurement setup of the test case guitar was not perfect and the foam used to damp the strings was placed in front of the soundhole. While this could have some effect on the low-frequency air modes, it was found to be negligible when compared to other measurements of the same guitar in a different mounting configuration. Further, the acoustic guitar measurements serve as a test case for the processing, not as a study of the instrument itself.

While the processing method is inspired by the physics of plucked string instruments, multiple assumptions, and simplifications were made in its current state. The strings are only processed in one dimension for simplicity and because I am not aware of any commercially available pickups that record both directions of the transverse string vibration. Non-commercial 2D pickups have been used in research [136], and 2D admittance measurements of the acoustic instrument could be incorporated, but this extension is something for future study. Similarly, the additional string modulation or string coupling, which has a more prominent effect with acoustic instruments and will occur minimally with the electric instrument were not addressed. The direct sound propagated by the vibrating strings in air has also been ignored at the moment but could be addressed with a microphone near the electric instrument and similar damping correction as applied to the bridge pickup signal.

Both guitars used for the test case were strung with the same set of strings, which simplified the method, but the user may want to achieve the sound of different strings. Since the reflectance damping correction in Sec. 4.2.3 takes the string impedance of both sets of strings into account, the damping due to the string-body interaction is accounted for. However, the damping caused by a string's bending stiffness and by viscous losses of the string moving through the air are not accounted

for. Further work could include factoring in approximate damping changes calculated from differing stiffness and diameters between strings of the electric and simulated acoustic instrument.

The processing is currently implemented offline, but future work includes implementing a real-time version for the guitar, allowing variability of the modeled guitar's modal parameters. The processing inherently works on individual strings since the body-induced damping of each string will be different for each string, resulting in the computational load scaling with the number of strings. With current computational power, it should be possible to run in real-time for most typical plucked-string instruments, though struck-string instruments, like the piano, may be too complex. While the frequency-warped FIR structure is fairly efficient, a fully IIR structure could possibly be made, which is more efficient and would also allow for easier variability of the modal parameters at run-time.

While it is unlikely that any processing can satisfactorily replace the full acoustic characteristics of an acoustic instrument, the hope is that this method could be used by musicians as an effect or by researchers and instrument builders to help study and design instruments.

Chapter 5

Studies in Guitar Measurement and Modeling

5.1 Study 1: Measurements of Acoustic Guitar Top Plates During The Voicing Process [92]

Acoustic guitar top plates are typically constructed out of extremely thin wood, which is not strong enough to withstand the stress caused by the high tension of the strings, leading to the use of wood struts as braces. The bracing design significantly affects the top plate's vibrational characteristics and is seen as one of the fundamental steps to producing a desirable-sounding instrument. Once a bracing pattern is chosen and the top plate is constructed, the braces are carved to minimize the added mass while maintaining stiffness. Luthiers often make voicing decisions by ear by tapping on the top plate and listening to the response. During this study, two steel string acoustic guitar top plates were measured throughout the brace-voicing process. The measurements were analyzed to show how the vibrational modes of the structure evolve as the braces are carved.

5.1.1 Introduction

The guitar is one of the most popular instruments in the world, and there are many different acoustic designs suited for different styles of music. Multiple books and research papers have been written about the construction of acoustic guitars. Still, there remains significant debate among the luthier and player communities into the best methods of construction [21, 38, 31, 46].

This section will focus on the design and construction of the steel string acoustic guitar, in particular, the carving of the braces used to strengthen the top plates of guitars. The top plate is considered to be the most acoustically important part of an acoustic guitar, so the bracing that

supports this thin wooden plate is critical [99]. There has been research that investigated standard and alternative bracing patterns, as well as some that looked at the theoretical effects of brace designs. Still, the actual brace voicing process remains largely lore [17, 62, 24, 25]. The carving of the braces with the goal of emphasizing a desired musical behavior is often referred to as “voicing” the top.

Many luthiers consider the brace carving to be one of the most important aspects of building a guitar and pay particular attention to it. A common method to test the effects of the brace voicing is to tap the guitar top and listen to the resulting vibrations; this is known as *tap testing*. A choice was made to focus on how the brace carving process can affect the vibrational modes of the guitar top throughout the voicing process, attempting to draw insight into this method.

To study the vibrational modes, input admittance measurements were made on the guitar tops. The mechanical input admittance is defined in the frequency domain as the velocity of the structural vibrations divided by an input driving force [131]. Input admittance measurements can be used to show the vibrational characteristics of the structure being measured. Input admittance measurements were taken on the guitar tops at the location where the bridge would later be placed, as this is the location where the strings will be most strongly coupled to the guitar body.

While it is acknowledged that the vibrational characteristics will continue to change as the guitar progresses through the construction process, it would be valuable to know how the effects of the top voicing propagate throughout the process. As well, knowing how the modes develop could help to teach apprentice luthiers to properly voice guitars based on the methods of master luthiers.

5.1.2 Brace Carving

While the main purpose of braces is to supply structural support to the thin guitar top, the braces can be carved to emphasize certain resonances. The bracing patterns used for this study were of the X-bracing style, a typical bracing pattern used for steel string acoustic guitars. Figure 5.1 shows the bracing pattern as well as the brace names.

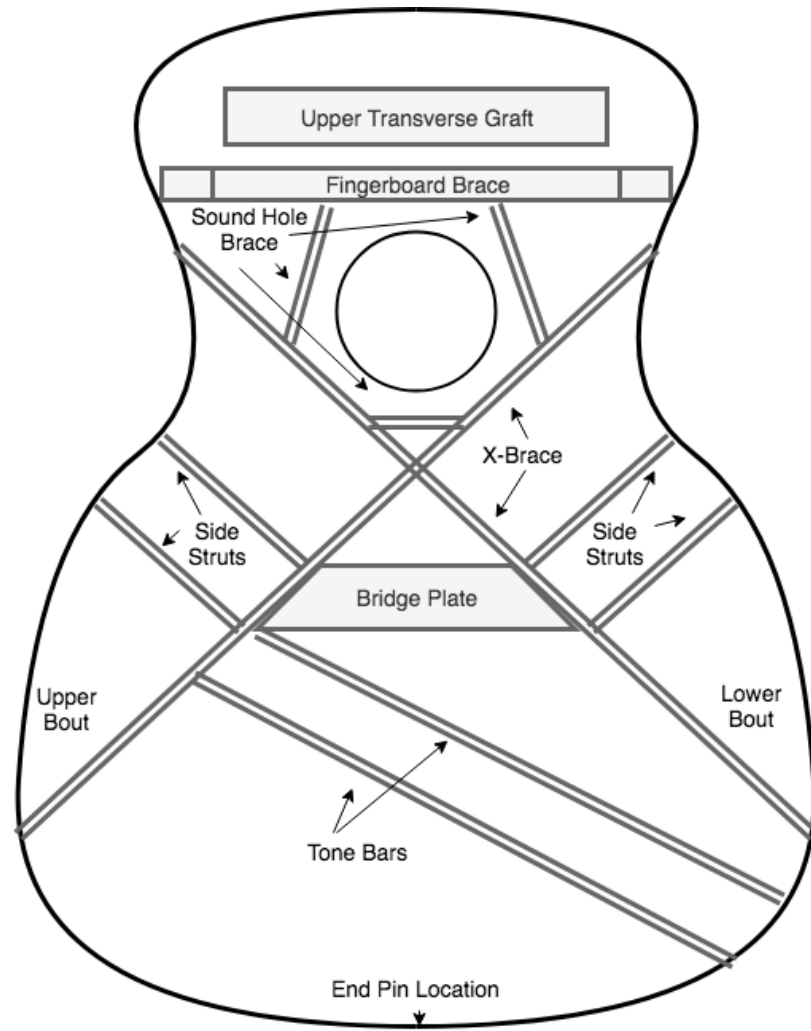


Figure 5.1: Bracing pattern diagram.

During the voicing, the upper transverse graft, soundboard braces, and bridge plate were either minimally carved or not modified. Similarly, the fingerboard brace received minimal carving, with only tapering of the ends to meet the top plate. The majority of the carving was done on the X-braces, tone bars, and side struts. The X-braces and tone bars were scalloped, meaning that wood was removed in the middle of the braces, leaving valleys and peaks. As well, significant tapering was done to the ends of these braces.

Two guitar tops were carved and measured for this study. Both guitar tops were shaped to become orchestra model (OM) sized guitars and will be referred to as OM1 and OM2. The wood used for both tops and their bracing was Adirondack red spruce. OM1 had a tapered thickness of

2.75 mm on the bass side and 2.95 mm on the treble side, while OM2 had a uniform thickness of 2.9 mm. The braces and top had a slight concave shape corresponding to that of a circle with a radius of 10.06 m.

The luthiers performed a tap test to listen to the response of the guitar tops. During the tap test, they would suspend the top with a finger or thumb through the sound hole and tap the front side of the top with a fingertip. The tapping method of the first luthier was to tap in multiple locations of the guitar top, listening to the decay of the different taps. The four main locations of tapping were: where the bridge will be located, on the lower bout, upper bout, and near the end pin. The tapping method of the second luthier was to tap only at the bridge location. While tapping, the perceived pitch and dominant frequencies heard at a particular location differed based on the tapping location. While the perceived pitch differed, the mode frequencies and damping will be the same since the guitar top can be approximated as a linear system, where only the mode amplitudes will change with excitation location. The overall goal of voicing the tops, as described by the luthiers, was to bring out the resonances heard in the tap and try to create a rich tap tone from which multiple overtones could be heard.

Both luthiers followed a general method of carving, which determined the points at which to measure the guitar tops. Figure 5.2 shows the braces at the beginning as well as after three carving steps of OM2. The first carving step involved removing a significant amount of wood to advance the guitar top to a reasonable starting point for more detailed voicing. This means tapering each brace and scalloping the general outline of the X-braces and tone bars. The following carving steps involved more detailed carving where the luthiers were aiming to bring out musical qualities in the tap tone.

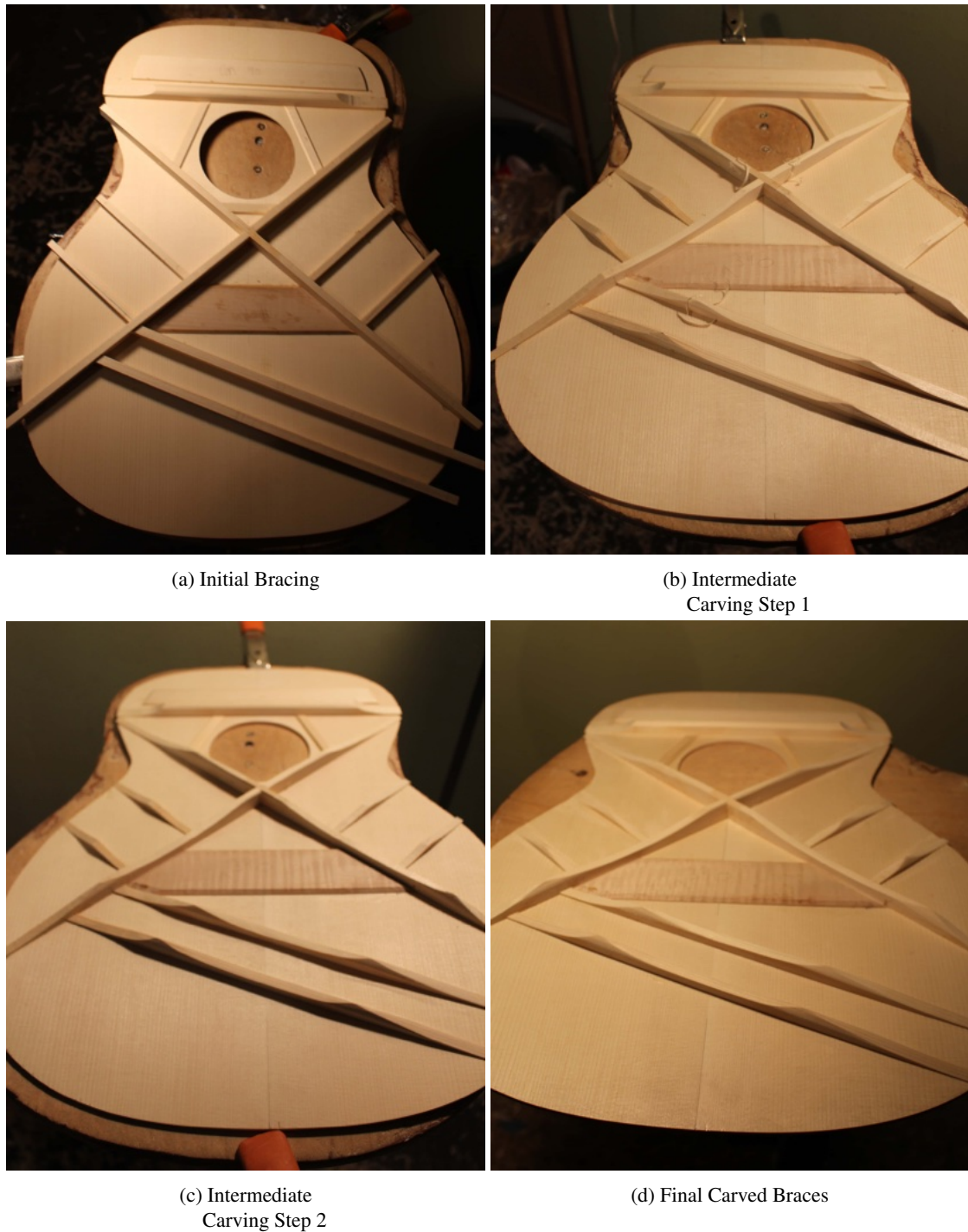


Figure 5.2: Brace carving of OM2.

5.1.3 Measurements

Admittance measurements were taken on the guitar tops using a force-sensing impact hammer (PCB 086E80) to impart a known force and a laser Doppler vibrometer (Polytec PDV 100) to measure the resulting velocity. The coherence was observed throughout the process, and poor-quality measurements were discarded. Although the guitar tops did not yet have bridges, it was decided that admittance measurements would be taken at the location where the bridge would later be placed, as this is where the strings will later be coupled to the instrument. These measurements will be referred to as the pseudo-bridge admittance. Two microphones were also used to record the sound radiated by the impulses, but the measurements were made in an active luthier shop, thereby rendering the microphone signals noisy and not useful. The guitar tops were suspended vertically from the sound hole using a padded arm, which minimized movement of the tops which is similar to how the luthiers would suspend the tops from their thumb while tap testing. The measurement setup is shown in Fig. 5.3. To ensure that the untreated wood was not damaged by the impact hammer, a vinyl tip was used, effectively bandlimiting the signal to around 2 kHz.

Each guitar top was measured before the braces were carved, at two intermediate carving stages, and after the braces were fully carved. The ambient temperature and humidity were 47 % and 22 °C during the carving of OM1, and 49 % and 22 °C during the carving of OM2.



Figure 5.3: Measurement setup.

5.1.4 Results

5.1.4.1 Pseudo-Bridge Admittance

The pseudo-bridge admittance was calculated for each top voicing step by deconvolving the force impulse recorded by the impact hammer from the velocity measurement recorded by the vibrometer. Single admittance measurements are shown in Figs. 5.4 and 5.5 for OM1 and OM2 respectively. The admittance measurements were not averaged, as it was chosen to fit the modes to the individual measurements, then average the modal parameters. It is noted that the velocity measurements of OM1 were slightly clipped and reconstructed. The reconstructions were not perfect, and I do not have confidence in the measurements below approximately 120 Hz.

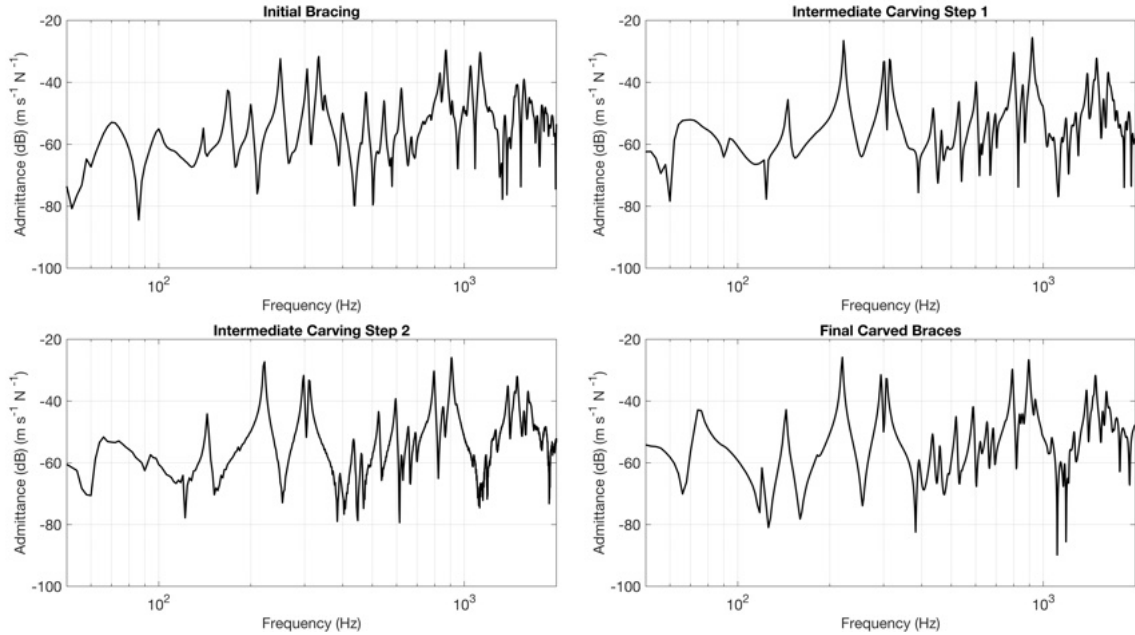


Figure 5.4: Pseudo-bridge admittance of OM1 at the four bracing stages.

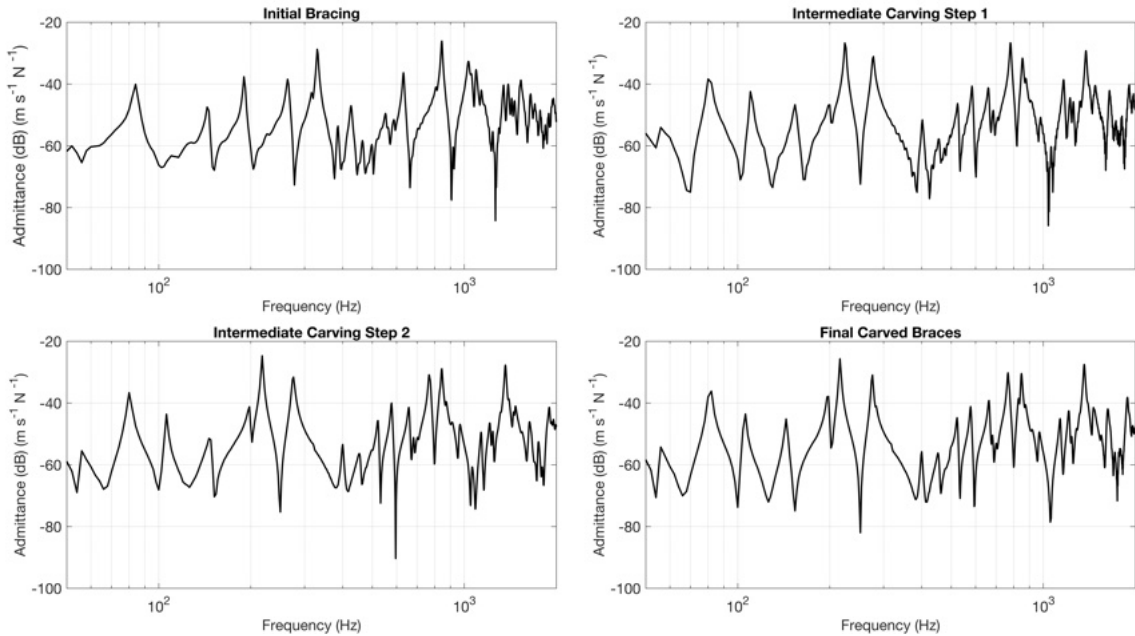


Figure 5.5: Pseudo-bridge admittance of OM2 at the four bracing stages.

5.1.4.2 Mode Fitting

Mode fitting was performed on the pseudo-bridge admittance measurements to gain insight into the mode frequencies, damping, and amplitudes. The mode fitting was performed assuming the modal response of a damped harmonic oscillator having an impulse response of the form,

$$h(t) = \sum_{m=1}^M \gamma_m e^{(i\omega_m - \zeta_m \omega_m)t}, \quad (5.1)$$

where γ_m , ω_m , and ζ_m are the amplitude, natural frequency, and damping ratios of modes $m = 1, 2, \dots, M$ [14, 4]. There are multiple classical modal parameter extraction methods as discussed in Chapter 3, however, the mode fitting was performed using a method derived by Jonathan Abel involving analysis of the eigenstructure of a Hankel matrix of impulse response samples [2]. The model order was derived from the M largest singular values of this decomposition, which can be viewed as the singular values associated with the signal space as opposed to the noise space. Figure 5.6 shows the mode fitting for two admittance measurements of OM2 taken at different voicing steps.

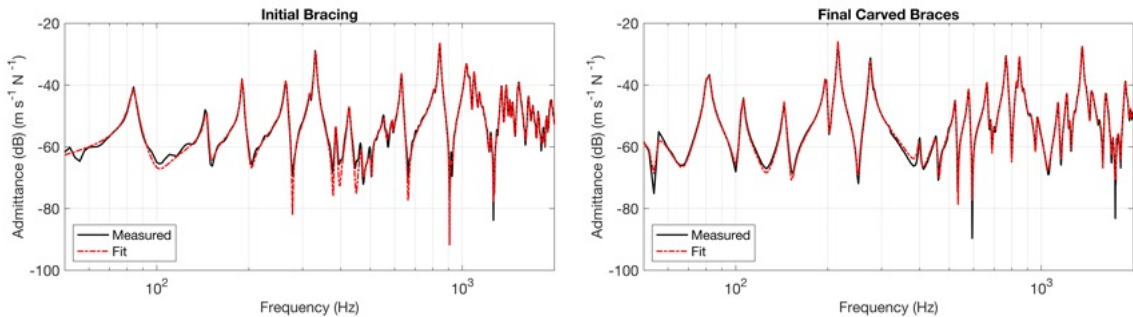


Figure 5.6: Example of mode fitting for OM2.

To facilitate comparison of how the modes develop as the braces are carved, the mode frequencies and damping rates of a number of prominent modes are shown in Fig. 5.7 for each guitar top at various stages of the voicing process. The modes chosen were those below 1 kHz with admittance greater than -50 dB. Only the modes found in the intermediate bracing steps and final bracing are shown here because the modes change quite drastically from those present with the initial uncarved braces. The average mode frequency and damping rate extracted from the mode fittings of multiple measurements are shown, as well as the uncertainty of \pm one standard deviation in the frequency and decay rate. The averaging was done with between 3-5 measurements for OM1 and 9-10 measurements for OM2.

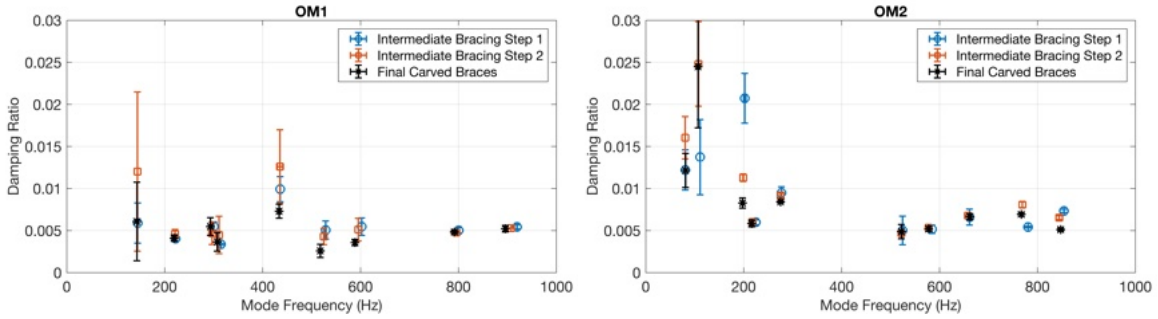


Figure 5.7: Mode frequencies and damping ratios of select modes of OM1 and OM2 \pm one standard deviation.

5.1.5 Discussion

Upon inspecting the admittance frequency response measurements shown in Figs. 5.4 and 5.5, it is clear that the biggest changes to the modes occurred between the initial bracing stage and the intermediate carving stage 1. This is understandable since the brace carving during this step involved removing quite a bit of wood while scalloping out the braces to get to a reasonable starting point for the finer tuning. The parts of the braces hanging over the sides of the guitar tops were also removed during this step. Unlike the initial bracing, the admittance at the intermediate steps and after the tops when fully carved are quite similar, with only subtle differences.

Both guitar tops have a similar overall pseudo-bridge admittance mode layout of a few strong modes below 350 Hz, a slight lull around 400 Hz, a group of stronger amplitude modes around 800 Hz, and another lull around 1 kHz. While the guitar tops may have similar mode amplitude envelopes, there is quite a large variance in the mode frequencies between the two guitar tops. These differences could be explained by the different thicknesses of the top plates, the material properties of each specific piece of wood, or the bracing methodology of the different luthiers.

Figure 5.7 allows us to take a closer look at how a few select low-frequency modes develop as the tops are voiced. In general, the modes shift slightly lower in frequency as more wood is carved away, which implies that the overall stiffness is decreasing at a faster rate relative to the decrease in mass. For some modes, the damping ratio is decreased quite significantly, while for some, the change is subtle. In most cases, the modal damping ratios decrease slightly, meaning the modes will take longer to decay. This confirms the goal of the luthiers to make the guitar body more resonant. However, the damping ratio of some modes actually increases, so there must be a balance to be made regarding the damping characteristics of each mode.

One possible use for measurements like this would be to aid apprentice luthiers in the process of voicing guitar tops. If they were able to see how the modes can change, it could help them gain an understanding of how carving each brace will alter the sound. Knowing information about the initial modal response could also be used to avoid problem areas by shifting the frequencies of

specific modes.

Future work may include investigating an ideal damping ratio for a mode to resonate well in a certain musical context. A low damping ratio will mean that the string energy is easily transferred to the instrument at that frequency, possibly resulting in a strongly radiated sound. However, if the string energy is transferred to the instrument too quickly, it will result in a shorter string decay, known as a dead note [29].

These measurements were part of an ongoing project, including measurements made when the tops were glued to their backs and sides and when the final guitars were completed. The measurements throughout the building process are analyzed in Sec. 5.2. The goal of tracking the progress was to see if predictions could be made about the final modal response based on the modes at intermediate stages.

5.2 Study 2: Measurements of an Acoustic Guitar During the Full Construction Process [88]

Vibration measurements were taken at various stages of the construction of three steel-string acoustic guitars. The construction stages include: the unaltered top plate, braced top plate at multiple steps during the brace carving, glued guitar body before and after sanding, and the completed guitar. Measurements were taken with a laser Doppler vibrometer and force hammer to analyze the mode frequencies, damping, and amplitudes, and track how they evolved. The motivation is to investigate which building steps create the most significant vibrational changes and gain insight into the significance of each change. This knowledge can help instrument builders know at which stage they can make specific alterations and how much variation they can expect to see during the remainder of the construction.

5.2.1 Introduction

The study in Section 5.1 focused on the top plate voicing of two guitars. This study explores measurements of the guitars as their construction was completed. Additionally, a third guitar built by the author was studied. These measurements are of an exploratory nature with the purpose of trying to see which trends appear in the modal structure of the guitars as they are being built.

5.2.2 Guitars

Two of the guitars studied were the same orchestra model guitars built by the Santa Cruz Guitar Company as described in Section 5.1. The reader is directed to Sec. 5.1.2 for more details. These guitars are again referred to as OM1 and OM2.

The third guitar was the first guitar constructed by the author. This guitar was built from a kit purchased from StewMac, a luthier supply store [116]. The guitar is based on a 1930s Martin 000-28 which is an X-braced acoustic guitar with the body and neck meeting at the 12th fret. This guitar will be referred to as the 000-28. The back and sides of the guitar are Indian rosewood, the neck is mahogany, and the fingerboard is ebony. The top plate and braces are torrefied Sitka spruce. Torrefied wood is thermally treated wood, which modifies the structure of the wood, generally with an attempt to replicate naturally aged wood. Studies of torrefied wood have shown that the parameters relevant to instrument soundboard materials, such as density, longitudinal stiffness, radiation coefficient, and damping can be significantly altered [23]. The author does not know what heating parameters were used for the wood for this guitar as it was already torrefied when purchased, so the study is not an in-depth study into torrefied wood for guitar making, but some observations can be drawn. While the guitar was built from a kit, the kit consisted of mostly rough cutting and carving, meaning that all construction and final decisions were left to the builder. Notable

construction steps that largely affect the sound, such as the top and back thicknessing and sanding, and brace carving were left to the builder.

Professional luthiers constructed the two OM guitars, while the 000-28 was constructed by an amateur, so naturally, the methods used for construction were different. The guitars are also not of the same geometry or woods so they cannot be directly compared. Some notable construction differences are pointed out here in case the reader is interested. The two OMs have dovetail neck joints, while the 000-28 has a bolt-on neck. The two OMs were finished with a nitrocellulose finish, while the 000-28 has a hand-rubbed shellac French polish. The OMs have 1930s-style “belly” bridges, while the 000-28 has a “pyramid” style bridge, typical of guitars older than the 1930s. The OMs are 14-fret guitars, meaning that the neck meets the body at the 14th fret, while the 000-28 is a 12th-fret guitar. The OMs have “paddle” style heads while the 000-28 has a “slotted” head.

5.2.3 Measurements

The OM top measurements are described in Sec. 5.1.3. The further measurements of these guitars were performed in a similar manner in the guitar shop. The 000-28 was constructed at the Center for Computer Research in Music and Acoustics (CCRMA) by the author, so many more measurements could be made since it was always close to the lab and equipment.

5.2.3.1 Measurement Setup

The further measurements of the OMs and all measurements of the 000-28 were performed with a force-sensing impact hammer (PCB 086E80) and laser Doppler vibrometer (Polytec PDV-100). The impact location was chosen as where the bridge would eventually be located to perform pseudo-bridge admittance measurements when there was no bridge and actual bridge admittance measurements once the bridges were attached.

The OMs were measured in a guitar shop, so there was more noise than if measured in a lab environment. The 000-28 was measured in a lab with closer to ideal conditions. All measurements were done by mounting the guitar or partially constructed guitar sitting vertically supported by the upper bout as shown in Fig. 5.8. The guitar is mounted on two metal rods wrapped in foam. Ideally, the instrument would be mounted in free conditions, but considering the different stages of construction, this was not possible, so the described mounting was used.



Figure 5.8: Measurement setup for guitar stages.

5.2.3.2 Measurement Stages

The OMs were measured at three stages in addition to the top plates being carved. The 000-28 was measured at many more stages, as described below, with photos to demonstrate the progress made.

Top Carving The 000-28 top with braces was measured at four stages, similar to those of the two OMs as shown in Fig. 5.9. The first stage consisted of the uncarved rectangular braces. The second and third stages were intermediate stages, as the braces were carved down to lower their mass. The fourth stage is when the braces are completely carved.



Figure 5.9: 000-28 top carving stages. Un-carved (top left), carving stage 1 (top right), carving stage 2 (bottom left), and the final carving (bottom right)

Box Not Sanded

The two OMs were measured again once the box was completed, meaning that the top and back were glued to the sides, as shown in the bottom row of Fig. 5.10. For these measurements, the top and back were not yet trimmed to be flush with the body and thus overhanded slightly. This

measurement stage was not done for the 000-28.

The 000-28 was measured with the top and sides joined but without the back. Additionally, the 000-28 was measured once the box was completed and the binding had been installed, but before the final sanding occurred. These stages are shown in the top row of Fig. 5.10



Figure 5.10: Guitar box before final sanding. 000-28 with top and sides (top left), 000-28 box (top right), OM1 box (bottom left), and OM2 box (bottom right)

Box Sanded The next stage was when the box was fully built, the binding was attached, and the top, back, and sides were sanded, as shown in Fig. 5.11. All three guitars were measured at this stage. This stage is of particular interest because it is the final step when significant changes, such as altering the thickness of the top and back can be made. After this step, the finish is applied, so the only structural change that can be made is to trim the braces from the inside of the guitar, which is possible but rather difficult. Note that the 000-28 has the neck joint pocket cut at this stage, but the two OMs do not. This should not have a significant effect on the vibratory response.



Figure 5.11: Guitar box after final sanding: OM1 (top left), and OM2 (top right), and 000-28 (bottom)

During Finish The 000-28 box was measured during three stages when the finish was applied, as shown in Fig. 5.12. This guitar had a hand-rubbed French polish finish which was applied in roughly 50 very thin coats. The measurements were spread out at about 1/3, 2/3, and 3/3 of the coats.

After each coat, a slight amount of mass is added to the instrument as the shellac is rubbed on.



Figure 5.12: 000-28 finish stages. First coat (top left), Four coats (top right), and fully polished (bottom left).

Completed Guitar All three guitars were measured once complete, strung up, and tuned to pitch. The 000-28 is shown at the bottom of Fig. 5.13, and the OMs are shown in Fig. 5.14. The 000-28 was also measured with the neck attached and no bridge, as well as once the bridge was glued on,

but with no strings as shown in the top row of Fig. 5.13.



Figure 5.13: 000-28 stages with neck: with neck (top left), with bridge (top right), and complete (bottom left).



Figure 5.14: OM1 (left) and OM2 (right) complete.

5.2.4 Results and Conclusions

The pseudo-admittance and admittance measurements for each stage of the three guitars are shown here, with some discussion of the changes. The box and further stages of the OMs are shown in Figs. 5.15 and 5.16. All stages of the 000-28 are shown in Figs. 5.17–5.20. Mode fitting is performed on all of the measurements so that the modal evolution of some of the modes can be shown in Figs. 5.21–5.23.

Looking at both OMs, the third mode, around 350 Hz is not present when the box is built but not sanded. This mode begins to appear when the box is sanded but is not nearly as prominent as it is with the completed guitar. The frequencies of the lowest observable modes shift lower as the guitar is finished, likely due to the mass of the finish being applied. Additionally, the amplitudes of these modes decrease as the guitar is completed. In both guitars, a cluster of high amplitude modes is present, centered around 700 Hz. Once the finish is applied and the neck is added, these modes are reduced in amplitude in addition to likely shifting in frequency. Unfortunately, mode shape scan measurements were not made, so these upper modes cannot be reliably tracked between measurements.

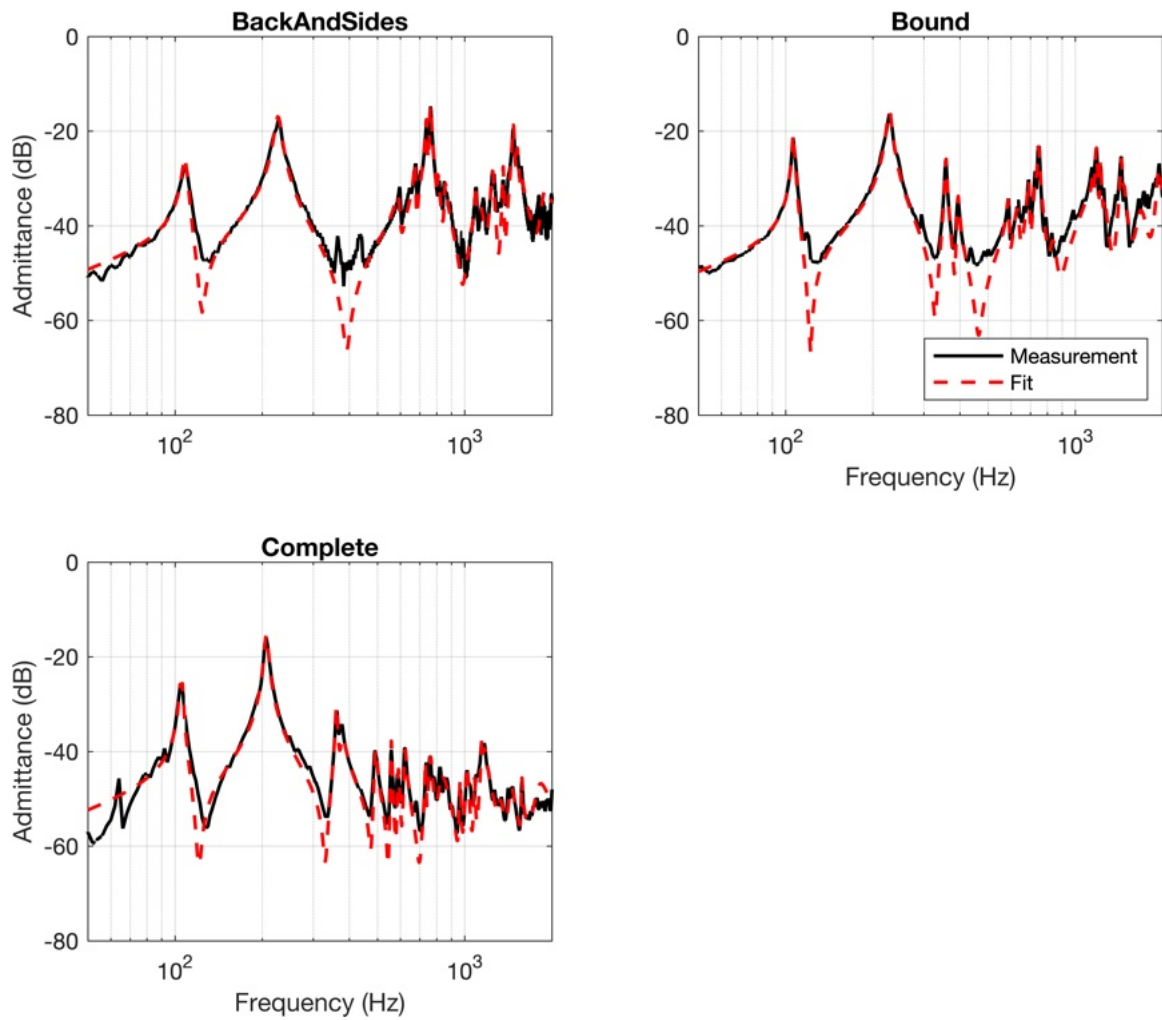


Figure 5.15: OM1 Body stages measurements.

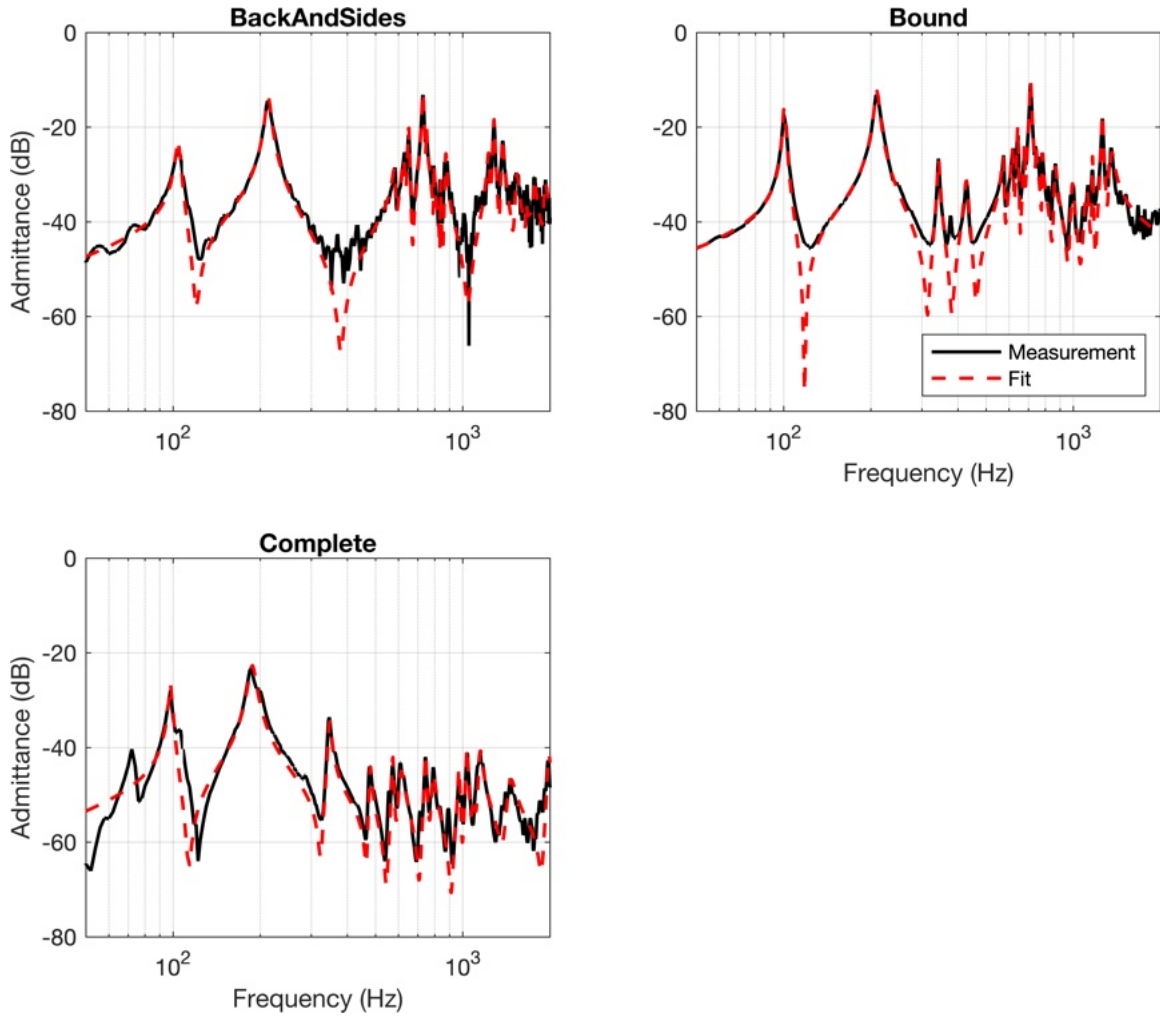


Figure 5.16: OM2 Body stages measurements.

Similar to the OMs, it is difficult to track significant progress as the top is carving, but general observations can be made by viewing the graphs in Fig. 5.17, such as the highest amplitude mode around 240 Hz lowers in frequency and increases in amplitude as the braces are carved. In general, the modes have an increased amplitude as the top is carved, which is likely a desirable outcome.

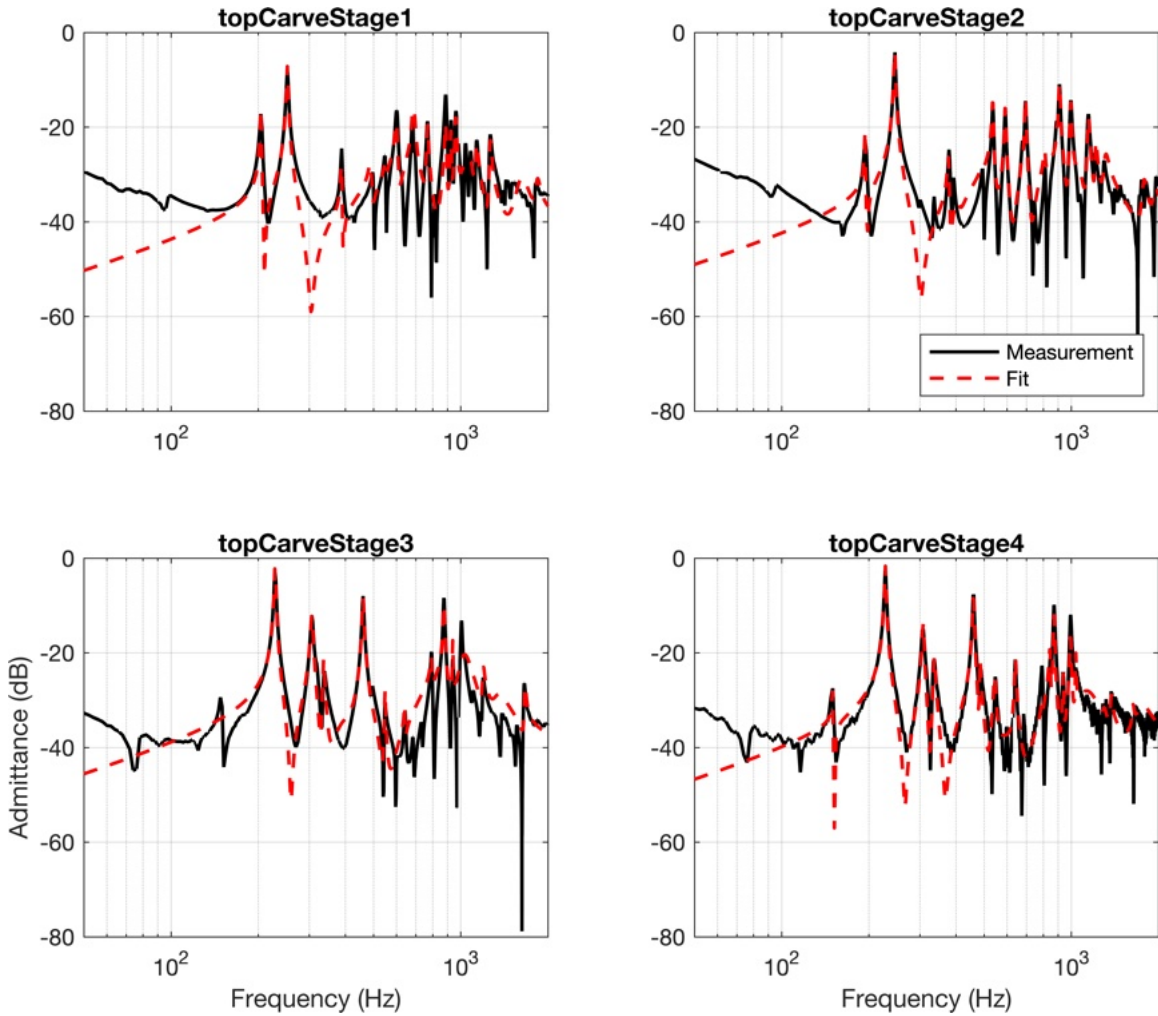


Figure 5.17: 000-28 top carve measurements.

The body stage measurements of 000-28 are shown in Fig. 5.18. When just the top and sides are included, there is a strong resonance from the top plate at around 240 Hz. There is also a resonance around 150 Hz, likely associated with the sides which are essentially in free boundary conditions where the back should be. Once the back is attached, the typical breathing modes at around 120 and 240 Hz appear as the air coupling between the top and back arises.

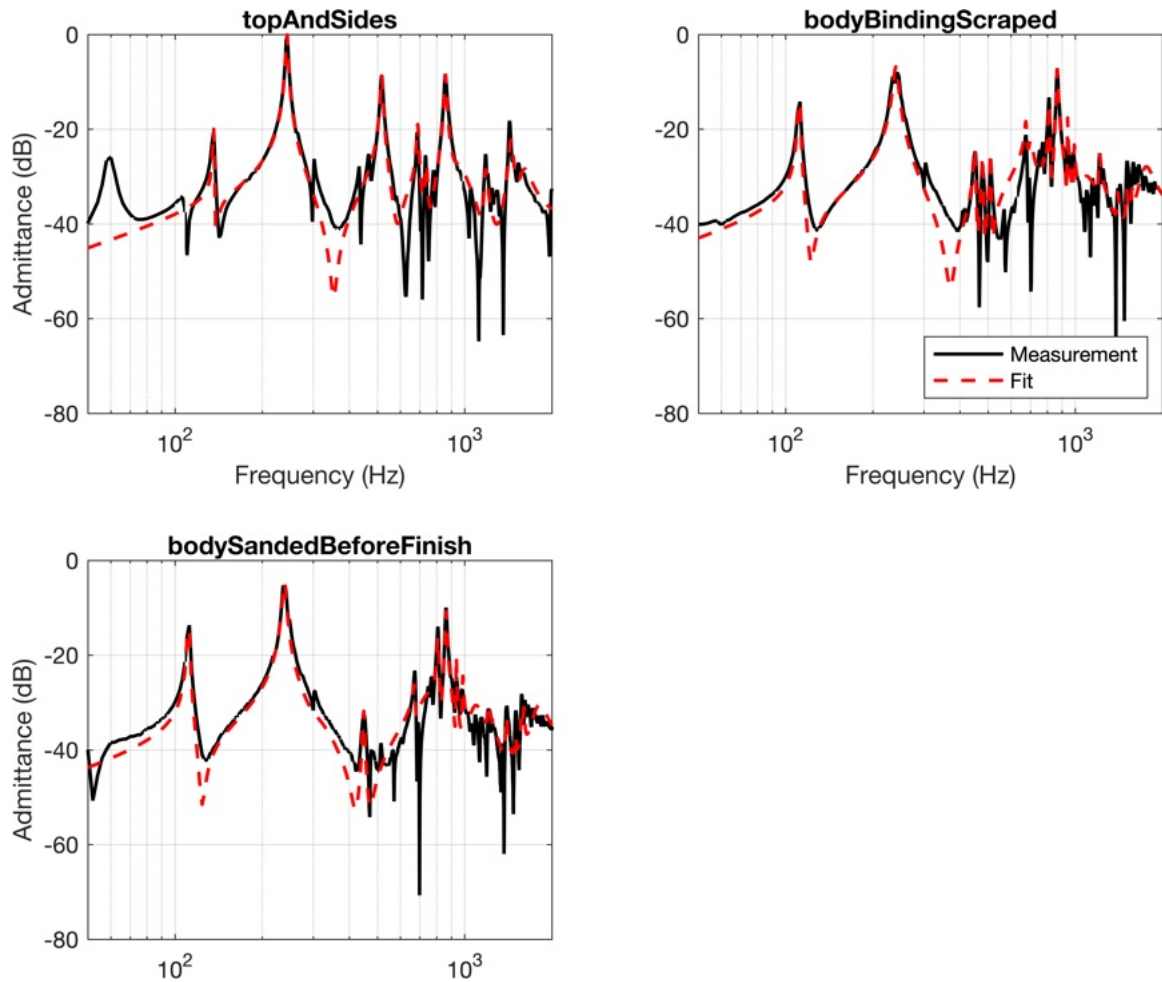


Figure 5.18: 000-28 body stage measurements.

Observing the changes as the finish is applied to the 000-28 as shown in Fig. 5.19, it can be observed that the breathing modes decrease in amplitude and frequency as more coats of finish are applied.

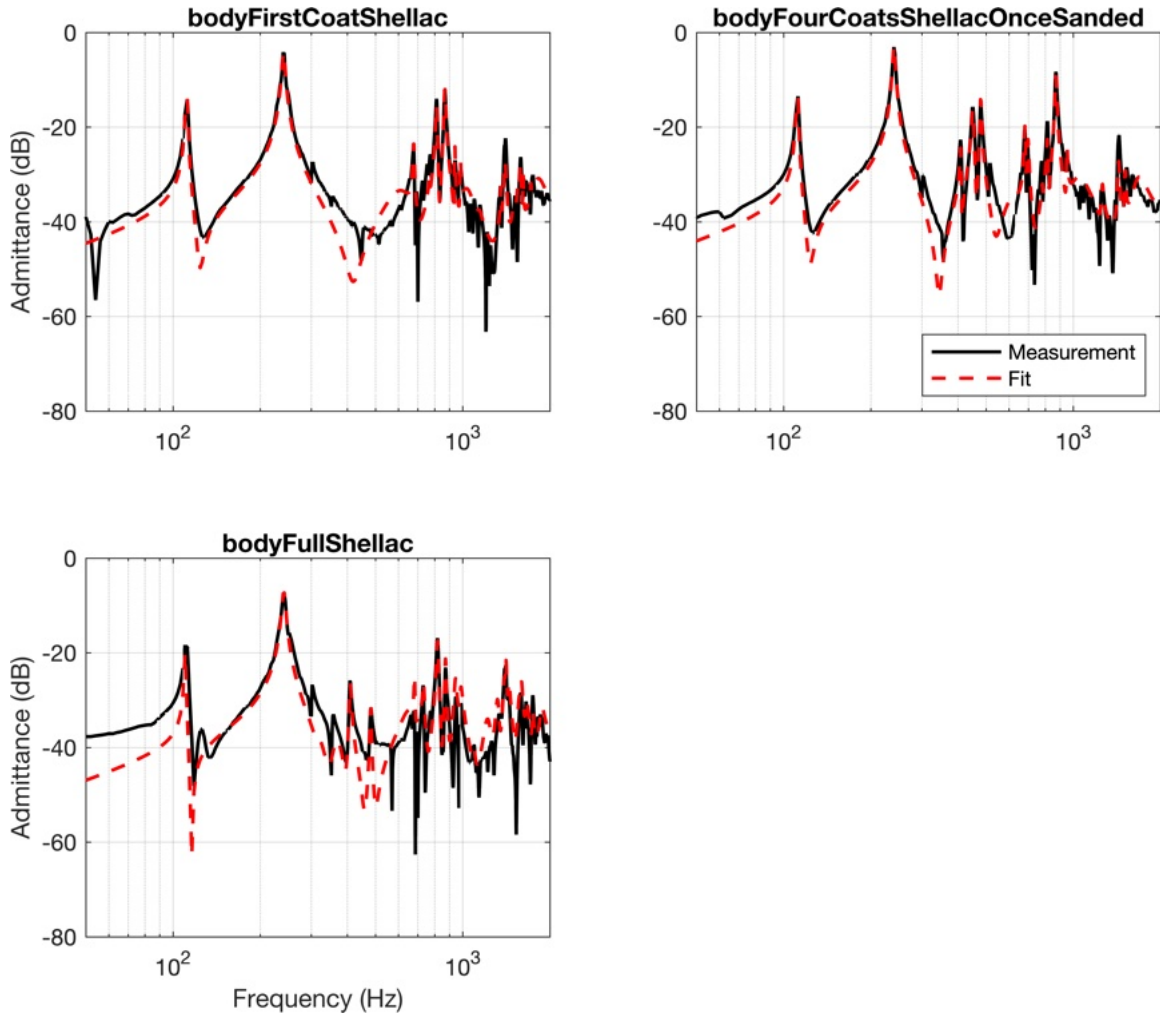


Figure 5.19: 000-28 finishing stage measurements.

Figure 5.20 shows the 000-28 with the neck attached and no bridge, with the bridge but no strings, and the completed guitar. There are noticeable changes to the admittance when the bridge is glued to the instrument, which makes sense as a significant mass is being added to the top plate. The ~ 240 Hz mode is lowered significantly in frequency by about 20 Hz, and the amplitude is also decreased slightly. The cluster of modes around 1000 Hz is also decreased in amplitude when the bridge is added. The changes with and without the strings are quite small.

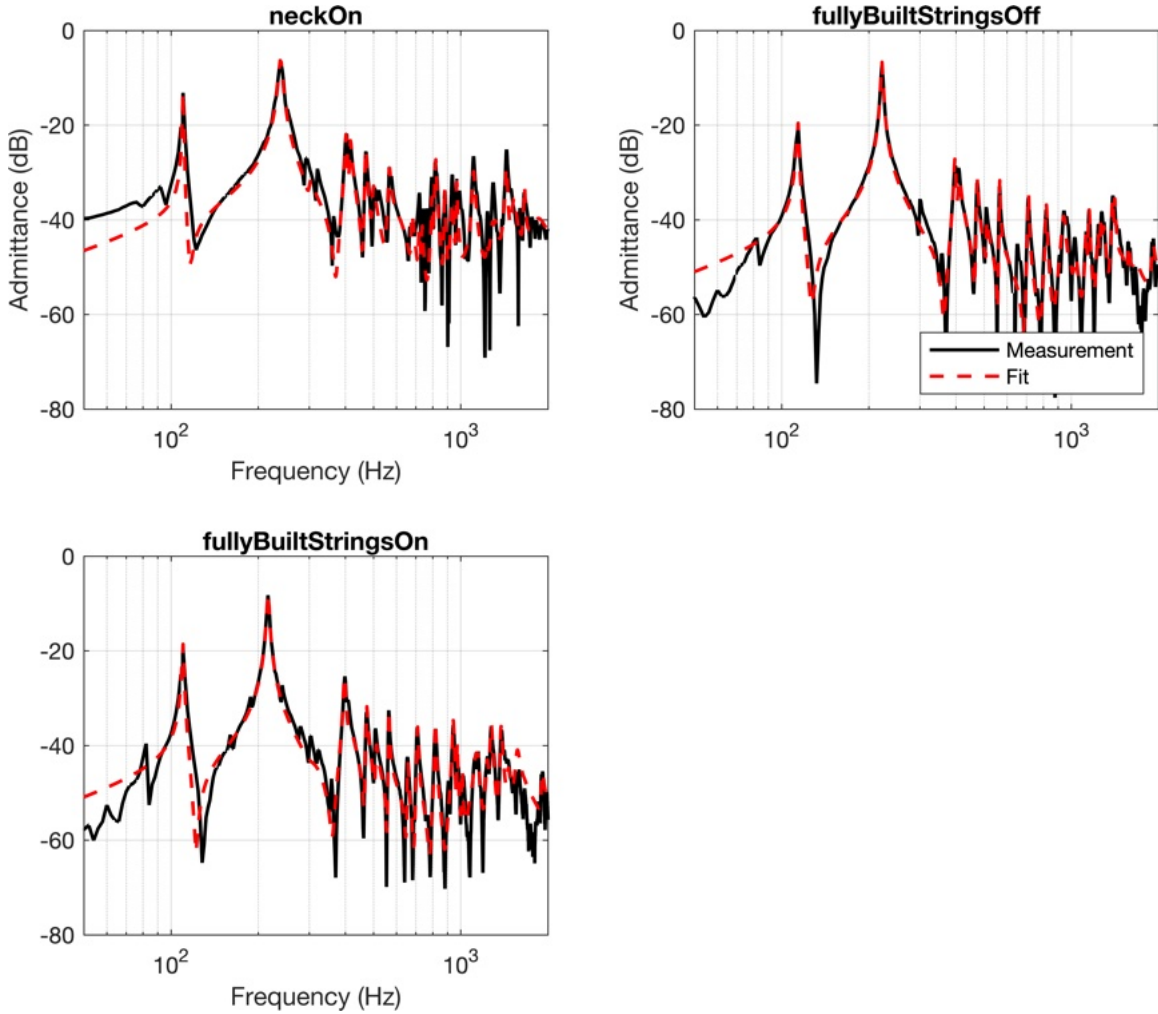


Figure 5.20: 000-28 neck on stage measurements.

It is difficult to pick out specific trends from only viewing admittance graphs, so Figs. [5.21]-[5.23] show the trends show some modal trends. These figures show the modal evolution of the frequencies, damping ratios, and amplitudes of the first three significant modes, notably those around 110 Hz, 220 Hz, and 350 Hz.

Figure [5.21] shows the frequency evolution. For each instrument, the first and second modes decrease in frequency as the instrument is built. Interestingly, in each guitar, the first mode decreased minimally from the completed box to the completed guitar, while the second mode decreased by roughly 20 Hz. While the two OM's have the same geometry, barring bracing differences, the frequencies of the first three modes are significantly lower for OM2 than for OM1, suggesting that the major differences are in the materials used. Unfortunately, the material parameters of the woods used are

not known for these guitars. The 000-28 has even higher frequencies for the first three modes than the two OMs, even though the internal volume is larger. This suggests that the wood for the OM is significantly different, likely having a higher stiffness-to-density ratio, which is supported by other literature on torrefied woods [23].

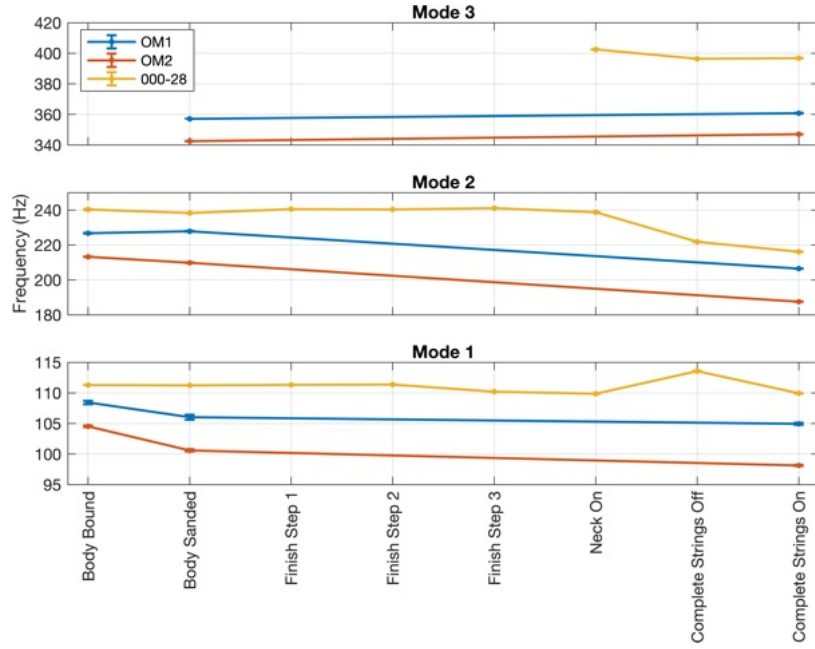


Figure 5.21: Mode frequency evolution of OM1 (blue), OM2 (orange), and 000-28 (yellow).

Figure 5.22 shows the damping ratio evolution for the first three modes. There don't appear to be clear trends in the progression of the modal damping ratios, but some observations can be made. Interestingly, the damping ratios for each of the three modes for OM2 increase as the guitar goes from the box to the completed guitar, while the same damping ratios decrease for OM1; I am unsure what would cause these changes. A notable observation is that for modes 1 and 2, the damping ratios for 000-28 are significantly lower than for the OMs. This follows with what would be expected for torrefied spruce, but further study should be done.

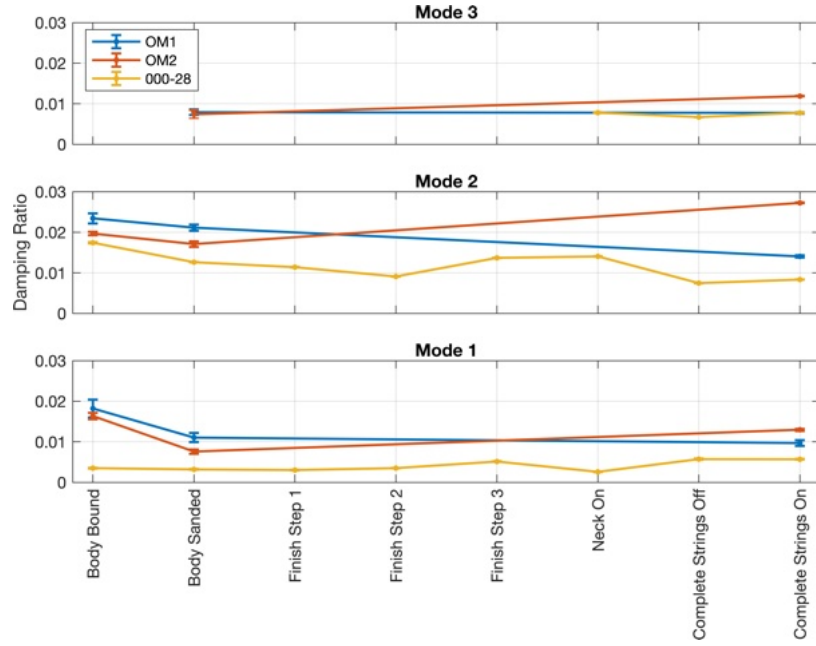


Figure 5.22: Mode damping ratio evolution of OM1 (blue), OM2 (orange), and 000-28 (yellow).

Figure 5.23 shows the amplitude evolution for the first three modes. The amplitudes are shown such that the first measurement stage is set at 0 dB, and the following stages are adjusted relative to this level. As the box is sanded, the amplitudes increase slightly, but as the guitar is built further, the mode amplitudes decrease, which is expected since more mass is being added with the finish and bridge.

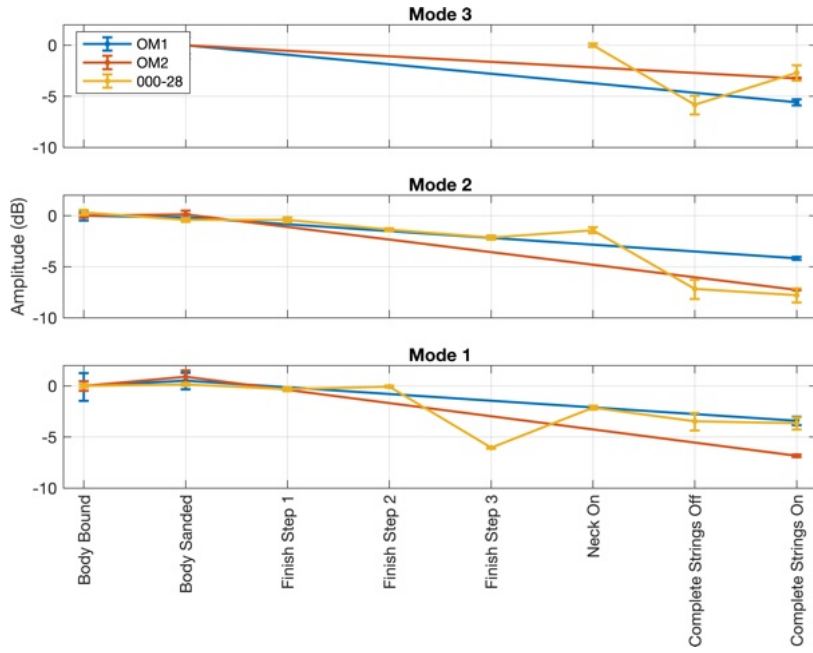


Figure 5.23: Mode amplitude evolution of OM1 (blue), OM2 (orange), and 000-28 (yellow).

This study shows pseudo-bridge admittance measurements of three guitars as they were constructed. Some trends and conclusions can be made, but it is not an easy problem since the same modal structure is not present at each construction stage, so individual modes cannot be reliably followed except in some instances. Some general suggestions and observations are presented here but are not definitive.

If a builder wishes to make measurements of an instrument and vary the geometry for consistency, and map this to the final instrument, I would suggest making the final measurements just before the finish is applied and making changes to the top and back thickness at this point. Any alterations before this point could be difficult to map precisely with a predictable outcome. Further changes could be made once the guitar is completed by reaching into the sound hole and further carving the braces, but this is physically difficult.

If a builder wishes to track individual modes of the instrument, the first two breathing modes are reliably present at each measurement stage once the box is closed. These modes are quite strong and isolated, so it is possible to fit the frequencies, damping ratios, and amplitudes reliably. The higher frequency modes are not present to a significant degree at each measurement stage. They are also located closer to other modes, making it difficult to reliably track their progress without mixing up the modes.

5.3 Study 3: An Exploration of Guitar Neck Admittance Measurements Taken at Different String Stopping Locations [94]

String instrument synthesis models have typically ignored the influence of the string-stopping position when modeling the string boundary conditions at the neck. This simplification neglects the differences between frequency-dependent wave reflection phenomena taking place at the string boundary when it is stopped at different positions along the neck. Driving-point admittance measurements were taken at the bridge of an electric guitar, and also at various stopping positions along the neck: open string, 2nd, 4th, 6th, 8th, and 10th fret. The acquired data is explored and comparisons are made between the boundary reflectance functions as computed for the bridge and the various stopping positions. As a test case, the measured and theoretical string decay times for one particular note are compared.

5.3.1 Introduction

Stringed instruments, such as guitars, involve the transfer of vibrational energy from a set of strings into a body, which serves as a more efficient radiator of acoustic energy. The energy of vibrating guitar strings is transferred to the instrument at the string termination points, the bridge, and the stopping location along the neck. The mechanical “input admittance” or “driving point mobility” is defined in the frequency domain as the velocity of the structure divided by the input force driving the structure at a given location and in a given direction. The admittance shows the ability of the guitar body to be displaced as a function of frequency, providing insight about the vibrational modes and string decay time [69] [130]. Input admittance is often measured at the bridge on a hollow instrument as this will give a good estimate of the instrument’s vibrational characteristics which will result in sound [130]. Admittance is the inverse of impedance, which can be used to calculate the string reflection coefficient

$$r = \frac{Z_b - Z_c}{Z_b + Z_c} \quad (5.2)$$

where Z_c and Z_b respectively represent the characteristic string and bridge impedance functions at the boundary. This amplitude reflection coefficient is the ratio of an incoming wave amplitude to the reflected wave amplitude. The string termination along the rigid neck will not result in a significant amount of sound compared to the termination at the mobile bridge, so this termination is often ignored when considering the instrument’s radiated sound [28]. However, this termination will affect the stopping location string reflectance as there are vibrational modes of the neck, affecting the string decay rates [28].

The purpose of this work is to use input admittance measurements to study the boundary conditions at the bridge and stopping location along the neck of an electric guitar. A first exploration of how much energy is lost at the string ends is performed by computing the corresponding reflectances,

with the aim of foreseeing the importance of including a model for the neck losses to attain accurate string decay times in a future synthesis model.

The rest of the section is organized as follows. Section 5.3.2 gives details on the experimental setup used to measure neck and bridge admittances as well as string decay times. In Section 5.3.3, the admittance measurements as well as an example of computed reflectance functions are presented. A simplified method to predict string decay times is presented and compared to an example of measured string decay. Section 5.3.4 discusses the measurements, missing factors in the decay time prediction, and proposes future steps.

5.3.2 Measurements

Admittance measurements were made on a guitar to observe the body and neck vibrations. String decay measurements were then made to explore the relationship between the neck vibrations and the string decay. A hollow-body electric guitar with a floating bridge and two electromagnetic pickups was measured. The measurements were taken in a semi-anechoic room with the guitar hung from the ceiling by the tuning pegs, and lightly resting against foam for stability. The setup for the admittance measurements is shown in Figure 5.24. The guitar was strung with flatwound strings which were tuned to pitch.



Figure 5.24: Experimental setup for admittance measurements.

5.3.2.1 Admittance

To measure the admittance of the guitar, the instrument was struck with a force-sensing hammer (B&K 8203) while a laser Doppler vibrometer (Polytec PDV 100) was used to measure the velocity. The hammer strike and laser measurement locations are made as close as possible to obtain a driving point admittance. The signals were pre-amplified to the appropriate level and recorded through a National Instruments data acquisition card with a sample rate of 44.4k Hz and 16-bit sample resolution. All strings were damped using a combination of thick card stock and elastic bands. Each measurement was triggered as soon as the impact hammer came in contact with the guitar

and lasted for 2 seconds. For each location, 5 consecutive measurements were made and averaged, observing the coherence between the measurements and discarding any erroneous measurements. The bridge admittance was measured in the vertical (normal to the guitar top plate) and horizontal (along the direction of the bridge) directions. The impacts were made near the low E string; this position was chosen because the low E is the thickest string, thus providing strong coupling to the body. Admittance measurements were also made on the neck at the open position, 2nd, 4th, 6th, 8th, and 10th frets. The open position admittance was measured with a driving point on the nut in the vertical and horizontal directions. The admittance was measured at each fret position on the fret for the vertical direction, and near the fret on the side of the neck for the horizontal direction. All admittance measurements were also recorded with calibrated microphones to later calculate the instrument's radiativity for synthesis purposes.

5.3.2.2 String Decay

In order to justify the stopping location admittance method and evaluate later synthesis, string decay measurements were made. A “wire break” method was used as it is more reproducible than a human pluck. A copper wire is looped around and pulled across the string such that it abruptly snaps at a repeatable level of stress, imparting an approximate step function (being more flat at low frequencies and rolling off at high frequencies above 10 kHz) in a known direction. It is difficult to know the exact force the wire exerts when it snaps, but it is consistent between tests, and the measurements are only concerned with the relative amplitude of vibrations [129]. Copper wire of gauge 40 on the American wire gauge scale (0.0799 mm) was chosen as it produced a string displacement similar to that of an average guitar plectrum. The signals were pre-amplified to the appropriate level and recorded through a National Instruments data acquisition card with a sample rate of 44.4 kHz and 16-bit sample resolution. Each measurement was triggered as soon as the wire broke and lasted for 10 seconds. The output from the electromagnetic pickup nearest to the neck was recorded with the guitar’s tone and volume controls at a maximum value, imparting no additional filtering. The vibrational axis of the strings will change with time [102], but guitar pickups are most sensitive in the direction perpendicular to the top plate of the guitar [77], so the measurements will approximate the vertical transverse string motion. The string plucks were also recorded with two calibrated microphones to later compare the radiated sound to that of the strings alone, as measured by the electromagnetic pickups. The strings were plucked at a constant distance away from the bridge at an angle of 45° between the vertical and horizontal axes. In order to measure the fretted notes, a “capo” (a device that clamps all of the strings to a particular fret) was placed on the corresponding fret. All strings that were not being measured were damped using heavy card stock and elastic bands.

Once recorded, the string decays measured through the electromagnetic pickup were analyzed. A short-time Fourier transform was used to determine the amplitudes of the first five harmonics at

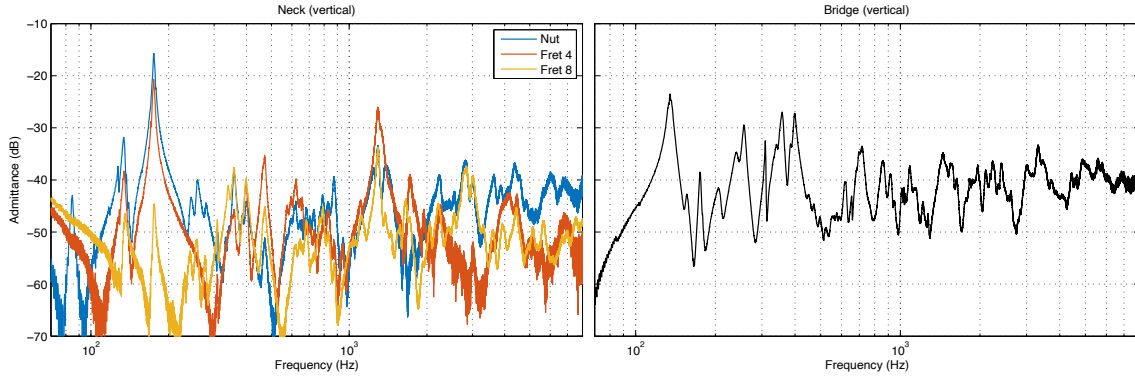


Figure 5.25: Magnitude response of the vertical admittance measurements made at the bridge, open position, 4th fret, and 8th fret.

each time frame. The peaks of the first five harmonics were determined in a general range based on their theoretical frequency. Since the string frequencies will vary slightly over the duration of the decay, the frequency and amplitudes were calculated more carefully by using parabolic interpolation. The harmonics were then analyzed to determine the time each took to decay by 15 dB, assuming an exponential decay.

5.3.3 Observations

Bridge admittance measurements in the vertical and horizontal directions are shown in the right columns of Figures 5.25 and 5.26. The left columns of Figures 5.25 and 5.26 show the vertical and horizontal admittance measurements made at the stopping locations corresponding to the open position, 4th fret, and 8th fret. When observing Figures 5.25 and 5.26, it can be seen that there are three modes of high amplitude at 85, 175, and 332 Hz, which are likely caused by the neck bending modes. The amplitudes of the modes at 175 and 332 Hz decrease at positions along the neck approaching the bridge, suggesting that they are near the nodes of the bending modes.

Figure 5.27 shows the magnitude responses of the bridge and open position admittance in the vertical and horizontal directions as well as string decay plots, which show the time for the first 5 harmonics to decay by 15 dB in the vertical direction as measured through the electromagnetic pickup. Each circle colour corresponds to the first five harmonics of an individual string. This serves as a way to observe the overall decay rate of the strings with respect to the measured admittance.

The reflection coefficient functions for the bridge, open position, 4th fret, and 8th fret of the low E string were calculated as described in equation 5.3.1, and the amplitude is shown in Figure 5.28. The string characteristic impedance was calculated from manufacturer data to be to $0.8702 \text{ N m s}^{-1}$ [22]. As it can be observed, losses at the neck should not be neglected: for some frequencies, they are comparable to those at the bridge.

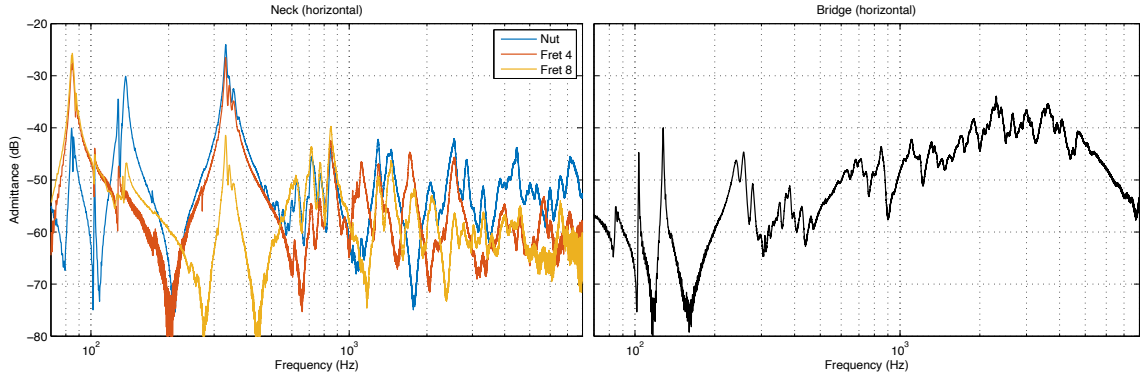


Figure 5.26: Magnitude response of the horizontal admittance measurements made at the bridge, open position, 4th fret, and 8th fret.

Assuming that energy is only lost through the bridge admittance, neck admittance, and propagation losses, the change in amplitude ratio G over one period can be calculated as

$$G = \frac{A}{A_0} = r_B \cdot r_N \cdot r_S \quad (5.3)$$

where A_0 is the original amplitude, A is the final amplitude after one period, r_B is the bridge reflection coefficient, r_N is the stopping location reflection coefficient, r_S is the propagation loss coefficient for one period of vibration. The reflection coefficients r_B and r_N represent the losses through one reflection from each end, respectively. This can be arranged to calculate the decay time t_L for the transverse string motion to decay by a certain amplitude as follows

$$t_L = \frac{\gamma_L}{f_0 20 \log_{10}(r_B r_N r_S)} \quad (5.4)$$

where f_0 is the fundamental frequency in Hertz, and γ_L is the decay amplitude ratio in dB. This method can be used to predict the vertical and horizontal transverse string decay by using the respective vertical and horizontal reflection coefficients.

Table 5.1 shows the measured decays as well as the computed vertical transverse decays of the first 5 harmonics of a pluck of the open low E string. The amount of decay, γ_L was set to -15 dB and the string air propagation loss r_S is assumed to be equal to 1 at all frequencies as an initial simplification. As expected from the imposed simplifications, significant differences were observed.

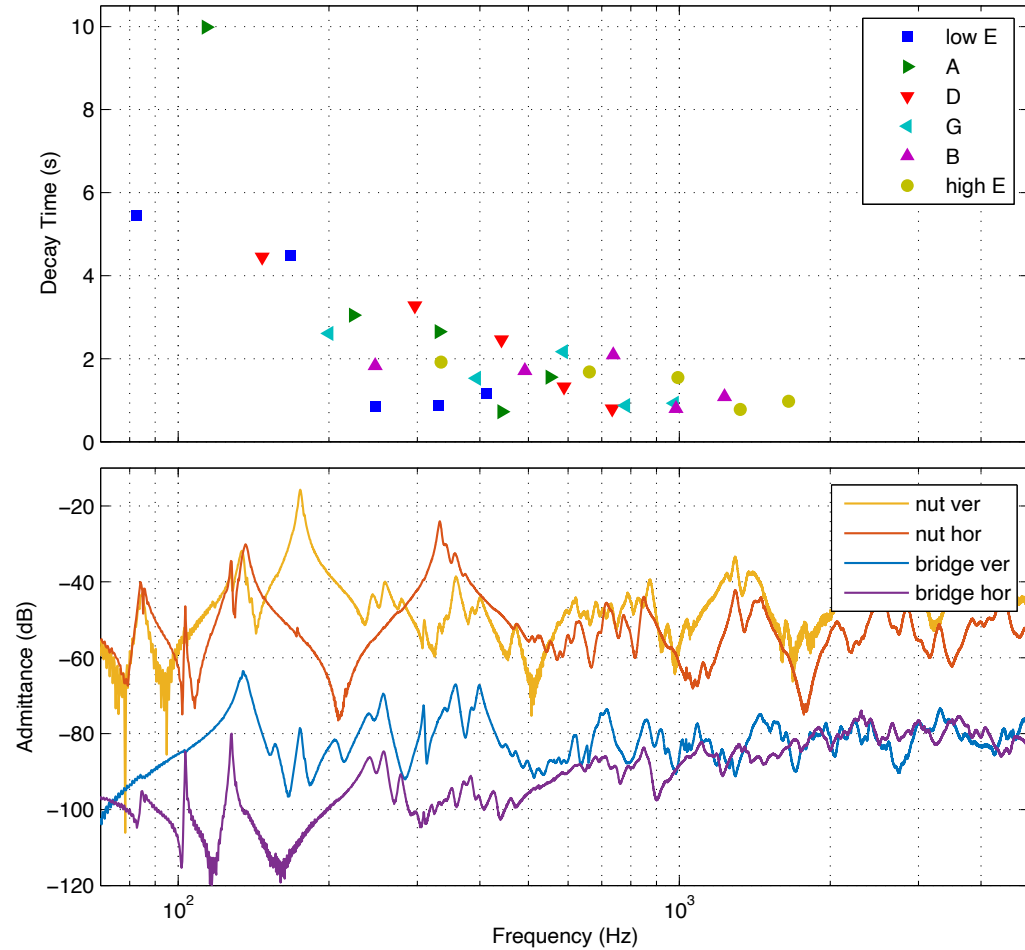


Figure 5.27: Magnitude responses (lower) of the bridge and open position admittance in the vertical and horizontal directions. The bridge admittance measurements are scaled by -40 dB for clarity. String decay times (upper plot) for the first 5 harmonics to decay by 15 dB.

| Harmonic | 1 | 2 | 3 | 4 | 5 |
|---------------------|-------|------|------|------|------|
| Measured Decay (s) | 5.45 | 4.49 | 0.86 | 0.87 | 1.12 |
| Predicted Decay (s) | 13.29 | 0.68 | 0.24 | 0.33 | 0.33 |

Table 5.1: Measured and predicted decay times for the first 5 harmonics of the open low E string to decay by 15 dB.

5.3.4 Discussion and Future Work

Observing the admittance measurements, it is clear that the neck modes absorb a significant amount of energy and will affect the string decays. The stopping location reflection coefficient will change as the note is stopped at different positions along the string, suggesting that multiple stopping location transmission coefficients should be used for accurate string decay synthesis across the instrument.

A practical method for measuring the propagation losses in the string from simple measurements is not known, and it would be useful if these could be learned from string decay and boundary admittance measurements. I hoped that it would be possible to approximate these frequency-dependent losses from the above analysis, but some of the predicted decay times are shorter than the measured decays. This suggests that the boundary conditions are more complicated than stateless reflectances, and that horizontal-vertical transverse motion coupling, and string-body and string-neck coupling should not be ignored as was done in this preliminary simplification. Future work will look into predicting the amount of energy transferred back into the string from the motion of the body and neck terminations if modeled as resonant systems.

Along these lines, further steps will be to perform mode fitting on the admittance measurements made at the bridge as well as the neck-stopping locations. This will result in efficient digital filters which are different at each end of the string termination, providing more accurate string decay rates for a digital waveguide model using the technique described in [64]. Multiple stopping location filters will be used with a different filter corresponding to each fretted note position. Synthesis examples will be computed, both including the stopping location filters, and without them. The synthesis will be compared to the measured decay rates to further validate the effectiveness of this method at correctly synthesizing the string decay.

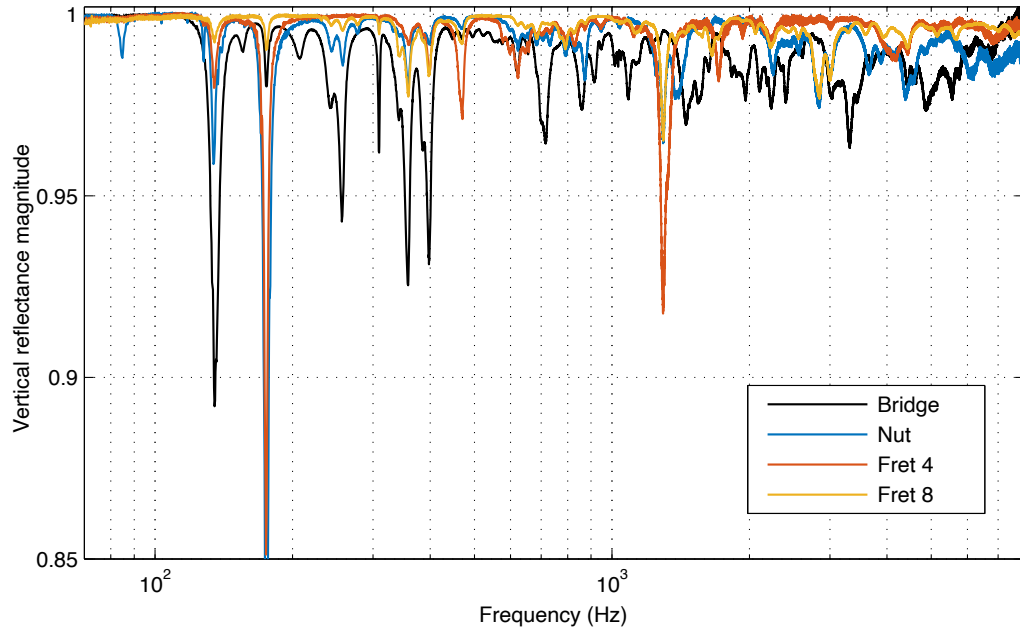


Figure 5.28: Low-E string reflectance magnitudes for the vertical direction, corresponding to the bridge and different stopping locations.

5.4 Study 4: Measurement and modeling of a resonator guitar [97]

Resonator guitars are acoustic instruments that have one or more spun metal cones embedded in the top plate, with strings driving the cone directly through a bridge. They were originally designed to be louder than traditional acoustic guitars and are often played with a metal slide. The vibrational characteristics of resonator guitars having a single inverted cone are studied as the basis for a synthesis model. The small-signal input admittance is obtained using an impact hammer and laser Doppler vibrometer. As well, sinusoidal sweeps are made using a modal shaker at various driving amplitude levels. The shaker measurements show that some of the modes exhibit nonlinear characteristics. These measurements are used to design body resonator filters with time-varying resonant modes for a digital waveguide model of the resonator guitar.

5.4.1 Introduction

During the early twentieth century, the playing levels of American bands were increasing due to the use of brass instruments and percussion. Conventional stringed instruments were not loud enough to compete, leading to the invention of “resophonic” or “resonator” instruments. Resonator instruments have a similar construction to their traditional counterparts, with the addition of one or more spun metal cones replacing the majority of the top plates. With the introduction of electronically

amplified musical instruments, the need for louder acoustic instruments was reduced, but by this time, resophonic instruments had already become part of the canon of American music, such as blues and traditional music. While there are resophonic versions of many instruments, such as banjos, mandolins, and ukuleles, by far the most popular variant is that of the guitar.

There are three main styles of resonator cone instruments: the single-cone “biscuit”, single inverted cone, and tricone designs [124]. The biscuit design uses a large cone having an approximately 24 cm diameter, mounted flush with the instrument’s top plate, with the bridge mounted at the peak of the cone. The inverted cone design uses a similar cone, but with it being inverted, and a small protrusion where the bridge is mounted. Tricone resonators use three smaller cones, typically of the biscuit style, with the bridge mounted to a metal structure connecting the peaks of each cone.

In addition to the different cone styles, there are two different neck setups commonly found on resonator guitars. Some resonator guitars have a standard round neck and can be played with a slide or with fingers to stop the notes. This style of guitar is played in the same manner as a standard guitar and is favored by blues musicians. The other category of resonator guitars has a thick square neck and is played on the musician’s lap. The strings are roughly 1 cm above the fretboard so it is only possible to play with a slide. Square neck resonator guitars are most often played by traditional and bluegrass musicians.

There is not much literature on resophonic instruments, with only brief mentions of them, but they have interesting properties that warrant further investigation [104]. In this study, a square-neck inverted cone-style resonator guitar is measured. Driving point admittance measurements are made using a hammer strike method to study the small signal response of the instrument. Resonator cones are made of very thin aluminum, typically less than 0.5 mm, which is quite thin as compared to the standard top plate thickness of roughly 3 mm for traditional acoustic guitars. The cone of the guitar measured is 0.35 mm thick. Since the cones are thin, it is more likely that the instrument will exhibit nonlinear characteristics when played in normal conditions. To measure potential nonlinearities of the instrument, a modal shaker was used to drive the instrument with various amplitude sinusoidal sweeps.

Mode fitting is performed on the small and large signal admittance measurements to be used as a body filter for a waveguide string synthesis model [112, 55, 113, 67, 68]. A modal architecture is used for this body filter so that the frequency, damping, and amplitude of each resonance can be adjusted during the synthesis. Some of the resonances observed with the shaker are shown to exhibit nonlinear weakening spring characteristics, resulting in a lowering of resonance frequency at high amplitude. These nonlinear resonances are approximated as time-varying linear modes using the modal architecture to vary the resonant frequency in relation to the amplitude of the bridge velocity at each mode. Synthesis examples are generated and compared to determine if this nonlinear behavior is audible and worth including in a model where a trade-off between accuracy

and computational complexity has to be taken into account.

The outline is as follows. Section §5.4.2 describes the measurements of the resonator guitar. Then, in §5.4.3, I describe the modal analysis and how the parameters are obtained. The waveguide synthesis model is described in §5.4.4. The results are discussed in §5.4.5. Finally, in §5.4.6, concluding remarks are provided.

5.4.2 Measurements

A square neck resonator guitar with a single inverted cone was measured as part of this study. Small signal driving point admittance measurements were made using a hammer strike method, while large-signal measurements were made with a modal shaker.

5.4.2.1 Measurement Setup

The guitar was suspended vertically by its tuning pegs, and the bottom end pin was supported lightly with foam to ensure the instrument remained mostly stationary. The strings were tuned to a common tuning of GBDGBD having frequencies 98.00, 123.47, 146.82, 196.00, 246.94, and 293.66 Hz. While the body resonances were being measured, all strings were damped using foam. A replacement bridge was manufactured for the instrument so as not to harm the original bridge when the shaker was attached. This bridge caused the low strings to be slightly offset from their normal position. The bridge was used for all measurements, including when the shaker was not used. The measurement setup is shown in Fig. 5.29.

5.4.2.2 Small Signal Measurements

Small signal bridge admittance measurements were taken by striking the bridge perpendicular to the instrument string's lengthwise direction. The miniature force hammer (PCB 086E80) was suspended as a swinging pendulum and dropped remotely. A Polytec PDV-100 laser Doppler vibrometer (LDV) was used to measure the resulting vibrations. The laser was focused as close as possible to the striking location of the hammer to measure the driving point velocity. The measured driving point force and velocity are used to compute the admittance in the frequency domain as $\Gamma(\omega) = V(\omega)/F(\omega)$, where V and F are the velocity and force, and ω is the frequency. Bridge admittance measurements were taken with the force hammer and vibrometer in the direction perpendicular to the top plate of the guitar. Measurements were also taken in the direction parallel to the top of the guitar and normal to the string, and with the hammer striking along this direction and the vibrometer measuring perpendicular to the top plate. These additional measurements allow for a two-dimensional model that includes both directions of transverse string vibration to be constructed with coupling between the directions, but for simplicity, only a one-dimensional string model was constructed at this time.



Figure 5.29: Measurement setup showing the LDV, force hammer, and shaker. Note the shaker's force sensor is not shown.

5.4.2.3 Large Signal Measurements

In order to check if the resonator guitar's modes exhibit nonlinear behavior, the instrument was driven with a signal having greater force. A modal shaker (Modal Shop 2004E) was used to drive the instrument. A force sensor (PCB 208C01) was used to measure the force imparted by the shaker. The LDV was again used to measure the resulting velocity of the instrument's vibrations. Epoxy was used to glue the shaker tip to the bridge of the guitar, ensuring that the shaker would stay attached as the instrument was driven. Twenty-second-long linear sinusoidal sweeps ranging from 50-2000 Hz were played through the shaker at thirteen different amplitude levels. Sine sweep measurements were made, increasing from 50-2000 Hz, and decreasing from 2000-50 Hz to check if the resonant behavior included hysteresis.

5.4.3 Modal Analysis

The bridge admittance measurements are used to form efficient digital filters to be used in a waveguide synthesis model. Modal fitting is performed on the admittance measurements to form a parallel bank of second-order filters, which simulate the instrument's vibrational characteristics.

5.4.3.1 Mode Fitting

Mode fitting was performed on the hammer and sweep bridge admittance measurements to gain insight into the resonant frequencies, damping, and amplitudes. Modes were fit assuming the system

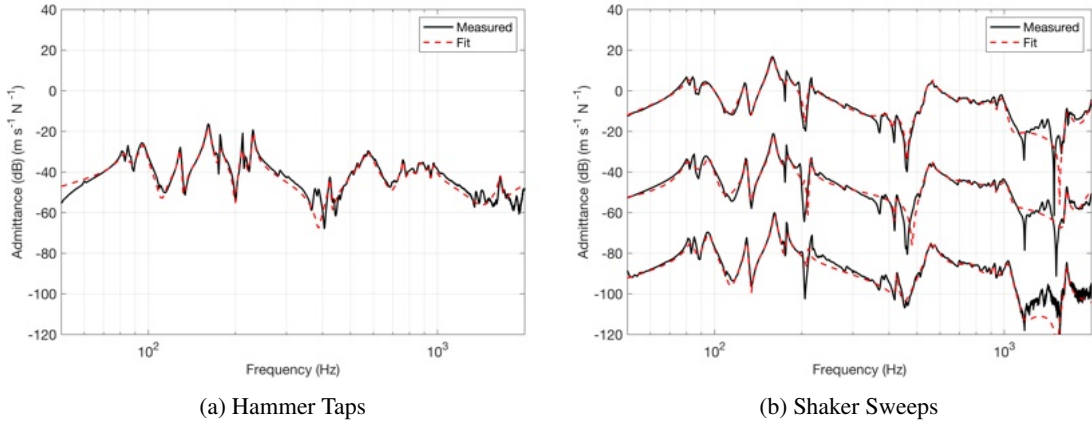


Figure 5.30: Figure 5.30a shows the measured and fit admittance from the hammer taps with $M = 24$ modes. Figure 5.30b shows the measured and fit admittance from the shaker sweeps having RMS velocity of 0.000041, 0.0032, and 0.0102 m s^{-1} with $M = 14$, 16, and 18 modes respectively. The shaker sweeps are offset by -40, 0, and 40 dB for clarity.

has damped harmonic oscillator behavior with an impulse response of the form,

$$h(t) = \sum_{m=1}^M \gamma_m e^{2\pi f_m t(i - \zeta_m)}, \quad (5.5)$$

where γ_m , f_m , and ζ_m are the amplitude, natural frequency, and damping ratios of modes $m = 1, 2, \dots, M$ [14, 4].

The mode fitting was done using the method described in Appendix A.2. The M largest singular values of this decomposition can be viewed as the singular values associated with the signal space as opposed to the noise space, and thus M was used as the model order. This mode-fitting architecture does not guarantee positive-real modes which are needed to ensure the stability of the filters. However, the measurements were of high enough quality that when properly processed, the fitting yielded positive-real modes. The complex amplitudes were obtained using least squares to minimize the error between the measured admittance and a basis of the fit modes. Figure 5.30a shows the measured and fit admittance as measured with the hammer tap method.

5.4.3.2 Nonlinear Resonances

Figure 5.30b shows the measured and fit admittance as measured with the shaker sweep method at three different levels. The sweeps were made at different amplitudes, and since the waveguide model will be constructed to model transverse velocity and force waves, the sweep levels are characterized here by the root mean square (RMS) velocity of the measured velocity during the sweep.

Figure 5.31 shows a zoomed in version of the low frequency portion of the admittance measured using the shaker for 13 different amplitude levels of the upward frequency trajectory sweeps. Note

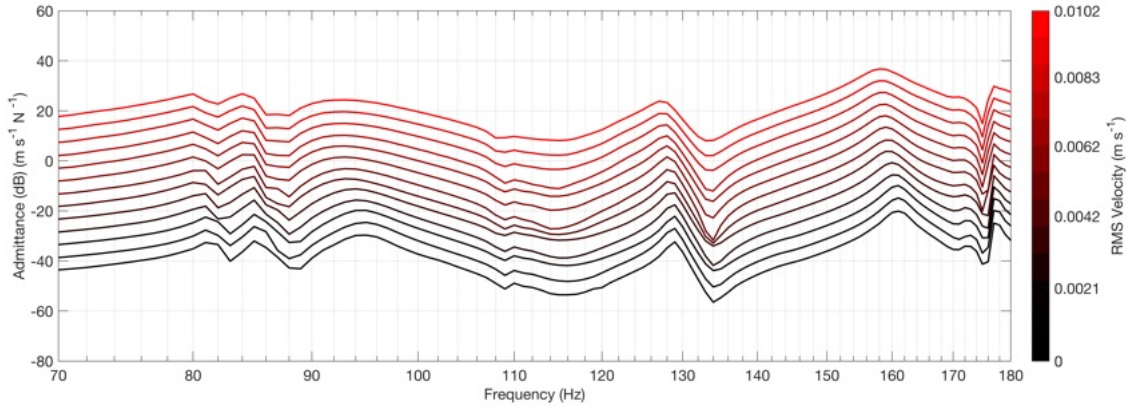


Figure 5.31: Admittance from the upward frequency trajectory shaker sweep measurements at 13 different levels. The 12 highest levels are offset in increments of 5 dB for clarity.

that for some of the modes, the resonant frequency shifts to a lower frequency at higher amplitudes. This phenomenon is known as a weakening spring if the modes are approximated as a nonlinear spring system such as a Duffing oscillator [57, 7]. The downward frequency trajectory sweeps show similar behavior, and no hysteresis is observed, so only the upward trajectory sweeps are shown.

5.4.4 Digital Waveguide Model

To simulate the resonator guitar, the digital waveguide architecture is used where samples stored in delaylines represent the transverse velocity waves of the simulated strings. The left and right traveling velocity waves are represented by $v^+(n)$ and $v^-(n)$, and the force waves are represented by $f^+(n)$ and $f^-(n)$ for each string. The transverse velocity and force at the bridge junction are $v(n) = v^+(n) + v^-(n)$ and $f(n) = f^+(n) + f^-(n)$. To calculate the reflected velocity waves at the bridge, the reflection scattering junction,

$$S_b(z) = \frac{R_B(z) - R_s}{R_B(z) + R_s}, \quad (5.6)$$

can be calculated from the string characteristic impedance, R_s , and the bridge impedance $R_B(z) = 1/\Gamma(z)$. The string impedance is calculated as $R_s = \sqrt{T\varepsilon}$, where the tension, T , and the linear mass density, ε , of the string are calculated from manufacturer-provided data [2]. The reflection scattering junction is implemented as a parallel bank of second-order filters as in [68] and used to calculate the reflected transverse velocity samples at the bridge.

For simplicity, and since the resonance nonlinearity is the focus of this section, only a 1D string with no string-to-string coupling is implemented. The neck termination is treated as a simple lossless reflection. The string losses are modeled in a simplified way using a 2nd order FIR lowpass filter, shown as $S(z)$. Two delay lines are used, one for $v^+(n)$ and one for $v^-(n)$. They are each of length $Q = \frac{f_s}{2f_0}$, where f_s is the sample rate and f_0 is the fundamental frequency of the string being simulated.

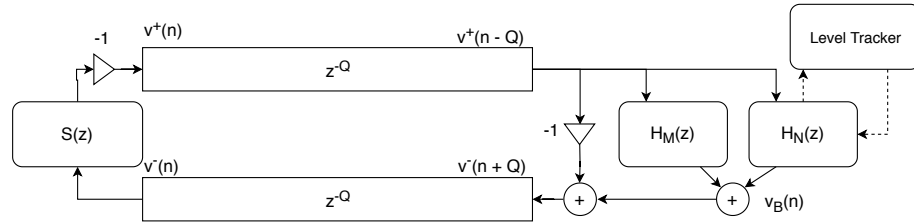


Figure 5.32: Block diagram of the waveguide synthesis architecture.

At this time, the instrument radiation is not simulated, and the output is taken as the bridge velocity $v_B(n)$.

A block diagram of the waveguide synthesis is shown in Fig. 5.32, and the details of the bridge termination filter will be explained in the following two subsections.

5.4.4.1 Bridge Termination Filter Architecture

The bridge reflectance filter is constructed as a parallel bank of second order filters which can include linear and nonlinear resonances. The shaker admittance measurements were not as reliable as the hammer taps, so the hammer tap measurement modes are used as the basis for the reflectance filter bank. However, 5 distinct nonlinear resonances were found using the shaker sweep measurements, they are at 83.2, 95.7, 128.8, 161.1, and 177.5 Hz. These are likely not the only nonlinear resonances, but they were found with more confidence than other modes, so only this set will be modeled as nonlinear resonances, while the rest are modeled as linear modes. This leaves $M = 19$ linear modes and $P = 5$ nonlinear resonances.

The filter banks are constructed in terms of their center frequency, damping ratio, and complex amplitude to give the two parallel filter banks as:

$$H_m(z) = \gamma_m \frac{1 - z^{-2}}{1 + a_{m,1}z^{-1} + a_{m,2}z^{-2}}, \quad (5.7)$$

$$H_p(z) = \gamma_p \frac{1 - z^{-2}}{1 + a_{p,1}z^{-1} + a_{p,2}z^{-2}}, \quad (5.8)$$

where $a_{m,1} = -2r_m \cos(2\pi f_m/f_s)$, and $a_{m,2} = r_m^2$, with $r_m = \exp(-2\pi f_m \zeta_m/f_s)$ being the pole radius, and f_s the sampling rate. The variables indexed with m represent the linear modes with $M = 19$ being used, and the variables indexed with p represent the nonlinear resonances with $P = 5$.

The nonlinear resonances are modeled as time-varying linear modes. As a first approximation, only the center frequency of the modes will be varied. The center frequencies and peak velocity of each of the nonlinear resonances were calculated at each RMS velocity level. To parameterize the nonlinear resonance frequency as a function of the instantaneous velocity, v_p , linear fits were made

of the form, $f_p(v_p) = c_m \times v_p + f_m$, where f_p is the calculated nonlinear resonance center frequency, c_m is the slope of the fit, and f_m is the center frequency calculated from the hammer tap measurement. During the shaker measurements, the instrument was mass loaded by the force sensor, decreasing the center frequencies, so the center frequencies from the hammer measurements are used as the base frequencies for the nonlinear resonances. The parameters of the linear fitting are shown in Table 5.2.

Table 5.2: Center frequency and slope of the linear fitting to calculate the amplitude-dependent nonlinear resonance center frequencies.

| | | | | | |
|--|------|-------|-------|-------|-------|
| Center Frequency, f_m (Hz) | 83.2 | 95.7 | 128.8 | 161.2 | 177.5 |
| Frequency Slope, c_m (m^{-1}) | -8.3 | -12.6 | -21.4 | -16.7 | -0.6 |

5.4.4.2 Level Tracking

To vary the center frequencies of the nonlinear resonances, an estimate of each mode's component of the bridge velocity, $v_p(n)$, was needed. The level detection is done on the output of each nonlinear resonance's associated filter using a leaky integrator-based peak detector. This is implemented using the update equation,

$$\text{if } |v_p(n)| > \lambda: \\ \lambda \leftarrow \lambda + (1 - e^{\frac{-1}{\tau_a f_s}})(|v_p(n)| - \lambda) \quad (5.9)$$

else:

$$\lambda \leftarrow \lambda + (1 - e^{\frac{-1}{\tau_r f_s}})(|v_p(n)| - \lambda),$$

where λ is the level estimate, $v_p(n)$ is the bridge velocity at each mode, τ_a is the time constant when the level detection is increasing, and τ_r is the time constant when it is decreasing. The attack and release time constants were chosen as $\tau_a = 0.1$ ms, and $\tau_r = 100$ ms, so that transients are detected quickly, but the level does not drop directly after the transients [138].

5.4.5 Results and Discussion

String pluck approximations were generated by initializing the delaylines with a triangular string displacement, which was used to calculate the transverse velocity at each sample of the delayline. Example plucks are generated using only linear modes and using the hybrid linear-nonlinear model. Audio examples can be found online¹. Figure 5.33 shows a linear and a nonlinear pluck as well as

¹<https://ccrma.stanford.edu/~mrau/ISMA2019/>

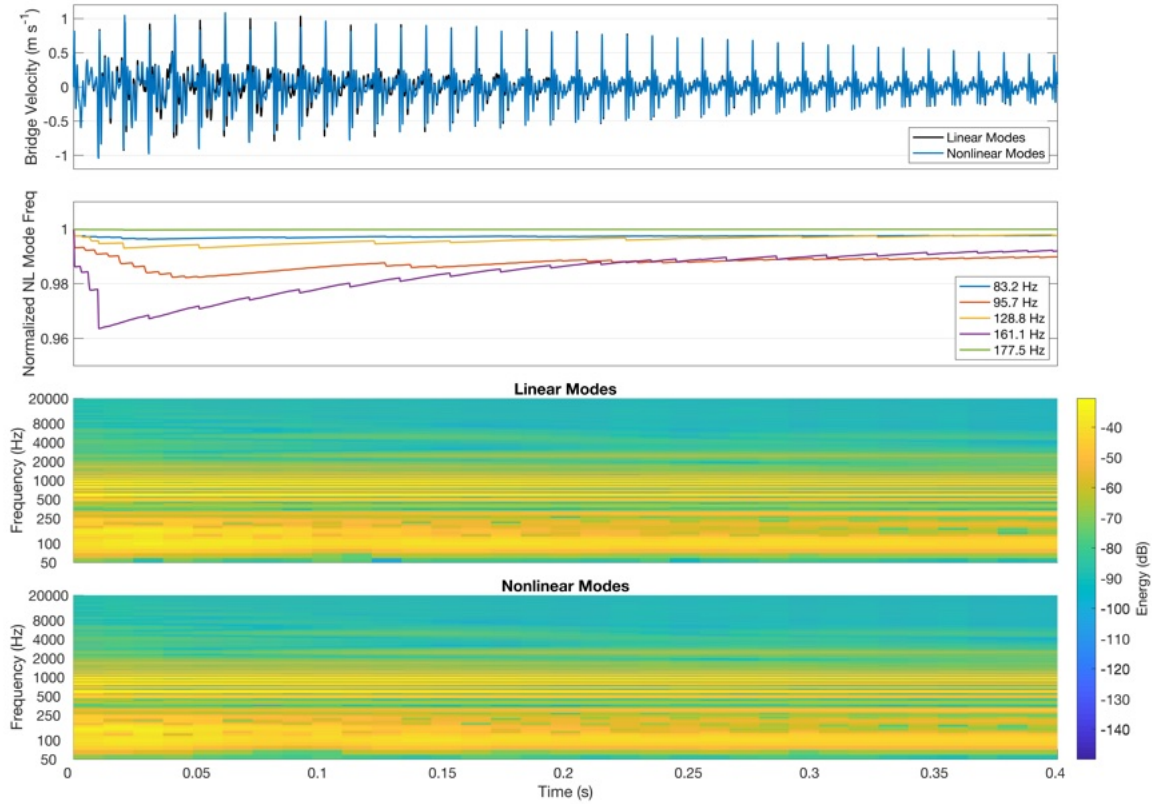


Figure 5.33: Bridge velocity and normalized frequencies of the nonlinear resonances during a pluck of the low G string at 98 Hz. Spectrograms are shown, one with only linear modes, and one which includes the nonlinear resonances.

the normalized frequencies of the nonlinear resonances during the nonlinear pluck. It is clear that the waveforms are quite similar but deviate, especially when the bridge velocity is high.

Informal listening suggests that the linear and and nonlinear models are quite similar, but do have a slight timbre difference, especially during the attack of the plucks. However, this evaluation is informal, and a formal listening test would be required to give more conclusive results of the timbre differences.

5.4.6 Conclusions

Measurements of a resonator guitar were made with small and large signal excitations as a basis for modal analysis. The small signal hammer excitation provided high-quality measurements to perform modal fitting, while the large signal shaker measurements revealed that some of the instrument's resonances behave nonlinearly. These linear and nonlinear resonance parameters were used to create a digital waveguide model of the resonator guitar.

This study provides preliminary results that suggest that modeling the weakly nonlinear resonances of resonating instruments may be important to properly model the timbre, especially during transients. However, this study is not complete, and there is plenty of room for future work. First, the model constructed is only one-dimensional and does not include string-string coupling. Expanding on this model would likely aid in the accuracy. As well, the signals used to synthesize the pluck are not physical, as a higher energy pluck will not be an exactly scaled version of a low energy pluck. The model uses the bridge velocity as the output signal, but a more accurate model would include radiation modeling [68].

The nonlinear resonances were approximated as time-varying linear modes, but this assumption should be checked to see how well it perceptually compares to a more complicated model. A more complicated model may also include varying the damping ratios and complex amplitudes of each resonance.

In addition to improvement to the waveguide model, more measurements could be made to improve the modal fitting. More shaker sweeps could be made at other amplitude levels and on different days to confirm the results. As well, other similar instruments could be measured and modeled to see how this approach translates to similar or dissimilar instrument modeling.

Chapter 6

Conclusions

This dissertation focused on stringed instrument acoustics, measurement, and modeling, particularly relating to the guitar. Acoustic and vibration measurement techniques and devices were described, along with examples of their use in the study, synthesis, and processing of guitar signals. This chapter provides summaries of each chapter and outlines areas of interest for future work.

In addition to work relating to guitars, I worked on multiple tangentially related projects while at CCRMA. Appendix [B](#) provides references for all the published papers and conference talks I contributed to during my time at CCRMA.

6.1 Chapter 1

Chapter [1](#) introduced the main topics of this thesis, the measurement, modeling, and synthesis of the guitar, with applications to luthiery. The motivation for the thesis was discussed, while a brief overview of the work was introduced. A concise history of the American guitar was given. Next, a review of the acoustics of the guitar was presented, though more detail was given in subsequent chapters. Finally, the modal formulation of the guitar and its acoustics was presented.

6.2 Chapter 2

Chapter [2](#) focused on vibration and acoustic measurement methods for stringed instruments. The mounting of the instrument was discussed, as this can affect the damping of the instrument's vibrations. Standard methods for taking admittance and radiation methods were presented with a particular emphasis on impact hammer and laser Doppler vibrometer measurements. While making vibration measurements, I designed multiple lab tools to aid in the process. I designed an automatic impact hammer controlled by a microprocessor that can be either controlled via a USB connection or manually triggered. To perform scanning laser Doppler vibrometer measurements, I designed an

inexpensive mirror galvanometer system to augment a single-point laser vibrometer. Both of these tools were described in this chapter. Expensive lab equipment is often out of reach for instrument builders and hobbyists, so I worked on low-cost alternatives. I discussed impact hammers and vibration sensors I built using 3D printing and inexpensive piezoelectric sensors. Finally, a device designed to measure the material and vibrational parameters of wood boards meant for guitar top plates was presented.

6.3 Chapter 3

In chapter 3, parameter extraction from measurements was discussed. To learn about the modal frequencies, damping, and amplitudes of a vibration measurement, these parameters need to be extracted from the measurement. Multiple methods exist to extract these parameters, and I present a comparison between three common methods and one less common algorithm which I have had success with. In addition to the information of a vibrating object, one may want to know the material parameters. This is especially important with wooden boards since they are orthotropic materials, and there is a wide range of material parameters between different species and even among boards cut from the same tree. Chapter 2 presented a measurement method to approximate some of the orthotropic material parameters but not all. This chapter presented a method to better predict the measured and unknown material parameters by comparing the mode frequencies found from a measurement and finite element model. The model material parameters were optimized to minimize the modal frequency error between the measurement and the model.

6.4 Chapter 4

Chapter 4 presented a new method to process an electric guitar to sound like an acoustic guitar. The bridge impedance of a solid-body electric guitar is much higher than that of an acoustic guitar and has fewer body resonances. The body resonances cause a frequency-dependant note sustain difference between the two guitars, with the electric guitar having notes that ring for significantly longer. This method models the physical bridge impedance differences between a solid-body electric guitar and an acoustic guitar in a manner that replicates the equalization and sustain characteristics of the acoustic guitar. These changes are implemented with time-varying filters applied to a hexaphonic bridge pickup on a solid-body electric guitar. The algorithm is fully parameterized by the modal frequencies, damping ratios, and amplitudes of the virtual acoustic guitar. This allows the user to alter the modal structure of the virtual guitar, opening up possibilities for use as a method to study the audible results of changes to a guitar's structure.

6.5 Chapter 5

While the previous chapters primarily discussed methods to study the guitar and its acoustics, Chapter 5 presented studies using these and other methods to investigate the guitar. The first study presented admittance measurements of two guitar tops and braces as the braces were carved. Further measurements show these two guitars and an added third as the guitars were being built. Measurements were made at multiple stages of the guitars' construction, including the top carving, closed box before and after sanding, as the finish is applied, and the completed guitar. The final study uses measurements of a resonator guitar to show that some modes exhibit non-linear behavior and change in frequency when driven at high amplitudes. This behavior was demonstrated with a waveguide synthesis model.

6.6 Future Work

A Ph.D. may seem long, but there are always more research directions to pursue. Here, I will discuss some projects I hope to continue or start in the future.

Some instrument makers incorporate vibration and acoustic measurement in their building practice, but many do not. One significant hurdle is the cost of measurement equipment and software to run and analyze the measurements. I have worked on low-cost measurement tools and hope to distribute them more widely. In addition to these existing and new measurement devices, I hope to distribute free software aimed at makers to make and analyze measurements easily. Having this type of tool can hopefully help both the maker and researcher by having more data points and directions in which to look.

One question that still puzzles me as a musician and researcher is the perceptual evaluation of instruments. My personal belief is that any instrument which is set up correctly and plays well can be used to make great music as long as it is used in the correct setting. For example, an inexpensive instrument may have a sound more suited to a particular style of music than an expensive instrument. This notion is especially true with guitars since the instrument is used for so many genres and styles of music. However, even given the view that all instruments can have a “good” sound, different players still prefer some, and this area is not well studied. I own multiple guitars and prefer to play different ones for different purposes, but even I struggle to explain why these preferences arise. I hope to conduct studies into the preference of instruments based on genre, style, and personal taste. Ideally, these studies will include vibration and acoustic measurements, syntheses, numerical modeling, and perceptual tests. Using the method of Chapter 4, I hope to study the modal characteristics of instruments to learn more about these preferences.

One area I am particularly interested in and feel is understudied is research into the damping ratios of the associated modes of guitars and how they relate to the perceived sound. Instrument makers often talk about the “tap-tone” of a wood board, which is a result of the frequencies, damping,

and amplitudes of the board's modes. Once the board is modified, these parameters will change as the guitar is completed. The mode frequency and shapes are relatively well studied and can be studied with numerical simulations such as finite element models. However, the damping is related to the internal structure of the wood, and most models used in simulations, such as Rayleigh damping, do not account for the complexities of the wood's internal damping. Damping is also one of the parameters that can be significantly altered by thermal and chemically modified woods and is likely related to any differences reported with aged woods and instruments. There is some research looking into damping, but more could be done.

The traditional way to design an instrument is to choose the materials and geometry and build the instrument to see later how it sounds. Skilled luthiers have great intuition and knowledge through years of practice to achieve the desired sound in the finished instrument, but this methodology still has variability. I hope to work towards the idea of reverse engineering a guitar based on the desired sound as the driving factor. Methods such as that of Chapter 4 could be used to determine the ideal sound of the finished guitar. Then, once the target sound is chosen, measurements and modeling could be used before and during the construction of the guitar in an attempt to match this sound. I hope to continue working in this direction, building on the related research of others.

Most importantly, I want to continue conversing and collaborating with instrument builders and work on research directions relevant to luthiers. I feel that the best musical acoustics research occurs when the researcher is fully immersed in the musical, creative, and building practices of those with whom they collaborate. I have learned a great deal from the luthiers I have talked with and find that for every question I start to understand the answer to, three more questions arise. These questions relating to the guitar and its acoustics, measurement, and modeling will inspire me for years to come.

Appendix A

Electric-to-Acoustic Pickup Processing

A.1 Notch Filter Design

This appendix presents the formulas for the coefficients of a second-order notch filter fit to the reflectance filters in (4.9).

The second-order filter,

$$H(z) = \frac{b_0 + b_1 z^{-1} + b_2 z^{-2}}{a_0 + a_1 z^{-1} + a_2 z^{-2}}, \quad (\text{A.1})$$

with coefficients given by

$$a_2 = \frac{2Q - \sin \omega_c}{2Q + \sin \omega_c}, \quad (\text{A.2})$$

$$a_1 = b_1 = -(1 + a_2) \cos \omega_c, \quad (\text{A.3})$$

$$b_0 = \frac{1}{2}(1 + a_2) + \frac{1}{2}(1 - a_2)v, \quad (\text{A.4})$$

$$b_2 = \frac{1}{2}(1 + a_2) - \frac{1}{2}(1 - a_2)v, \quad (\text{A.5})$$

where ω_c is the center frequency, Q is the inverse bandwidth, and v is the gain at the center frequency. The parameters, v and Q can be calculated to fit the reflectance filters in (4.9) as

$$v = \left| \frac{(1 - R_s \gamma_m) - 2r \cos(\omega_c) e^{-i\omega_c} + (r^2 + R_s \gamma_m) e^{-2i\omega_c}}{(1 + R_s \gamma_m) - 2r \cos(\omega_c) e^{-i\omega_c} + (r^2 - R_s \gamma_m) e^{-2i\omega_c}} \right|, \quad (\text{A.6})$$

$$Q = \frac{1}{2} \left[\frac{v\beta \sin^2 \omega_c}{2 \cos \omega_c - \beta} \right]^{\frac{1}{2}}, \quad (\text{A.7})$$

$$\beta = \frac{16 \cos \omega_c + v \zeta^2 \sin^2 \omega_c - \zeta^2 \sqrt{v^2 \sin^4 \omega_c + \frac{32v \sin^2 \omega_c \cos \omega_c}{\zeta^2}}}{32 \cos^2 \omega_c}. \quad (\text{A.8})$$

A.2 Mode Fitting

Starting with the impulse response of (4.7) and assuming the number of samples, N is even, the goal is to estimate the modes of a noisy impulse response $h(n)$. A Vandermonde matrix with the m^{th} column representing the time impulse response of the m^{th} mode, $h_m(n)$,

$$\mathbf{V} = \begin{bmatrix} \mathbf{v}_1 & \dots & \mathbf{v}_M \end{bmatrix}, \quad (\text{A.9})$$

$$\mathbf{v}_m = \begin{bmatrix} e^{\omega_m(i-\zeta_m)0} & \dots & e^{\omega_m(i-\zeta_m)(N/2-1)} \end{bmatrix}^\top, \quad (\text{A.10})$$

where $[.]^\top$ represents the non-Hermitian transpose. The outer product of \mathbf{V} with a diagonal matrix of the mode amplitudes, $\mathbf{G} = \text{diag}[\gamma_1 \dots \gamma_M]$ is equivalent to a Hankel matrix formed by the impulse response samples as

$$\mathbf{H} = \mathbf{V} \mathbf{G} \mathbf{V}^\top, \quad (\text{A.11})$$

$$\mathbf{H} = \begin{bmatrix} h(0) & h(1) & h(2) \dots & h(N/2-1) \\ h(1) & h(2) & & \vdots \\ h(2) & & \ddots & \vdots \\ \vdots & & & \ddots \\ h(N/2-1) & \dots & \dots & h(N-1) \end{bmatrix}. \quad (\text{A.12})$$

An offset Hankel matrix, \mathbf{K} can be formed similar to in the ESPRIT [105] method with a similar outer product as

$$\mathbf{K} = \mathbf{V} \Psi \mathbf{G} \mathbf{V}^\top, \quad (\text{A.13})$$

$$\mathbf{K} = \begin{bmatrix} h(1) & h(2) & h(3) \dots & h(N/2) \\ h(2) & h(3) & & \vdots \\ h(3) & & \ddots & \vdots \\ \vdots & & & \ddots \\ h(N/2) & \dots & \dots & h(N) \end{bmatrix}, \quad (\text{A.14})$$

where Ψ is the diagonal matrix of mode exponential kernels,

$$\Psi = \text{diag} \left[e^{\omega_1(i-\zeta_1)} \dots e^{\omega_M(i-\zeta_M)} \right] \quad (\text{A.15})$$

Post multiplying \mathbf{K} by the pseudoinverse of \mathbf{H} gives

$$\mathbf{K} \mathbf{H}^+ = \mathbf{V} \Psi \mathbf{V}^{-1}, \quad (\text{A.16})$$

where the diagonal elements of Ψ are the generalized eigenvalues, and the mode frequency and damping can be found by taking the real and imaginary parts of the logarithm of the eigenvalues,

$$\ln(\psi_m) = \omega_m(i - \zeta_m). \quad (\text{A.17})$$

The number of modes is determined by choosing the M largest eigenvalues which produce a good fit.

Appendix B

Publications at CCRMA

B.1 Journal Articles

1. **M. Rau**, J. S. Abel, D. James, and J. O. Smith III, “Electric-to-acoustic pickup processing for string instruments: An experimental study of the guitar with a hexaphonic pickup,” *The Journal of the Acoustical Society of America*, vol. 150, no. 1, pp. 385–397, 2021.

B.2 Conference Papers

1. **M. Rau**, J. O. Smith, J. S. Abel, “A comparison of modal parameter extraction methods when applied to measurements of stringed instruments,” *Proceedings of the Forum Acusticum*, Turin, Italy, 2023.
2. T. Zhang, M. Sheinin, D. Yao Chan, **M. Rau**, M. O’Toole, and S. Narasimhan, “Estimating physical interactions using transient surface wave imaging,” *Proceedings of the IEEE/CVF Conference on Computer Vision and Pattern Recognition*, 2023.
3. S. Clarke, R. Gao, M. Wang, **M. Rau**, J. Xu, J.H. Wang, D. James, and J. Wu, “RealImpact: A dataset of impact sound fields for real objects,” *the Proceedings of the IEEE/CVF Conference on Computer Vision and Pattern Recognition*, 2023.
4. S. Clarke, N. Heravi, **M. Rau**, R. Gao, J. Wu, D. James, and J. Bohg, “DiffImpact: Differentiable rendering and identification of impact sounds,” in *5th Annual Conference on Robot Learning*, 2021.
5. J. Chowdhury, E. K. Canfield-Dafilou, and **M. Rau**, “Water bottle synthesis with modal signal processing,” in *23rd Int. Conf. Digital Audio Effects (DAFx-20)*, Virtual, Sep. 9–11, 2020.

6. **M. Rau**, O. Das, and E. Canfield-Dafilou, “Improved carillon synthesis,” in 22nd Int. Conf. Digital Audio Effects (DAFx-19), Birmingham, England, Sep. 2–6, 2019.
7. **M. Rau** and J. O. Smith III, “Measurement and modeling of a resonator guitar,” International Symposium on Musical Acoustics, September 13–17, 2019.
8. **M. Rau** and R. Hoover, “Measurements of acoustic guitar top plates during the voicing process,” in 26th International Congress on Sound and Vibration, July 7–11, 2019.
9. **M. Rau**, J. S. Abel, and J. O. Smith III, “Contact sensor processing for acoustic instrument recording using a modal architecture,” in 21st Int. Conf. Digital Audio Effects (DAFx-18), Aveiro, Portugal, pp. 304–311, Sep. 4–8, 2018.
10. **M. Rau** and O. Das, “An “infinite” sustain effect designed for live guitar performance,” in Audio Engineering Society Convention 143. Audio Engineering Society, 2017.
11. P. Murgai, **M. Rau**, and J.-M. Jot, “Blind estimation of the reverberation fingerprint of unknown acoustic environments,” in Audio Engineering Society Convention 143. Audio Engineering Society, 2017.
12. **M. Rau**, E. Maestre, J. O. Smith, and G. Scavone, “An exploration of guitar neck admittance measurements taken at different string stopping locations,” International Symposium on Musical Acoustics, pp. 73–76, June 18–22, 2017.

B.3 Conference Presentations

1. C. Darabundit and **M. Rau**, “Modeling and correction of piezoelectric string instrument pickups,” in 183rd Meeting of the Acoustical Society of America, Nashville, TN, Dec 5–9, 2022.
2. **M. Rau**, R. Hoover, R. Barto, and J. O. Smith, “A self-contained and automated tonewood measurement device,” Vienna Talk on Musical Acoustics, Vienna, Austria, September 11–14, 2022.
3. **M. Rau**, J. O. Smith, and D. L. James, “Augmenting a single-point laser Doppler vibrometer to perform scanning measurements,” in 182nd Meeting of the Acoustical Society of America, Denver, CO, May 23–27, 2022, published abstract.
4. **M. Rau**, “Measurements and analysis of acoustic guitars during various stages of their construction,” in 180th Meeting of the Acoustical Society of America, Virtual, June 8–10, 2021.
5. **M. Rau**, J. S. Abel, J. O. Smith, and D. L. James, “String instrument acoustic transfer processing,” in 179th Meeting of the Acoustical Society of America, Virtual, December 7–11, 2020.

6. **M. Rau** and J. O. Smith III, “A comparison of nonlinear modal synthesis using a time-varying linear approximation and direct computation,” in 178th Meeting of the Acoustical Society of America, San Diego, CA, December 2–6, 2019.
7. **M. Rau**, J. O. Smith, and J. S. Abel, “String synthesis using individually modeled termination scattering filters,” in 177th Meeting of the Acoustical Society of America, Victoria, Canada, Nov. 5–9, 2018, presentation by invitation.

Bibliography

- [1] Jonathan S. Abel. Method and system for designing a modal filter. *US Patent App. No. 62-726325*, 2018.
- [2] Jonathan S. Abel. Direct modal filter design. *Personal Communication*, November 2018.
- [3] Jonathan S Abel and David P Berners. Filter design using second-order peaking and shelving sections. In *ICMC*, 2004.
- [4] Agilent Technologies. Fundamentals of modal testing. 2000.
- [5] Randall J Allemand and David L Brown. Experimental modal analysis and dynamic component synthesis. volume 3. modal parameter estimation. 1987.
- [6] Martin Alnæs, Jan Blechta, Johan Hake, August Johansson, Benjamin Kehlet, Anders Logg, Chris Richardson, Johannes Ring, Marie E Rognes, and Garth N Wells. The fenics project version 1.5. *Archive of Numerical Software*, 3(100), 2015.
- [7] Marco Amabili. *Nonlinear vibrations and stability of shells and plates*. Cambridge University Press, 2008.
- [8] Bishner Saroop Atal. Automatic speaker recognition based on pitch contours. *The Journal of the Acoustical Society of America*, 52(6B):1687–1697, 1972.
- [9] Tony Bacon. *History of the American Guitar: 1833 to the Present Day*. Rowman & Littlefield, 2012.
- [10] LR Baggs. Electric guitar bridges.
<https://www.lrbaggs.com/pickups/electric-guitar-acoustic-pickup>. (Last viewed Feb 8, 2021).
- [11] LR Baggs. LR Baggs - voiceprint DI acoustic guitar impulse response pedal.
<https://www.lrbaggs.com/voiceprint-di-acoustic-guitar-impulse-response-pedal>. (Last viewed Feb 8, 2021).

- [12] Balázs Bank and Matti Karjalainen. Passive admittance synthesis for sound synthesis applications. *Journal of the Acoustical Society of America*, 123(5):3521–3521, 2008.
- [13] John S Bogdanovich. *Classical guitar making: a modern approach to traditional design*. Sterling Publishing Company, Inc., 2007.
- [14] Anders Brandt. *Noise and Vibration Analysis: Signal Analysis and Experimental Procedures*. John Wiley & Sons, 2011.
- [15] D. Brown, R. Allemand, R. Zimmerman, and M. Mergeay. Parameter estimation techniques for modal analysis. Technical report, SAE Technical paper, 1979.
- [16] Graham Caldersmith. Guitar as a reflex enclosure. *The Journal of the Acoustical Society of America*, 63(5):1566–1575, 1978.
- [17] Graham Caldersmith. Designing a guitar family. *Applied acoustics*, 46(1):3–17, 1995.
- [18] GW Caldersmith and EV Jansson. Frequency response and played tones of guitars. *Quarterly Report STL-QPSR*, 4(1980):50–61, 1980.
- [19] Antoine Chaigne and Jean Kergomard. *Acoustics of musical instruments*. Springer, 2016.
- [20] Clockwise Tools. DIGR-0105 Digital Indicator. <https://clockwisetools.com/products/clockwise-tools-digr-0105-digital-indicator-0-1-25-4mm>. Accessed 05-10-2023.
- [21] Willian R. Cumpiano and Jonathan D. Natelson. *Guitarmaking: Tradition and technology: A complete reference for the design & construction of the steel-string folk guitar & the classical guitar*. Chronicle Books, 1994.
- [22] D'Addario. Catalog Supplement/String Tension Specifications: A complete technical reference for fretted instrument string tensions. 2019.
- [23] Anna Danihelová, Zuzana Vidholdová, Tomáš Gergel', Lucia Spišiaková Kružlicová, and Michal Pástor. Thermal modification of spruce and maple wood for special wood products. *Polymers*, 14(14):2813, 2022.
- [24] Patrick Dumond and Natalie Baddour. Can a brace be used to control the frequencies of a plate? *SpringerPlus*, 2(1):558, 2013.
- [25] Patrick Dumond and Natalie Baddour. A structured approach to using a rectangular brace to design a soundboard section for a desired natural frequency. In *Proceedings of the Stockholm Music Acoustics Conference*, pages 613–618, 2013.
- [26] eFunda. Hooke's law for orthotropic materials, https://www.efunda.com/formulae/solid_mechanics/mat_mechanics/hooke_orthotropic.cfm

- [27] David Ewins. *Modal Testing: Theory and Practice*, volume 15. Research studies press Letchworth, 1984.
- [28] Helmut Fleischer. Mechanical Vibrations of Electric Guitars. *Acta Acustica united with Acustica*, 84(January):758–765, 1998.
- [29] Helmut Fleischer and Tilmann Zwicker. Investigating dead spots of electric guitars. *Acta Acustica united with Acustica*, 85(1):128–135, 1999.
- [30] Neville H Fletcher and Thomas D Rossing. *The physics of musical instruments*. Springer Science & Business Media, 2012.
- [31] Richard Mark French. *Engineering the guitar: Theory and practice*. Springer Science & Business Media, 2008.
- [32] Richard Mark French. *Engineering the guitar: theory and practice*. Springer, 2009.
- [33] Richard Mark French. *Technology of the Guitar*. Springer Science & Business Media, 2012.
- [34] Vincent Fréour, François Gautier, Bertrand David, and Marthe Curtit. Extraction and analysis of body-induced partials of guitar tones. *The Journal of the Acoustical Society of America*, 138(6):3930–3940, 2015.
- [35] Claudia Fritz, Ian Cross, Brian CJ Moore, and Jim Woodhouse. Perceptual thresholds for detecting modifications applied to the acoustical properties of a violin. *The Journal of the Acoustical Society of America*, 122(6):3640–3650, 2007.
- [36] Christophe Geuzaine and Jean-François Remacle. Gmsh: A 3-d finite element mesh generator with built-in pre-and post-processing facilities. *International journal for numerical methods in engineering*, 79(11):1309–1331, 2009.
- [37] Trevor Gore. Wood for guitars. In *Proceedings of Meetings on Acoustics*, volume 12. AIP Publishing, 2011.
- [38] Trevor Gore and Gerard Gilet. *Contemporary acoustic guitar design and build: Build*, volume 2. Trevor Gore, 2011.
- [39] Trevor Gore and Gerard Gilet. *Contemporary Acoustic Guitar: Design and Build*. Trevor Gore, 2016.
- [40] Aki Härmä, Matti Karjalainen, Lauri Savioja, Vesa Välimäki, Unto K Laine, and Jyri Huopaniemi. Frequency-warped signal processing for audio applications. *Journal of the audio engineering society*, 48(11):1011–1031, 2000.

- [41] Joseph Howse. *OpenCV computer vision with python*, volume 27. Packt Publishing Birmingham, 2013.
- [42] Carleen Maley Hutchins. The acoustics of violin plates. *Scientific American*, 245(4):170–187, 1981.
- [43] Daniel J Inman. Engineering vibration. upper saddle, 2008.
- [44] Instructables. Arduino Laser Show With Real Galvos.
<https://www.instructables.com/Arduino-Laser-Show-With-Real-Galvos/>. Accessed 04-10-2023.
- [45] Instructables. Arduino Scale With 5kg Load Cell and HX711 Amplifier. <https://www.instructables.com/Arduino-Scale-With-5kg-Load-Cell-and-HX711-Amplifi/>. Accessed 05-10-2023.
- [46] Ra Inta. *The acoustics of the steel string guitar*. PhD thesis, University of New South Wales, 2007.
- [47] Erik V Jansson. A study of acoustical and hologram interferometric measurements of the top plate vibrations of a guitar. *Acta Acustica united with Acustica*, 25(2):95–100, 1971.
- [48] Erik V Jansson. Acoustical properties of complex cavities. prediction and measurements of resonance properties of violin-shaped and guitar-shaped cavities. *Acta Acustica united with Acustica*, 37(4):211–221, 1977.
- [49] Erik V Jansson. Admittance measurements of 25 high quality violins. *Acta Acustica united with Acustica*, 83(2):337–341, 1997.
- [50] Erik V Jansson. *Acoustics for violin and guitar makers*. Kungl. Tekniska högskolan, Department of Speech. Music and Hearing, 2002.
- [51] Richard Johnston and Dick Boak. *Martin guitars: A history*, volume 1. Hal Leonard Corporation, 2008.
- [52] M. Karjalainen, H. Penttinen, and V. Välimäki. Acoustic sound from the electric guitar using DSP techniques. In *Acoustics, Speech, and Signal Processing, 2000. ICASSP'00. Proceedings. 2000 IEEE International Conference on*, volume 2, pages II773–II776. IEEE, 2000.
- [53] M. Karjalainen, H. Penttinen, and V. Välimäki. More acoustic sounding timbre from guitar pickups. in *2nd Workshop on Digital Audio Effects (DAFx-99), Trondheim, Norway*, 10:1–4, Dec. 9–11, 1999.

- [54] M. Karjalainen, V. Välimäki, H. Penttinen, and H. Saastamoinen. DSP equalization of electret film pickup for the acoustic guitar. *Journal of the Audio Engineering Society*, 48(12):1183–1193, 2000.
- [55] Matti Karjalainen, Vesa Välimäki, and Tero Tolonen. Plucked-string models: From the Karplus-Strong algorithm to digital waveguides and beyond. *Computer Music Journal*, 22(3):17–32, 1998.
- [56] Mykel J Kochenderfer and Tim A Wheeler. *Algorithms for optimization*. Mit Press, 2019.
- [57] Lev Landau and Evgenii Lifshitz. *Course of theoretical physics: Mechanics*, volume 1. Elsevier, 2013.
- [58] Mikael Laurson, Cumhur Erkut, and Vesa Välimäki. Methods for modeling realistic playing in plucked-string synthesis: analysis, control and synthesis. In *Proceedings of the COSTG-6 Conference on Digital Audio Effects (DAFx-00)*, Verona, Italy, December 7-9, 2000.
- [59] Mikael Laurson, Cumhur Erkut, Vesa Välimäki, and Mika Kuuskankare. Methods for modelling realistic playing in acoustic guitar synthesis. *Computer Music Journal*, 25(3):38, 2001.
- [60] Jean-Loic Le Carrou, Arthur Paté, and Baptiste Chomette. Influence of the player on the dynamics of the electric guitar. *The Journal of the Acoustical Society of America*, 146(5):3123–3130, 2019.
- [61] Timothy W Leishman and Samuel D Bellows. Musical instrument directivity measurements. *The Journal of the Acoustical Society of America*, 146(4):2822–2822, 2019.
- [62] Dan Luo. *Measuring the frequency response function of X-braced guitar top and guitar*. PhD thesis, Tufts University, 2016.
- [63] Esteban Maestre and Gary Scavone. Creating virtual acoustic replicas of real violins. In *Proceedings of the International Symposium on Musical Acoustics (ISMA 2019)*, Detmold, Germany, September 13-17, 2019.
- [64] Esteban Maestre, Gary P. Scavone, and Julius O. Smith. Digital modeling of string instrument bridge reflectance and body radiativity for sound synthesis by digital waveguides. *2015 IEEE Workshop on Applications of Signal Processing to Audio and Acoustics, WASPAA 2015*, 2015.
- [65] Esteban Maestre, Gary P Scavone, and Julius O Smith. Design of recursive digital filters in parallel form by linearly constrained pole optimization. *IEEE Signal Processing Letters*, 23(11):1547–1550, 2016.

- [66] Esteban Maestre, Gary P Scavone, and Julius O Smith. Joint modeling of bridge admittance and body radiativity for efficient synthesis of string instrument sound by digital waveguides. *IEEE/ACM Transactions on Audio, Speech, and Language Processing*, 25(5):1128–1139, 2017.
- [67] Esteban Maestre, Gary. P. Scavone, and Julius. O. Smith III. Digital modeling of bridge driving-point admittances from measurements on violin-family instruments. In *Proc. of the Stockholm Music Acoustics Conference*, pages 101–108, 2013.
- [68] Esteban. Maestre, Gary. P. Scavone, and Julius. O. Smith III. Digital modeling of string instrument bridge reflectance and body radiativity for sound synthesis by digital waveguides. In *Proc. of the IEEE Workshop on Applications of Signal Processing to Audio and Acoustics*. IEEE, 2015.
- [69] Hossein Mansour, Vincent Fréour, Charalampos Saitis, and Gary P Scavone. Post-Classification of Nominally Identical Steel String Guitars Using Bridge Admittances. *Acta Acustica united with Acustica*, 101:1–14, 2015.
- [70] Max Mathews and Julius O Smith. Methods for synthesizing very high Q parametrically well behaved two pole filters. In *Proceedings of the Stockholm Musical Acoustics Conference (SMAC 2003)*, Stockholm, Sweden, August 6-9, 2003.
- [71] Sebastian Merchel, M Ercan Altinsoy, and David Olson. Perceptual evaluation of bracewood and soundboard wood variations on the preference of a steel-string acoustic guitar. *The Journal of the Acoustical Society of America*, 146(4):2608–2618, 2019.
- [72] Jürgen Meyer. Quality aspects of the guitar tone. *Function, Construction and Quality of the Guitar*, edited by EV Jansson (Royal Swedish Academy of Music, Stockholm, Sweden, 1983), pages 51–75, 1983.
- [73] MOKOSE. 4K Ultra HD Webcam. <https://www.mokose.com/products/>. Accessed 05-10-2023.
- [74] J Alonso Moral and EV Jansson. Eigenmodes, input admittance, and the function of the violin. *Acta Acustica united with Acustica*, 50(5):329–337, 1982.
- [75] Guild of American Luthiers. Guild of american luthiers. <https://luth.org/>. [Accessed 22-10-2023].
- [76] Ahmet Arda Ozdemir and Suat Gumussoy. Transfer function estimation in system identification toolbox via vector fitting. *IFAC-PapersOnLine*, 50(1):6232–6237, 2017.
- [77] Arthur Paté. *Lutherie de la Guitare Électrique Solid Body: Aspects Méchaniques et Perceptifs*. PhD thesis, L’Université Pierre Et Marie Curie, 2014.

- [78] PCB. Model 080A109 | PCB Piezotronics. <https://www.pcb.com/products?m=080a109>. Accessed 03-10-2023.
- [79] Henri Penttinens. Acoustic timbre enhancement of guitar pickup signals with digital filters. *Master's Thesis*, Helsinki University of Technology, 2002.
- [80] Henri Penttinens, Matti Karjalainen, and Aki Härmä. Morphing instrument body models. In *Proceedings of the COSTG-6 Conference on Digital Audio Effects (DAFx-01)*, Limerick, Ireland, December 6-8, 2001.
- [81] PJRC. Audio adaptor boards for teensy 3.x and teensy 4.x. https://www.pjrc.com/store/teensy3_audio.html. Accessed 05-10-2023.
- [82] PJRC. Teensy 4.0 development board. <https://www.pjrc.com/store/teensy40.html>. Accessed 05-10-2023.
- [83] PJRC. Teensy® 3.6 development board. <https://www.pjrc.com/store/teensy36.html>. Accessed 04-10-2023.
- [84] Martin Pollow, Gottfried K Behler, and Frank Schultz. Musical instrument recording for building a directivity database. *Fortschritte der ANustiN: Tagungsband d*, 36:6, 2010.
- [85] Polytec. PSV-500 Scanning Vibrometer. <https://www.polytec.com/eu/vibrometry/products/full-field-vibrometers/psv-500-scanning-vibrometer>. Accessed 04-10-2023.
- [86] Polytec. Vibrometry products - PSV-500-3D Scanning Vibrometer - Polytec. <https://www.polytec.com/eu/vibrometry/products/full-field-vibrometers/psv-500-3d-scanning-vibrometer>. Accessed 04-10-2023.
- [87] Mark Rau. See supplementary audio files at <https://ccrma.stanford.edu/~mrau/projects/PickupProcessingWithDamping/>, <https://ccrma.stanford.edu/~mrau/projects/PickupProcessingWithDamping/>, 2021.
- [88] Mark Rau. Measurements and analysis of acoustic guitars during various stages of their construction. in *180th Meeting of the Acoustical Society of America*, Virtual, June 8–10, 2021. published abstract.
- [89] Mark Rau, Jonathan S Abel, Doug James, and Julius O Smith III. Electric-to-acoustic pickup processing for string instruments: An experimental study of the guitar with a hexaphonic pickup. *The Journal of the Acoustical Society of America*, 150(1):385–397, 2021.

- [90] Mark Rau, Jonathan S Abel, and Julius O Smith III. Contact sensor processing for acoustic instrument recording using a modal architecture. In *in 21st Int. Conf. Digital Audio Effects (DAFx-18)*, Aveiro, Portugal, pages 304–311, September 4–8, 2018.
- [91] Mark Rau, Orchisama Das, and Elliot Canfield-Dafilou. Improved carillon synthesis. *in 22nd Int. Conf. Digital Audio Effects (DAFx-19)*, Birmingham, England, Sep. 2–6, 2019.
- [92] Mark Rau and Richard Hoover. Measurements of acoustic guitar top plates during the voicing process. *in 26th International Congress on Sound and Vibration*, July 7–11, 2019.
- [93] Mark Rau, Richard Hoover, Rick Barto, and Julius O Smith. A self-contained and automated tonewood measurement device. *Vienna Talk on Musical Acoustics*, Vienna, Austria, September 11–14, 2022. published abstract.
- [94] Mark Rau, Esteban Maestre, Julius O Smith, and Gary Scavone. An exploration of guitar neck admittance measurements taken at different string stopping locations. *International Symposium on Musical Acoustics*, pages 73–76, June 18–22, 2017.
- [95] Mark Rau, Julius O. Smith, and Jonathan S. Abel. A comparison of modal parameter extraction methods when applied to measurements of stringed instruments. *in 10th Convention of the European Acoustics Association*, Turin, Italy, Septembet 11–15, 2023.
- [96] Mark Rau, Julius O Smith, and Doug L James. Augmenting a single-point laser doppler vibrometer to perform scanning measurements. *in 182nd Meeting of the Acoustical Society of America*, Denver, CO, May 23–27, 2022. published abstract.
- [97] Mark Rau and Julius O Smith III. Measurement and modeling of a resonator guitar. *International Symposium on Musical Acoustics*, September 13–17, 2019.
- [98] Edwin Reynders. System identification methods for (operational) modal analysis: review and comparison. *Archives of Computational Methods in Engineering*, 19:51–124, 2012.
- [99] Bernard E Richardson. The acoustical development of the guitar. *Catgut Acoustical Society Journal*, 2(5):1–10, 1994.
- [100] Gert Roebben, B Bollen, A Brebels, Jan Van Humbeeck, and Omer Van der Biest. Impulse excitation apparatus to measure resonant frequencies, elastic moduli, and internal friction at room and high temperature. *Review of scientific instruments*, 68(12):4511–4515, 1997.
- [101] Robert J Ross et al. Wood handbook: wood as an engineering material. *USDA Forest Service, Forest Products Laboratory, General Technical Report FPL-GTR-190*, 2010: 509 p. 1 v., 190, 2010.
- [102] Thomas D. Rossing. *The Science of String Instruments*. Springer, New York, 2010.

- [103] Thomas D Rossing and Neville H Fletcher. *Principles of vibration and sound*. Springer Science & Business Media, 2012.
- [104] Thomas D. Rossing and Andrew Morrison. *The science of string instruments*. Springer, 2010.
- [105] Richard Roy and Thomas Kailath. Esprit-estimation of signal parameters via rotational invariance techniques. *IEEE Transactions on acoustics, speech, and signal processing*, 37(7):984–995, 1989.
- [106] Jaroslav Schmidt, Petr Pelech, Mark Dostálík, and Jiří Malík. Modal analysis - fenics solid tutorial 2019.0.2 documentation.
- [107] John Schneider. *The contemporary guitar*, volume 5. Univ of California Press, 1985.
- [108] Brian J Schwarz and Mark H Richardson. Experimental modal analysis. *CSI Reliability week*, 35(1):1–12, 1999.
- [109] Roger H Siminoff. *The Luthier's Handbook: A Guide to Building Great Tone in Acoustic Stringed Instruments*. Hal Leonard Corporation, 2002.
- [110] Julius O Smith. *Mathematics of the discrete Fourier transform (DFT): with audio applications*. Julius Smith, 2008.
- [111] Julius O. Smith. *Physical audio signal processing: For virtual musical instruments and audio effects*. W3K publishing, 2010.
- [112] Julius O. Smith III. Efficient synthesis of stringed musical instruments. In *Proc. of the International Computer Music Conference*, pages 64–71, 1993.
- [113] Julius. O. Smith III. *Physical Audio Signal Processing*. W3K Publishing, 2004. online book: [//ccrma.stanford.edu/~jos/pasp/](http://ccrma.stanford.edu/~jos/pasp/).
- [114] Ervin Somogyi. *The Responsive Guitar*. Luthiers Press, 2010.
- [115] Audio Sprockets. Tonedexter by audio sprockets.
<https://audiosprockets.com/tonedexter/>. (Last viewed Feb 8, 2021).
- [116] StewMac. StewMac Triple-O Acoustic Guitar Kit.
<https://www.stewmac.com/kits-and-projects/instrument-kits/acoustic-guitar-kits/stewmac-triple-o-acoustic-guitar-kit/>. Accessed 02-10-2023.
- [117] The MathWorks Inc. Modal parameters from frequency-response functions - matlab2017, 2017.
- [118] The MathWorks Inc. Matlab version: 9.13.0 (r2022b), 2022.

- [119] Thorlabs. Thorlabs - PK4DLP1 Discrete Piezo Stack, 150 V, 5.2 μm Displacement, 2.5 mm x 2.5 mm x 6.1 mm, End Hemisphere and Flat End Plate.
<https://www.thorlabs.com/thorproduct.cfm?partnumber=PK4DLP1>. Accessed 03-10-2023.
- [120] Cremona Tools. Cermona tools. *Cermona Tools*.
- [121] Harvey Turnbull. *The guitar: From the Renaissance to the present day*, volume 1. Bold Strummer, 2006.
- [122] Stan VanDruff. Association of Stringed Instrument Artisans — asiartisans.org.
<https://www.asiartisans.org/content/> [Accessed 22-10-2023].
- [123] Guido vanRossum. Python reference manual. *Department of Computer Science [CS]*, (R 9525), 1995.
- [124] Peter T. Veru. *The National-Dobro Guitar Company: How the resonator guitar survived the age of electric amplification*. The George Washington University, 2009.
- [125] Pauli Virtanen, Ralf Gommers, Travis E Oliphant, Matt Haberland, Tyler Reddy, David Cournapeau, Evgeni Burovski, Pearu Peterson, Warren Weckesser, Jonathan Bright, et al. Scipy 1.0: fundamental algorithms for scientific computing in python. *Nature methods*, 17(3):261–272, 2020.
- [126] Chris Waltham and Andrzej Kotlicki. Construction and calibration of an impact hammer. *American Journal of Physics*, 77(10):945–949, 2009.
- [127] Ulrike GK Wegst. Wood for sound. *American Journal of Botany*, 93(10):1439–1448, 2006.
- [128] Wonsung. 20kpps galvo galvanometer based optical scanner including show card for animation light.
https://www.amazon.com/Generic-Galvanometer-Optical-Scanner-Including/dp/B01IZPMUPO/ref=cm_cr_arp_d_product_top?ie=UTF8. Accessed 04-10-2023.
- [129] J. Woodhouse. Plucked guitar transients: Comparison of measurements and synthesis. *Acta Acustica united with Acustica*, 90(5):945–965, 2004.
- [130] J. Woodhouse and R. S. Langley. Interpreting the input admittance of violins and guitars. *Acta Acustica united with Acustica*, 98(4):611–628, 2012.
- [131] J Woodhouse and RS Langley. Interpreting the input admittance of violins and guitars. *Acta Acustica united with Acustica*, 98(4):611–628, 2012.
- [132] J Woodhouse, EKY Manuel, LA Smith, AJC Wheble, and Claudia Fritz. Perceptual thresholds for acoustical guitar models. *Acta Acustica united with Acustica*, 98(3):475–486, 2012.

- [133] Jim Woodhouse. On the synthesis of guitar plucks. *Acta Acustica united with Acustica*, 90(5):928–944, 2004.
- [134] Jim Woodhouse and Nicolas Lynch-Aird. Choosing strings for plucked musical instruments. 2019.
- [135] Howard Wright. *The acoustics and psychoacoustics of the guitar*. PhD thesis, Cardiff, 1998.
- [136] Ailin Zhang and Jim Woodhouse. Reliability of the input admittance of bowed-string instruments measured by the hammer method. *The Journal of the Acoustical Society of America*, 136(6):3371–3381, 2014.
- [137] Tianyuan Zhang, Mark Sheinin, Dorian Yao Chan, Mark Rau, Matthew O’Toole, and Srinivasa Narasimhan. Estimating physical interactions using transient surface wave imaging. In *Proceedings of the IEEE/CVF Conference on Computer Vision and Pattern Recognition*, 2023.
- [138] Udo Zölzer. *DAFX: Digital Audio Effects, 2nd Edition*. John Wiley & Sons Ltd, Hamburg, Germany, 2011.
- [139] Eberhard Zwicker and Hugo Fastl. *Psychoacoustics: Facts and models*, volume 22. Springer Science & Business Media, 2013.